

Chromium Complexes of Amine-bis(phenolate) Ligands as Copolymerization

Catalysts

by

© Hua Chen

A Thesis submitted to the School of Graduate Studies
in partial fulfillment of the requirements for the degree of

Master of Science

Department of Chemistry

Memorial University of Newfoundland

May 2014

St. John's,

Newfoundland

ABSTRACT

Alternating copolymerization of CO₂ with epoxides to provide polycarbonates is a promising reaction for the industrial production of biodegradable thermoplastics, which have been widely used in electronics, optical media, the automotive industry, the medical and healthcare industry, and many consumer goods. Homogeneous catalysts containing transition metals including Co, Cr and Zn have been active for this reaction. Previous work in the group involved using amine-bis(phenolates) with different metals to generate catalysts and reactive species for use in several reactions. It was found that Cr complexes of tetradentate amine-bis(phenolate) ligands were promising catalysts for the copolymerization of CO₂ with cyclohexene oxide (CHO) and propylene oxide (PO). This thesis seeks to further that research by investigating different amine-bis(phenolates) to study their structure-polymerization activity relationship.

The ligands used in this thesis were tridentate or tetradentate amine-bis(phenolates) where the substituents on the phenolate groups and pendant arm were varied. Three ligands used were 2-tetrahydrofurfuryl-*N,N*-bis(2-methylene-4,6-*tert*-butylphenol), H₂[**L1**], benzylamino-*N,N*-bis(2-methylene-4,6-di-*tert*-butylphenol), H₂[**L2**], and benzylamino-*N,N*-bis(2-methylene-4,6-di-*tert*-amylphenol), H₂[**L3**]. The synthesis and characterization of related lithium complexes **1**, **2** and **3** and also chromium^{III} complexes **4**, **5** and **6** were performed. Three chromium complexes were isolated and characterized by UV-Vis spectroscopy, mass spectrometry, elemental analysis and, for complex **5**, single-crystal X-ray diffraction.

The copolymerization of cyclohexene oxide with CO₂ to yield polycarbonates was investigated with these chromium^{III} amine-bis(phenolate) complexes. The resulting polymers were analyzed by ¹H and ¹³C NMR spectroscopy, MALDI-TOF mass spectrometry and gel permeation chromatography.

ACKNOWLEDGEMENTS

Firstly, I truly appreciated my supervisor Dr. Chris Kozak for providing the opportunity to work on this fascinating research project, his guidance and full support and also for his dedicated reading of my thesis chapters. Secondly, I would like to thank Dr. Fran Kerton for helpful discussions in group meetings and also valuable comments as a committee member in my program. I also thank my supervisory committee member Dr. Yuming Zhao for useful suggestions in my studies.

I am also so grateful to have had the opportunity to work with our Green Chemistry and Catalysis Group members. They have offered loads of help to me and I have also learned a lot from them through discussions in or out of the lab. Specifically, I would like to thank Katalin, Ali and Nduka for their constant help, advice, and support while conducting my research. I am also thankful to everyone in C-CART for their knowledge and advice for the instruments operation. Specially, I would like to thank Dr. Louise Dawe, Dr. Celine Schneider, and Linda Winsor in C-CART.

I would especially like to thank all the funding agencies who allowed me to complete my degree and attend many conferences during my program, NSERC, SGS, Department of Chemistry, Dean of Science and GSU. Last but not least, I would like to thank my family and friends for their continued support throughout my educational life. My parents, please accept my deepest gratitude and love for their dedication and the many years of support during my studies that provided the foundation for this work. The friendship of Yi and Qing is much appreciated and has led to many interesting moments in life. To all of you, thanks for always being there for me.

Table of Contents

ABSTRACT	ii
ACKNOWLEDGEMENTS	iv
List of Tables.....	viii
List of Figures	ix
List of Schemes	xii
List of Abbreviations and Symbols	xiii
Abbreviations for ligands used in this work	xvi
List of Appendices.....	xvii
Chapter 1	1
Introduction	1
1.1 Chromium Complexes	1
1.1.1 Introduction to the Element Chromium	1
1.1.2 Overview of Chromium Coordination Chemistry	2
1.2 [Cr(salen)] complexes	4
1.3 Copolymerization of CO ₂ /epoxide	9
1.3.1 Background	9
1.3.2 Polycarbonate	10
1.3.3 Catalyst Systems used in Copolymerization of CO ₂ /epoxides.....	12
1.3.4 Mechanism of Polymerization.....	19
1.3.5 Polymer Characterization.....	20

Chapter 2 Synthesis and Structure of Chromium ^{III} Amine-bis(phenolate) Complexes	22
2.1 Introduction.....	22
2.2 Synthesis of Chromium ^{III} Amine-bis(phenolate) Complexes.....	23
2.3 Characterization of Chromium ^{III} Amine-bis(phenolate) Complexes	25
2.3.1 MALDI-TOF MS.....	25
2.3.2 UV-Visible Spectroscopy.....	31
2.3.3 Single Crystal X-ray Diffraction	33
2.4 Experimental.....	38
2.4.1 General Experimental Conditions.....	38
2.4.2 Synthesis of Cr ^{III} Complexes.....	39
2.5 Conclusions.....	41
Chapter 3 Chromium Amine-bis(phenolate) Complexes for the Copolymerization of Cyclohexene oxide and Carbon Dioxide	42
3.1 Introduction.....	42
3.2 Copolymerization of Cyclohexene Oxide and CO ₂	43
3.3 Characterization of poly(cyclohexene) carbonate.....	49
3.3.1 NMR of polymer.....	49
3.3.2 Mass Spectrometry	52
3.3.3 Gel Permeation Chromatography	71
3.4 Experimental.....	72

3.4.1 General Experimental Conditions.....	72
3.4.2 Copolymerization Procedure.....	72
3.4.3 Mass Spectrometry.....	73
3.4.4 Gel Permeation Chromatography.....	74
3.5 Conclusions.....	74
References.....	77
Appendices.....	85

List of Tables

Table 2.1. Selected bond lengths (Å) and angles (°) for (5) ₂ ·LiCl·THF.	38
Table 3.1. Results of the Copolymerization of CHO and CO ₂ by Catalyst 5 and 6 with DMAP or PPNX salts. ^a	45
Table 3.2. Results of the Copolymerization of CHO and CO ₂ by Catalyst 4 and DMAP or PPNX salts. ^a	46
Table A1.1. Crystallographic and Structure Refinement Data for (5) ₂ ·LiCl·THF.	85

List of Figures

Figure 1.1. SalenH ₂ , salanH ₂ and salalenH ₂ ligands (from left to right).	5
Figure 1.2. β-diiminate zinc complexes used for the copolymerization of CO ₂ /CHO.....	14
Figure 1.3. Aluminum Schiff base complex used for the copolymerization of CO ₂ and CHO	15
Figure 1.4. [Co(salcy)OAc] complex used for the copolymerization of CO ₂ and propylene oxide.	15
Figure 1.5. Highly active cobalt ^{III} catalyst for CO ₂ /PO and CO ₂ /EO copolymerization...	16
Figure 1.6. General structure of chromium ^{III} salen catalyst used in the copolymerization of CO ₂ /epoxides.	17
Figure 1.7. Diamine-bis(phenolate) chromium ^{III} catalyst used in the copolymerization of CO ₂ /epoxides.....	18
Figure 2.1. MALDI-TOF mass spectrum (lower mass region) of CrCl[ONO] ^{BuBuBn} (5)..	26
Figure 2.2. Experimental (top blue) and theoretical (bottom, green) MALDI-TOF isotopic distribution pattern for the [M] ⁺ peak of 5	27
Figure 2.3. MALDI-TOF mass spectrum of (5) showing the higher mass region.	28
Figure 2.4. MALDI-TOF mass spectrum (lower mass region) of CrCl[ONO] ^{tAmtAmBenzyl} (6).....	29
Figure 2.5. Experimental (top, blue) and theoretical (bottom, green) MALDI-TOF isotopic distribution pattern for the molecular ion of the [M] ⁺ peak of 6	30
Figure 2.6. MALDI-TOF mass spectrum of (6) showing the higher mass region.	30

Figure 2.7. UV-Vis absorption spectrum of 5 in CH ₂ Cl ₂ . Inset: Expansion of visible region showing peak wavelength and molar extinction coefficients, and wavelength of two maximum absorptions in region 500-800 nm are assigned.....	32
Figure 2.8. UV-Vis absorption spectrum of 6 in CH ₂ Cl ₂ . Inset: Expansion of visible region showing peak wavelength and molar extinction coefficients, and wavelength of two maximum absorptions in region 500-800 nm are assigned.....	33
Figure 2.9. Molecular structure (ORTEP) and partially labelled numbering scheme of (5) ₂ ·LiCl·THF. Ellipsoids are shown at 50% probability. Hydrogen atoms and methyl groups on phenolate t-butyl groups are omitted for clarity. Symmetry operations used to generate equivalent atoms (*): -x+2, -x+y+1, -z+1/3.....	34
Figure 2.10. Structure of {[(<i>t</i> -Bu)NP(Ph) ₂ N(<i>t</i> -Bu)]Cr} ₂ (μ ₂ -Cl) ₃ (μ ₃ -Cl) ₂ {Li(THF) ₂ } containing bridging Cl ions and face-sharing octahedra.	36
Figure 3.1. Common co-catalysts used in CO ₂ /epoxide copolymerization reactions.	44
Figure 3.2. Typical ¹ H NMR spectrum of PCHC in CDCl ₃ (Table 3.1 Entry 1), EG = end group (see section 3.3.2).	50
Figure 3.3. Carbonyl region of the ¹³ C NMR spectrum (75.5 MHz, CDCl ₃) of CHO/CO ₂ copolymer prepared as described in Table 3.1, entry 1.	51
Figure 3.4. Stereochemistry of PCHC.	52
Figure 3.5. (A) MALDI-TOF MS of PCHC produced by 5 (Table 3.1, entry 4). (B) Magnified region of the spectrum (n = 24-27). (C) Magnified region of the spectrum (n = 45-48). Modeled isotopic masses and images for the polymer chains with end groups (a, b and c).....	55

Figure 3.6. (A) MALDI-TOF MS of PCHC produced by 5 (Table 3.1, entry 2). (B) Magnified region of the spectrum (n = 18-21). (C) Magnified region of the spectrum (n = 34-37) and modeled isotopic masses and images for the polymer chains with end groups (a-d).....	58
Figure 3.7. (A) MALDI-TOF MS of PCHC produced by 6 (Table 3.1, entry 5). (B) Magnified region of the spectrum (n = 22-25) and modeled isotopic masses and images for the polymer chains with end groups (a-c).	60
Figure 3.8. (A) MALDI-TOF MS of PCHC produced by 4 (Table 3.2, entry 1). (B) Magnified low molecular weight region of the spectrum (n = 18-20). (C) Magnified high molecular weight region of the spectrum (n = 44-47). Modeled isotopic masses and images for the polymer chains with end groups (a-f).	64
Figure 3.9. (A) MALDI-TOF MS of PCHC produced by 4 (Table 3.2, entry 4). (B) Magnified low molecular weight region of the spectrum (n = 24-26). (C) Magnified high molecular weight region of the spectrum (n = 47-50). Modeled isotopic masses and images for the polymer chains with end groups (a-d).	67
Figure 3.10. (A) MALDI-TOF MS of PCHC produced by 4 (Table 3.2, entry 5). (B) Magnified low molecular weight region of the spectrum (n = 9-11). (C) Magnified high molecular weight region of the spectrum (n = 32-35). Modeled isotopic masses and images for the polymer chains with end groups (a-g).	70

List of Schemes

Scheme 1.1. Preparation of SalenH ₂ and salen..	4
Scheme 1.2. Synthesis of Cr ^{III} -salen based complex.	6
Scheme 1.3. Synthesis of [CrCl(salen)] complex by <i>in-situ</i> CrCl ₂ formation.	6
Scheme 1.4. Synthesis of [Cr(Schiff base)] complex via salt metathesis.	7
Scheme 1.5. Epoxidation of <i>trans</i> -olefins by using oxo[Cr(salen)] complex.	8
Scheme 1.6. Enantioselective Diels-Alder reaction using Cr ^{III} -salen complex as catalyst.	8
Scheme 1.7. Traditional synthetic route to BPA-based polycarbonate	11
Scheme 1.8. Co-polymerization of racemic propylene oxide and CO ₂ by a mixture of diethylzinc and water as the catalyst	13
Scheme 1.9. Proposed mechanism of polycarbonates formation in the copolymerization of CO ₂ /epoxides.	19
Scheme 2.1. Synthetic routes to Cr ^{III} complexes.	25
Scheme 3.1. Copolymerization of CHO and CO ₂ .	44

List of Abbreviations and Symbols

et al.: and co-workers

Å: Angstrom (10^{-10} m)

amu: atomic mass unit

BDI: β -diiminate

BPA: bisphenol A

salan: N,N'-bis(phenolato)-1,2-diaminoethane

salen: N,N'-bis(salicylaldehydo)ethylenediamine (and related ligands)

PPNN₃: bis(triphenylphosphoranylidene)iminium azide

PPNCl: bis(triphenylphosphoranylidene)iminium chloride

cm: centimetre (10^{-2} m)

salalen: a combination of salan and salen ligands

J: coupling constant

CHC: cyclohexene carbonate

CHO: cyclohexene oxide

(°): degree

DHBA: 2,5-dihydroxybenzoic acid

DMAP: (4-dimethylamino)pyridine

d: doublet

dd: doublet of doublet

EO: ethylene oxide

Et: ethyl

g: gram

HH: head-to-head

HT: head-to-tail

HOMO: highest occupied molecular orbital

h: hour(s)

in situ: “in the reaction mixture”

MS: mass spectrometry

m/z: mass-to-charge ratio

MALDI-TOF: matrix assisted laser desorption/ionization time-of-flight

MeOH: methanol

Me: methyl

N-MeIm: 1-methylimidazole

μL : microlitre (10^{-6} L)

mmol: millimole (10^{-3} mol)

min: minute

M: molar (mols/L)

NMR: nuclear magnetic resonance

M_n : number average molecular weight

ORTEP: Oak Ridge thermal-ellipsoid plot program

trans: “on the other side”

cis: “on the same side”

ppm: parts per million

Ph: phenyl

PCHC: poly(cyclohexene carbonate)

PDI: polydispersity index

PPC: poly(propylene carbonate)

PC: propylene carbonate

PO: propylene oxide

ROP: ring-opening polymerization

s: singlet (in NMR)

SO: styrene oxide

scCO₂: supercritical carbon dioxide

TT: tail-to-tail

*t*Am: tertiary-amyl (tertiary-pentyl)

*t*Bu: tertiary-butyl

THF: tetrahydrofuran

TMS: tetramethylsilane

TOF: turnover frequency

TON: turnover number

UV-Vis: ultraviolet-visible

vs: “versus”

M_w : weight average molecular weight

Abbreviations for ligands used in this work

$\text{H}_2[\text{O}_2\text{NO}]^{\text{BuBu}}$ ($\text{H}_2[\mathbf{L1}]$): 2-tetrahydrofurfuryl-*N,N*-bis(2-methylene-4,6-*tert*-butylphenol)

$\text{H}_2[\text{ONO}]^{\text{BuBuBn}}$ ($\text{H}_2[\mathbf{L2}]$): benzylamino-*N,N*-bis(2-methylene-4,6-di-*tert*-butylphenol)

$\text{H}_2[\text{ONO}]^{t\text{Am}t\text{AmBn}}$ ($\text{H}_2[\mathbf{L3}]$): benzylamino-*N,N*-bis(2-methylene-4,6-di-*tert*-amylphenol)

List of Appendices

Table A1.1. Crystallographic and Structure Refinement Data for (5) ₂ ·LiCl·THF	84
Checkcif Report for (5) ₂ ·LiCl·THF.....	85

Chapter 1

Introduction

1.1 Chromium Complexes

1.1.1 Introduction to the Element Chromium

Chromium was first isolated from the rare mineral crocoite (PbCrO_4) by the French chemist Louis N. Vauquelin of France in 1797, and named for its various colors (*chroma*). It ranks 21st in elemental abundance at an average concentration of 100 ppm in the earth's crust. Chromium has the atomic number 24 and a relative atomic mass of 51.9961 ($^{12}\text{C} = 12.0000$). Only four (mass numbers 50, 52, 52 and 54) of the 13 known isotopes of Cr are stable.^[1]

Chromium compounds exist in a wide range of oxidation states, from $-IV$ to $+VI$. The most common oxidation states are $+II$, $+III$ and $+VI$ for inorganic chromium compounds. For chromium, the $+II$ oxidation state can be strongly reducing and the highest oxidation state $+VI$ is found to be a very strong oxidant. However, the most stable oxidation state of chromium is $+III$. The transition metal chromium has played a remarkable role in the development of inorganic chemistry.^[1] Chromium^{VI} compounds have been regarded as skin irritants. In contrast, chromium^{III} occurs in trace amounts in foods and water and shows no known toxic effects so far. The estimated average daily intake of chromium should be 25-35 μg , as it aids in the metabolism of glucose.^[1] Moreover, due to its high corrosion resistance and hardness, chromium has been

commercially used to electroplate surfaces to protect them from corrosion. In addition, Cr is often used for decorative purposes and Cr salts are used in the dyeing of leathers.^[1]

1.1.2 Overview of Chromium Coordination Chemistry

Alfred Werner, the father of modern coordination chemistry, proposed the octahedral configuration of transition metal complexes.^[2] His contribution developed the basis for modern coordination chemistry, leading to the discoveries of thousands of coordination complexes.^[3] Chromium^{III} coordination complexes became one of the most influential areas in the development of coordination chemistry for their prominent chemical and configurational stability.^[4]

Cr^{II} and Cr^{III} complexes were the focus of the early studies of Cr coordination chemistry and are dominated by octahedral complexes. As mentioned, Cr^{II} complexes are usually strongly reducing and easily affected by air oxidation. Cr^{III} comprises the majority of coordination compounds of chromium reported so far, for the reason that they are generally substitutionally inert and easily synthesized. The +IV and +V oxidation states are still considered unusual in chromium chemistry, whereas Cr^{VI} is a common oxidation state of chromium, usually as CrO₄²⁻ or other oxide-containing ions.^[1, 4]

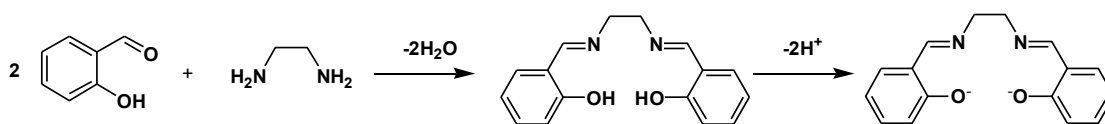
The area of monometallic coordination compounds and the chemistry of metal-metal bonded species are two subdivisions of the coordination chemistry of Cr^{II}. The first class is usually derived from blue [Cr(H₂O)₆]²⁺ ions and the second is derived from analogs of Cr₂(OAc)₄. Due to the Jahn-Teller effect, most Cr^{II} compounds are distorted, octahedral, high-spin d⁴ complexes. However, low-spin, octahedral complexes are formed with

strong-field ligands such as CN^- and CO and some four-coordinate complexes with different coordination geometries exist such as tetrahedral and square planar.^[4]

Since Werner's pioneering work in coordination chemistry, thousands of Cr^{III} coordination compounds have been published in the literature. A variety of ligands can be used in the synthesis of these Cr^{III} complexes and these ligands are usually inert allowing a great number of isolable complexes to be simply generated. A central feature of the reactivity of Cr^{III} complexes is very slow ligand substitution reactions, generating this unusual configurational stability. In organochromium chemistry, the most active area of research is the chromium–carbon σ -bond owing to its important application in catalytic processes (especially ethylene polymerization and oligomerization).^[5] Six-coordinate chromium complexes with octahedral arrangement of ligands are the key features of chromium^{III} coordination chemistry. In this geometry, the large ligand field stabilization energy of the d^3 configuration results in their chemical and structural stability.^[4] Chromium^{III} compounds with oxygen and sulfur ligands are well known, where the number of oxygen-donor ligand examples far exceeds the sulfur-containing ligands. The violet $[\text{Cr}(\text{H}_2\text{O})_6]\text{Cl}_3$, an important reagent for the production of commercially available CrCl -salts, is often used as a starting material in the synthesis process. In addition, CrCl_3 is probably the most important chromium halide, among which $\text{CrCl}_3 \cdot 6\text{H}_2\text{O}$ is the most common form. Moreover, $\text{CrCl}_3(\text{THF})_3$ can be easily synthesized by treating $\text{CrCl}_3 \cdot 6\text{H}_2\text{O}$ with trimethylsilylchloride in THF.^[6] Related to the research presented in this thesis, $\text{CrCl}_3(\text{THF})_3$ is the precursor used for the preparation of Cr^{III} compounds.

1.2 [Cr(salen)] complexes

Currently, considerable effort is being invested in developing new chelating ligands that can be utilized in homogeneous catalyst synthesis.^[7, 8] Particularly, the chelating salen (N,N'-bis(salicylidene)ethylenediamine) ligand, a [ONNO]-type Schiff base compound, can be coordinated to a variety of metal ions. The resulting complexes show great catalytic ability for a variety of reactions.^[9, 10] "Salen" is a contraction of salicylaldehyde and ethylenediamine, referring to the deprotonated dianionic species. Salen ligands, which possess an ethylene bridge between the nitrogen donors and two phenolate fragments that are often deprotonated giving dianionic tetradentate bonding modes, tend to wrap around transition metals forming complexes.^[11] All the structurally related chiral and achiral Schiff bases of this class of compounds are commonly referred to as "salen", often regardless of the nature of the fragment bridging the N-donors. SalenH₂ is commercially available. The ligand can also be easily prepared by the condensation of ethylenediamine, or other diamines, and salicylaldehyde, which may or may not possess substituents on the arene ring.^[12] (Scheme 1.1)



Scheme 1.1. Preparation of SalenH₂ and salen.

In addition to the salen-ligand, two related structural analogs exist, called salan and salalen. Salan^[11] ligands are saturated at the nitrogen; these compounds contain secondary or tertiary amines rather than imines. Salalens are a combination of salan and salen ligands: one side of the compound bears an imine, while the other side bears an amine.^[13] (Figure 1.1) These salen-related ligands can be easily synthesized and the desired steric and electronic properties of these ligands may be obtained through modifications of the substituents on the phenolate groups, which help tune the structure of electronic features of the metal complexes.

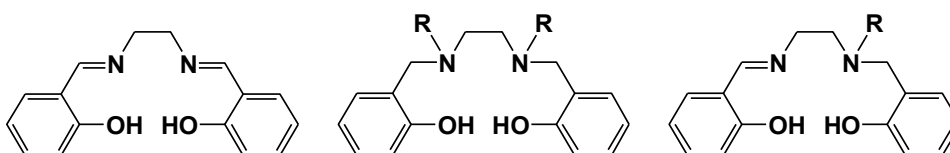
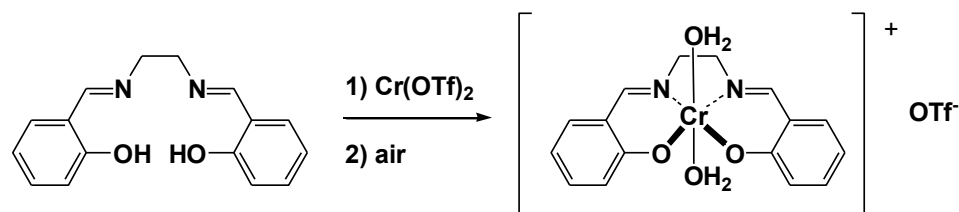


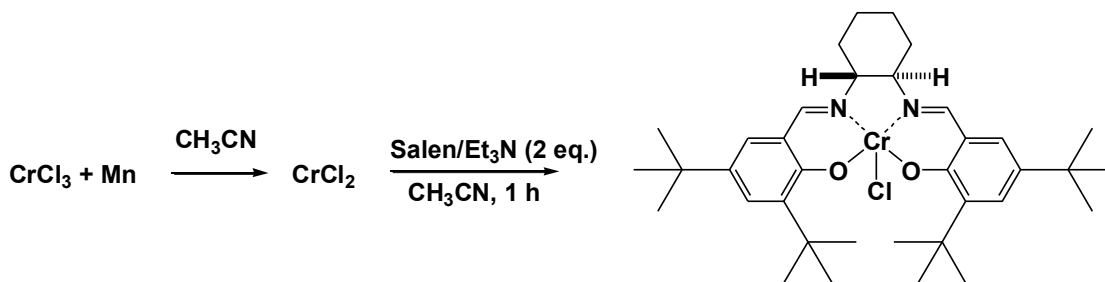
Figure 1.1. SalenH₂, salanH₂ and salalenH₂ ligands (from left to right).

The synthesis of metallo-salen complexes is normally conducted by mixing the ligand with the desired metal salt. However, several other synthetic methods that yield [Cr(salen)] complexes have been reported.^[11] The pioneering study was reported by Coggon *et al.* in 1970 on the synthesis of Cr^{III}-Schiff base complexes. The procedure involved using Cr(OTf)₂ and the oxidation of the intermediate [Cr^{II}(salen)] complex by air.^[14] (Scheme 1.2)



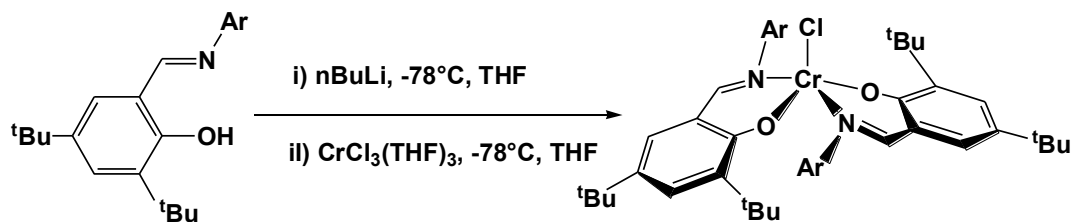
Scheme 1.2. Synthesis of Cr^{III}-salen base complex.

Bandini and coworkers have reported an alternative approach to the preparation of chromium-Schiff base species in 2001. The protocol involved using Mn as a reducing agent to produce CrCl₂ *in situ*. Reaction with chiral salen ligands in CH₃CN in the presence of 2 equiv. of Et₃N resulted in the [CrCl(salen)] complex (Scheme 1.3).^[15]



Scheme 1.3. Synthesis of [CrCl(salen)] complex by *in-situ* CrCl₂ formation.

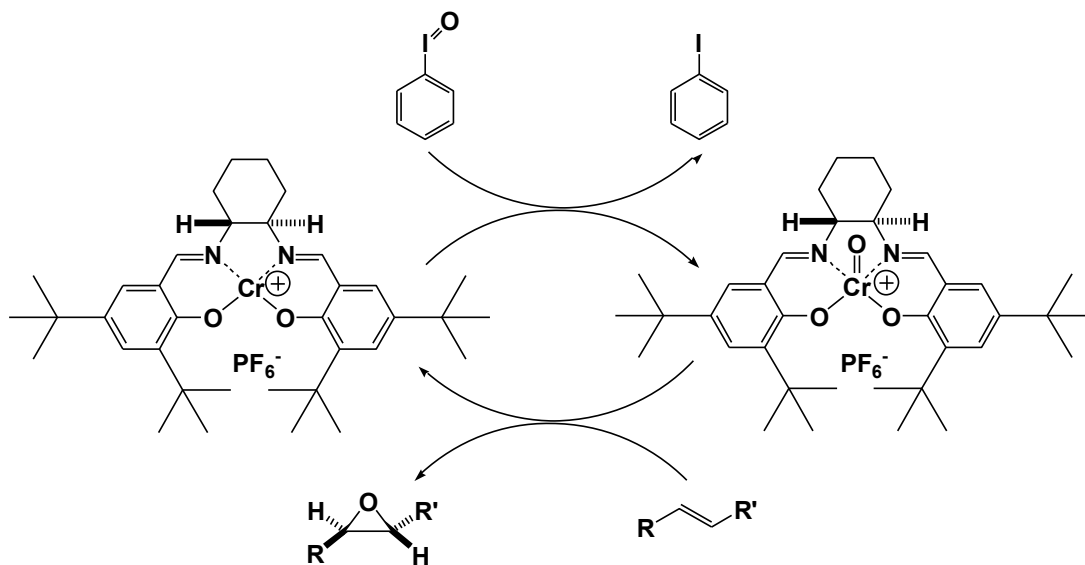
A more controlled synthetic approach starting from CrCl₃(THF)₃ has also been developed. A five-coordinate chromium complex bearing two salicylaldiminato ligands was prepared in high yield by treatment of CrCl₃(THF)₃ with 2 equiv. of the lithiated ligand precursor (Scheme 1.4).^[16] It is based on this salt-metathesis route that the synthesis of the Cr^{III} compounds in this thesis were prepared.



Scheme 1.4. Synthesis of [Cr(Schiff base)] complex via salt metathesis.^[16]

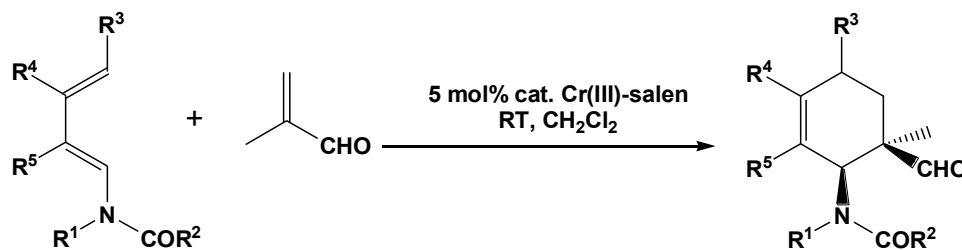
A variety of important Cr(salen) derivatives has been developed since the salen-ligand was firstly introduced. Salen Cr^{III} complexes have a wide range of applications, such as enantioselective Diels-Alder reactions,^[17-19] ring opening reactions of epoxides,^[20, 21] the coupling of CO₂ and epoxides,^[22, 23] copolymerizations of epoxides and CO₂^[24-26] and asymmetric epoxidations.^[27]

The first application of chromium-salen complexes as homogeneous catalysts was reported by Kochi and coworkers in 1983. Various [Cr(oxo)salen] complexes were used for catalysis of the epoxidation of olefins with iodobenzene.^[28] Subsequently, Gilheny and coworkers discovered chiral [Cr(salen)] complexes were effective in enantioselective epoxidation reactions. High efficiency of epoxidation of *trans*-olefins was obtained in the presence of oxo[Cr(salen)] complex and iodobenzene as the oxygen source (yield up to 77%) (Scheme 1.5).^[29, 30]



Scheme 1.5. Epoxidation of *trans*-olefins by using oxo[Cr(salen)] complex.^[31]

A broad range of substituted 1-aminobutadienes has been used in enantioselective Diels–Alder reactions with methacrolein in the presence of 5 mol % of Cr^{III}-salen complex. The reactions were carried out at room temperature and afforded the cycloadducts in high yields (Scheme 1.6).^[19]



Scheme 1.6. Enantioselective Diels-Alder reaction using Cr^{III}-salen complex as catalyst.^[19]

1.3 Copolymerization of CO₂/epoxide

1.3.1 Background

Fossil fuel resources remain the most important chemical feedstock of the day, which are widely used in industry. However, at current rates of consumption, worldwide fossil fuel reserves could be completely depleted by the year 2050, thus alternative, renewable carbon-based sources of raw materials are needed.^[32-35] Carbon dioxide is one possible source, which is released in many combustion processes and considered as one of the major green house gases.

According to current policies and regulations calling for limiting fossil fuel use, worldwide energy-related carbon dioxide emissions will increase from about 31 billion metric tons in 2010 to 36 billion metric tons in 2020.^[36] Carbon capture and storage (CCS) is one strategy assumed to considerably diminish the atmospheric CO₂ concentration via storage in the long term.^[37-39] A significant amount of research activities in this area indicates promising results in the near future. Since global climate change is the result of excessive combustion of fossil fuels, more emphasis should be placed on the restriction of CO₂ emissions by alternative methods. The utilization of CO₂ as a C1-feedstock for chemical reactions is one solution of great significance.^[40, 41]

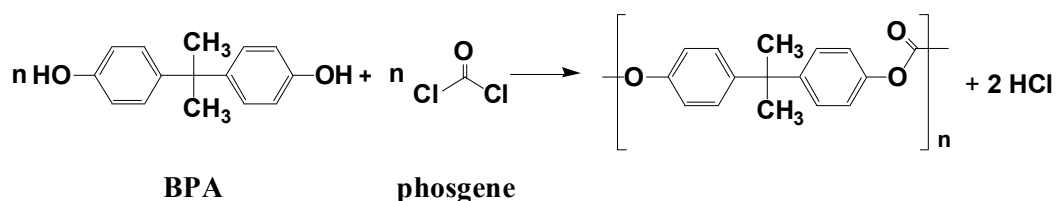
Currently, a promising reaction of utilizing CO₂ is the alternating copolymerization of CO₂ with epoxides to give polycarbonates.^[42, 43] Large-scale industrial application of CO₂ potentially lies in the production of biodegradable thermoplastics, such as poly(propylene carbonate) (PPC) and poly(cyclohexene carbonate) (PCHC). Although using CO₂ as a chemical feedstock will not significantly diminish global CO₂ levels, this

strategy potentially provides access to desirable products from a non-toxic, renewable and low-cost resource.

1.3.2 Polycarbonate

Traditional oil-based plastics have been widely used in a variety of packaging materials. However, the production of plastic uses fossil fuels which are finite, non-renewable resources, and lead to waste problems after use due to their poor biodegradability.^[44] Polycarbonates are polymers containing carbonate groups ($-O-(C=O)-O-$) in their backbone.

The conventional commercial synthesis of polycarbonate has used bisphenol A (BPA) as the monomer for many years (Scheme 1.7). BPA based polymer may display hydrolysis of the carbonate resulting in leaching of BPA. This potentially leads to widespread human exposure to this alleged endocrine disruptor.^[45] Besides, it is widely accepted that phosgene, which is needed in the polymerization reaction is one of the most acutely toxic substances in commercial use. Thus, it will be extremely beneficial with respect to risk reduction to eliminate the need for phosgene.^[46] New processes do not use $COCl_2$ but dimethyl carbonate or diethyl carbonate instead.^[47]



Scheme 1.7. Traditional synthetic route to BPA-based polycarbonate.

With current concerns about resource utilization and disposal in the plastics industry, polycarbonates produced from the copolymerization of carbon dioxide and epoxides are promising alternatives to petrochemical derived from polycarbonates.^[48] CO₂ represents an attractive co-monomer in the manufacture of polymers, not least because, as a gas, it would be compatible with many current polymerization processes. As the most highly oxidized state of carbon, CO₂ is the lowest energy state of all carbon-containing binary neutral species. Besides, CO₂ and water are the end-products of most energy releasing processes, including combustion and metabolic pathways.^[43, 49]

Polycarbonates possess outstanding properties. These include strength, lightness, durability, high transparency, heat resistance, and good electrical insulation.^[50] Hence, these materials have been widely used in electronics, optical media, the automotive industry, the medical and healthcare industry, and many other consumer goods. The thermo-mechanical properties of polymers, including glass transition temperature, crystalline melting temperature, tensile, compressive, and flexural strengths, fatigue and impact resistance, are highly dependent on molecular weight.^[43] On the other hand, cyclic carbonates have a wide range of applications, most importantly as high boiling and high flash point solvents with low toxicity in degreasing, paint stripping, and cleaning

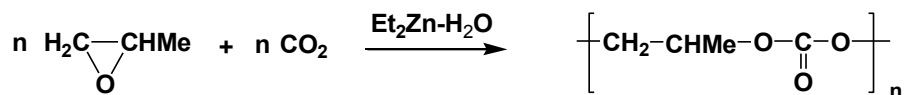
processes. These monomeric compounds are also extensively employed as reactive intermediates.^[51]

1.3.3 Catalyst Systems used in Copolymerization of CO₂/epoxides

The copolymerization of CO₂ and epoxides is a promising route to prepare new sustainable copolymers and materials. The success and viability of the copolymerization is critically dependent on the catalyst. The catalysts for the copolymerization are essential to control both the efficiency and the physical/chemical properties of polycarbonates.^[43, 49] The key evaluation criteria for catalyst activity include the productivity (defined as turn-over-number, TON), activity (turn-over-frequency, TOF) and the quality of the copolymer produced (% selectivity, the number average molecular weight (M_n)). In addition, another important aspect is the conditions under which the catalyst will operate, including the pressure of CO₂, temperature and any additives (co-catalysts).^[43] Since the development of high-activity catalysts will offer tremendous potential for the production of copolymers from CO₂, significant efforts have been devoted by a number of academic groups to the preparation and study of various homogeneous and heterogeneous catalyst systems for the reaction.

The discovery of metal-catalyzed copolymerization of carbon dioxide and epoxides by Inoue *et al.* dates back to the late 1960s, when the first successful polymerization of racemic propylene oxide and CO₂ was accomplished by a mixture of diethylzinc and water as the catalyst system.^[52] This was the first example of the use of carbon dioxide as

a monomer in the polymerization reaction with epoxides (see Scheme 1.8).



Scheme 1.8. Co-polymerization of racemic propylene oxide and CO₂ by a mixture of diethylzinc and water as the catalyst.

Since this discovery, copolymerization of carbon dioxide has been examined with many other monomers such as oxetane, thiirane, and aziridine. However, to date only CO₂/epoxide copolymers are considered sufficiently qualified for practical production and applications.^[53] The most commonly used epoxides are cyclohexene oxide (CHO), propylene oxide (PO), ethylene oxide (EO) and styrene oxide (SO). Regarding CO₂/epoxide copolymerization, a great deal of work has been carried out, mainly to develop highly active catalyst systems.^[26, 54-56] The activities and developments of different metal-centered catalysts will be discussed in the following part.

Coates and co-workers made a breakthrough by developing a series of zinc β-diiminate (BDI) complexes (Figure 1.2), which showed high activity in the CO₂/epoxides copolymerization reaction.^[54, 57, 58] A variety of substituents and initiating groups were investigated, and their influence was correlated with activity (Figure 1.2). For example, using [(BDI)ZnOAc] as the catalyst, the alternating copolymerization of CO₂/CHO proceeded rapidly under very mild conditions (20 °C, 6.9 bar) and gave the alternating copolymer (TOF = 135) in 2 h.^[54]

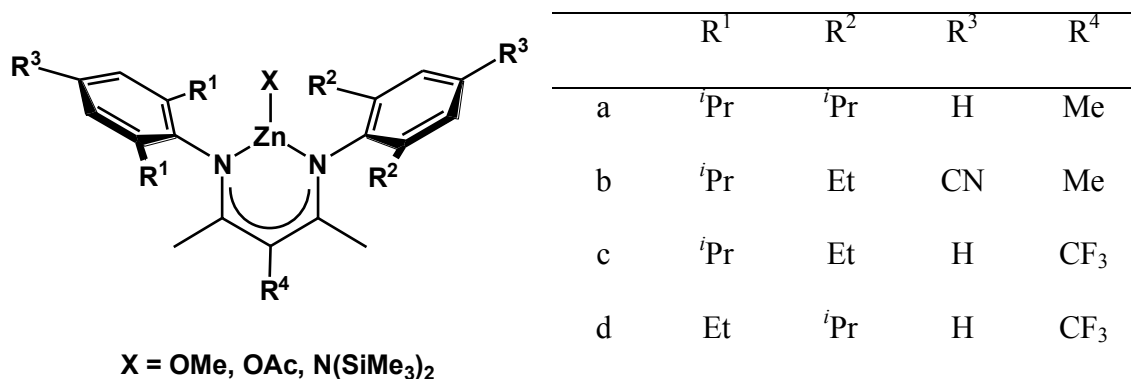


Figure 1.2. β -diiminate zinc complexes used for the copolymerization of CO₂/CHO.^[58]

In addition to zinc catalysts, aluminum catalysts also showed good activity towards copolymerization of CO₂/epoxides.^[59] A typical example is an aluminum Schiff base complex with tetraethylammonium acetate (Et₄NOAc) system (Figure 1.3).^[55] When the (Salen)AlMe–Et₄NOAc catalyst was mixed with CHO and CO₂ (80 °C, 51 bar) in CH₂Cl₂, the copolymerization of CO₂ and CHO gave a high polymer yield (96%) of polycyclohexene carbonate (PCHC) containing 94% carbonate linkages with M_n and M_w/M_n of 10,500 g/mol and 1.54, respectively in 24 h.

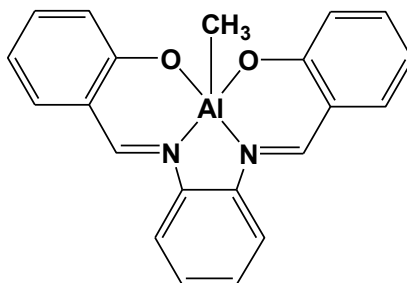


Figure 1.3. Aluminum Schiff base complex used for the copolymerization of CO₂ and CHO.^[55]

Transition-metal (especially Co and Cr) complexes are a very promising class of catalysts and have been intensively studied in recent years.^[43, 60] In the early study of cobalt catalysts, Coates and co-workers reported a cobalt salen complex (Figure 1.4) that provided over 99% selectivity for polypropylene carbonate (PPC) from CO₂ and propylene oxide (PO) with 99% carbonate linkages and TOF around 70 h⁻¹ at catalyst loadings of 0.2 to 0.5%.^[56]

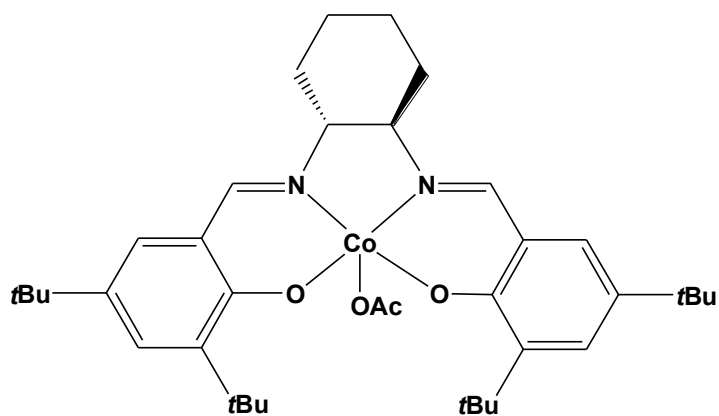


Figure 1.4. [Co(salcy)OAc] complex used for the copolymerization of CO₂ and propylene oxide.^[56]

The Williams research group reported three extremely active cobalt catalysts for the copolymerization of CO₂/CHO at just 1 bar pressure of carbon dioxide, with very high selectivity ($\geq 98\%$) for copolymerization and carbonate formation.^[61]

A series of highly active cobalt complexes possessing ligands tethering 4 quaternary ammonium salts was reported by Lee and co-workers.^[26, 62, 63] For instance, the salen-cobalt^{III} catalyst shown in Figure 1.5, not only showed high activity for CO₂/propylene oxide (PO) copolymerization (TOF = 22,000 h⁻¹),^[63] but also showed high activity (TOF = 25,900 h⁻¹) and high selectivity ($>98\%$) for CO₂/ethylene oxide (EO) copolymerization, resulting in polymers of high molecular weight ($M_n = 200,000\text{--}300,000$) with strictly alternating repeating units.^[26]

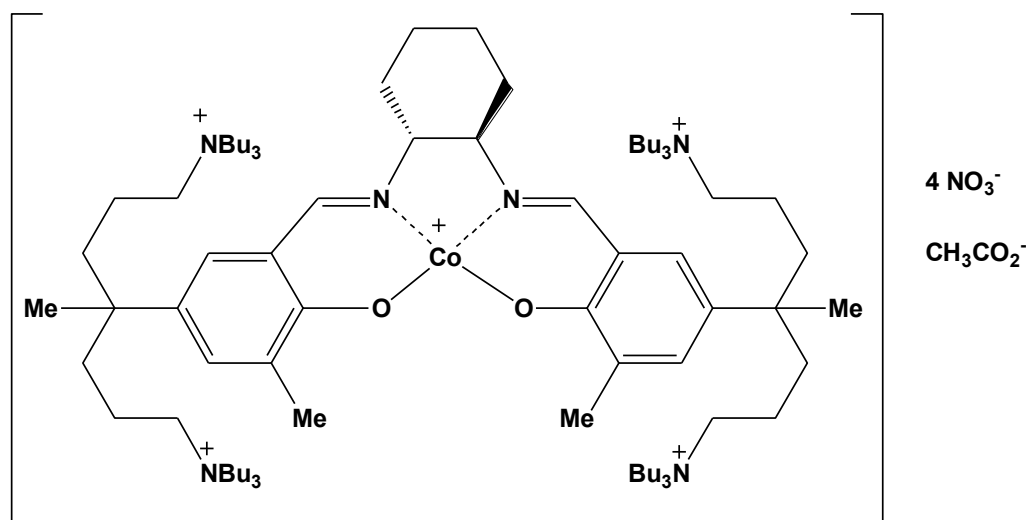


Figure 1.5. Highly active cobalt^{III} catalyst for CO₂/PO and CO₂/EO copolymerization.^[57]

The first example of using a chromium complex as a catalyst for CO₂/epoxide copolymerization came from the Holmes research group.^[64] A fluorinated chromium

porphyrin complex, tetra(pentafluorophenyl)porphyrin chromium^{III} chloride (CrTFPPCl), combined with (4-dimethylamino)pyridine (DMAP) co-catalyst was used to catalyze the copolymerization of 1,2-cyclohexene oxide (CHO) with carbon dioxide, showing a TOF exceeding 150 h⁻¹ for CHO (110 °C, 225 bar in supercritical CO₂, (scCO₂)).

After the introduction of Cr-porphyrin catalysts for the copolymerization of CO₂/epoxides, the Darensbourg research group investigated a wide variety of salen/salen-chromium catalyst with different ligand substitutions, initiating groups and co-catalysts over the past decade.^[60, 65, 66] Various (salen)CrX catalysts (Figure 1.6) with PCy₃ or PPN⁺ azide and chloride salts as co-catalysts, were found to be most effective at selectively producing poly(propylene carbonate) (PPC).^[67] When the chromium complex having R₃ = H and R₄ = *t*Bu was used in the copolymerization of CO₂/CHO, TOFs in the presence of 1 equiv. of co-catalyst were achieved in the range of 109-169 h⁻¹ at 60 °C, with selectivity for copolymer formation of 87-96%.^[67]

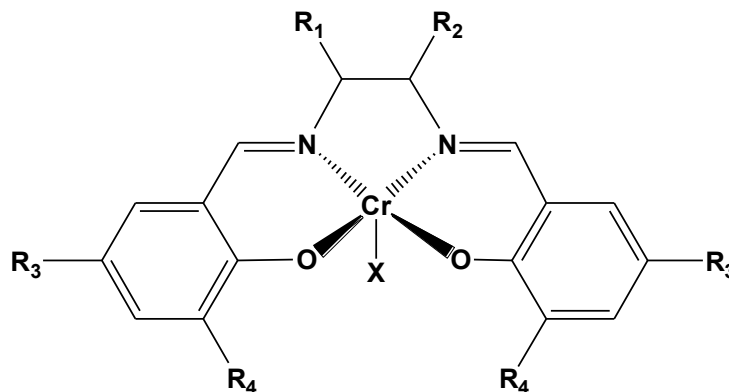


Figure 1.6. General structure of chromium^{III} salen catalyst used in the copolymerization of CO₂/epoxides.

A diamine-bis(phenolate) chromium^{III} catalyst, $\{\text{CrCl}[\text{O}_2\text{NN}']^{\text{t-Bu}}\}_2$, for copolymerization of CO_2 and epoxides was recently reported by the Kozak group.^[68, 69] In the presence of three co-catalysts (PPNCl, PPNN₃ or DMAP), the chromium catalyst shown in Figure 1.7 showed good activity towards the copolymerization of CO_2 and CHO/PO, producing polycarbonates with low dispersities. In the copolymerization of cyclohexene oxide and CO_2 , a turnover frequency of 219 h^{-1} was achieved by using this Cr catalyst and 1 equiv of DMAP as the co-catalyst at $80 \text{ }^\circ\text{C}$ and 24 bar CO_2 .^[68]

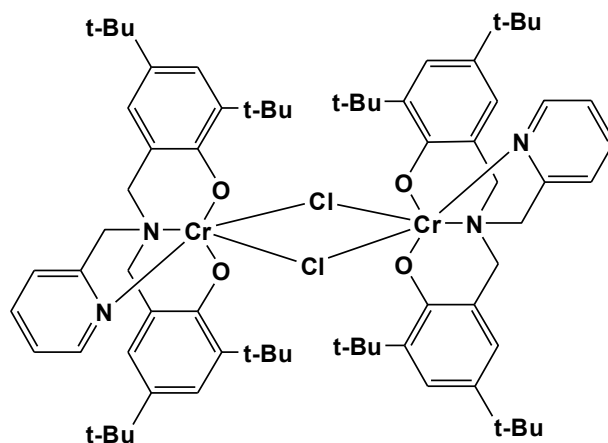


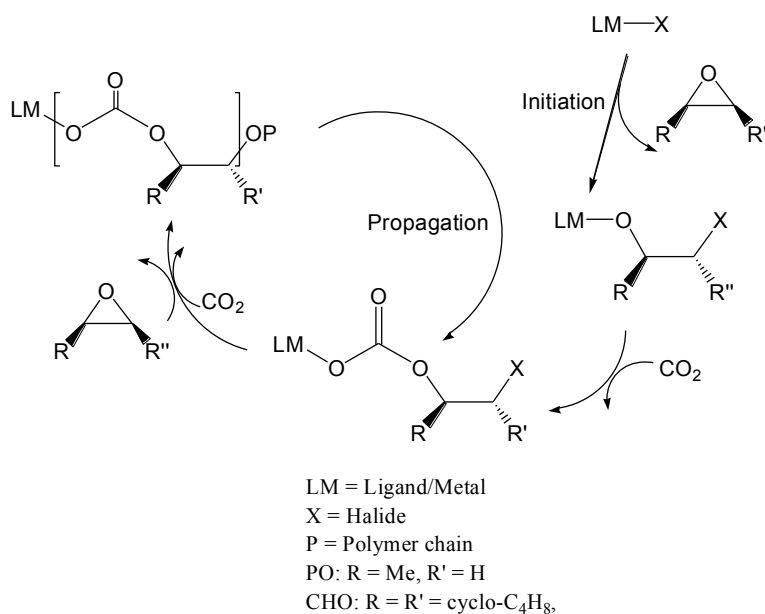
Figure 1.7. Diamine-bis(phenolate) chromium^{III} catalyst used in the copolymerization of CO_2 /epoxides.

The present study was undertaken to explore the potential of Cr^{III} amine-bis(phenolate) complexes for copolymerization of cyclohexene oxide and carbon dioxide. In Chapter 2, the synthesis and characterization of related Cr^{III} amine-bis(phenolate) complexes will be discussed. In Chapter 3, the use of these chromium complexes for the

copolymerization of cyclohexene oxide and carbon dioxide will be described. Also, Chapter 3 briefly summarizes the work described in this thesis and proposes new directions of investigation.

1.3.4 Mechanism of Polymerization

The general mechanism proposed for the formation of polycarbonates in CO₂/epoxide copolymerization was presented in Scheme 1.9. This coordination-insertion mechanism involves the insertion of CO₂ into a metal alkoxide bond, and then followed by the insertion of the epoxide into the resulting metal carbonate bond. Propagation continues with sequential additions of CO₂ and epoxides.



Scheme 1.9. Proposed mechanism of polycarbonates formation in the copolymerization of CO₂/epoxides.

Proposed mechanisms for CO₂/epoxide copolymerization by using chromium catalyst and different co-catalysts have been introduced detailedly in the literature.^[65, 69]

1.3.5 Polymer Characterization

GPC (Gel permeation chromatography) is the technique often used for polymer analysis. Most polymers are polydisperse which mean they contain more than one chain length. The average distribution of chain masses can be described in the weight average molecular weight (M_w), the number average molecular weight (M_n), the size average molecular weight (M_z), or the viscosity molecular weight (M_v).^[70] The dispersity of polymers, which is also known as PDI (polydispersity indices), can be calculated as the M_w divided by M_n . The M_n is the statistical average molecular weight of all the polymer chains in the sample, which is defined by “ $M_n = (\sum N_i M_i) / (\sum N_i)$ ” (where M_i is the molecular weight of a chain and N_i is the number of chains of that molecular weight.). Compared to M_n , M_w is defined by “ $M_w = (\sum N_i M_i^2) / (\sum N_i M_i)$ ”. PDI (polydispersity index) values indicate the breadth of the molecular weight distribution. Polymers that are monodisperse would have a PDI of 1.0. The PDI values approaching 1.0 for polymers should have very narrow molecular weight distributions, while the PDI values above 2.0 for polymers are usually considered having broad molecular weight distributions.^[70]

¹H NMR (nuclear magnetic resonance) is a useful method to determinate different characteristic peaks of polymers and also polymer conversion calculations from integration of the spectra.

MALDI-TOF MS (matrix assisted laser desorption/ionization time-of-flight mass spectroscopy) is an effective method to gain insight into experimental values of the number average molecular weights (M_n) of the copolymers and analysis of possible end-groups providing mechanistic details for the catalytic system.

The detailed characterization results of polymers will be described in Chapter 3, Section 3.3.

Chapter 2

Synthesis and Structure of Chromium^{III} Amine-bis(phenolate) Complexes

2.1 Introduction

As introduced in Chapter 1, metal salen complexes, especially Cr, Co, and Zn compounds have shown significant catalytic ability for a copolymerization of CO₂/epoxide in the literature. For chromium inorganic compounds, the most common oxidation states are +II, +III and +VI. The +II oxidation state can be strongly reducing, while the highest oxidation state of Cr^{VI} is found to be a very strong oxidant.^[1] For their prominent chemical and configurational stability, Cr^{III} coordination complexes became one of the most influential areas in the development of coordination chemistry.^[4] The electron configuration of mononuclear d³ octahedral Cr^{III} complexes arises from the large ligand field stabilization energy. Cr^{III} compounds are generally substitutionally inert and often the most stable oxidation state, making them easier to synthesize.^[1]

In the field of coordination chemistry, ligand design is crucial to control the reactivity of metal complexes. The amine-bis(phenolate) complexes offer new avenues for development of highly active catalysts.^[71] The modification of the central donor to a sp³-hybridized N atom results in non-planar geometries, and thus increases the flexibility of the ligand framework compared with salen ligands. Desired steric and electronic properties of these ligands may be obtained through modifications of the substituents on

the phenolate groups or pendant arms. This differs from salen and salan-based catalyst systems where only the phenolate groups are easily modified. Commonly, these amine-bis(phenolate) ligands can be easily synthesized in a one-pot Mannich condensation reaction.^[72]

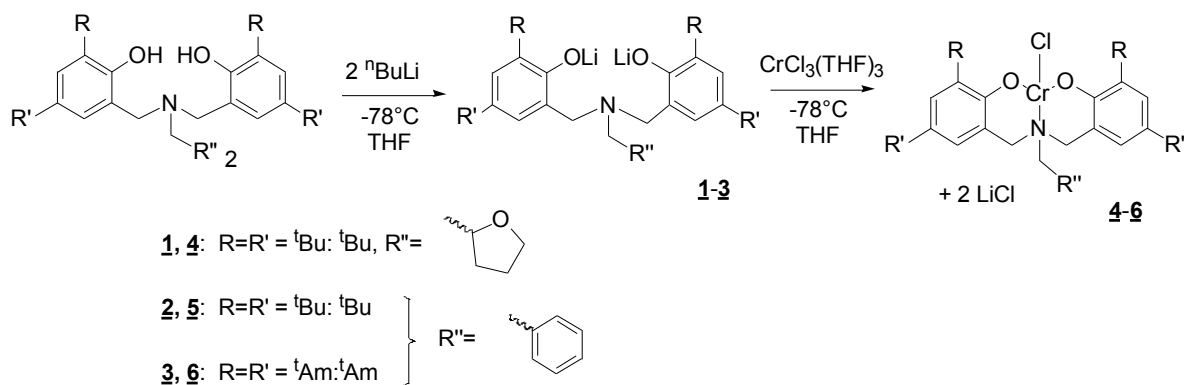
The first tetradentate tripodal amine bis(phenolate) ligand was introduced by Hinshaw in 1989.^[73] Amine-bis(phenolate) complexes are widely used as catalysts in reactions such as olefin polymerization and oxidation, where the metal centre acts as a Lewis acid. These complexes are also acted as bioinorganic model compounds. The group 4 amine-bis(phenolate) complexes used as olefin polymerization catalysts evolved from the need for alternatives to the well-studied and thoroughly patented group 4 metallocene catalysts.^[74, 75] In group 5, oxovanadium compounds are well-known precursors for catalyzed oxidations of organic substrates with peroxides.^[76] Another example was presented recently by Kozak and co-workers, in which iron^{III} amine-bis(phenolate) complexes were used to catalyze C–C cross-coupling of Grignard reagents with primary and secondary alkyl halides.^[77, 78] The copolymerization of epoxides and CO₂ is also an important reaction studied over the past years. In Chapter 3, reactions of cyclohexene oxide with CO₂ catalyzed by amine-bis(phenolate) Cr^{III} complexes will be described and discussed.

2.2 Synthesis of Chromium^{III} Amine-bis(phenolate) Complexes

The ligands 2-tetrahydrofurfuryl-*N,N*-bis(2-methylene-4,6-*tert*-butylphenol), H₂[O₂NO]^{BuBu} H₂[L1], benzylamino-*N,N*-bis(2-methylene-4,6-di-*tert*-butylphenol),

$\text{H}_2[\text{ONO}]^{\text{BuBuBn}} \text{H}_2[\mathbf{L2}]$, and benzylamino-*N,N*-bis(2-methylene-4,6-di-*tert*-amylphenol), $\text{H}_2[\text{ONO}]^{\text{tAm/AmBn}} \text{H}_2[\mathbf{L3}]$ were prepared according to previously reported procedures.^[31, 72, 79] The synthesis of the corresponding Li complexes involved stirring a mixture of $\text{H}_2[\mathbf{L1}]$, $\text{H}_2[\mathbf{L2}]$ or $\text{H}_2[\mathbf{L3}]$ and *n*-butyllithium under nitrogen for 2 h, giving $\{\text{Li}_2[\text{O}_2\text{NO}]^{\text{BuBu}}\}_2$ (**1**), $\{\text{Li}_2[\text{ONO}]^{\text{BuBuBn}}\}_2$ (**2**), $\{\text{Li}_2[\text{ONO}]^{\text{tAm/AmBn}}\}_2$ (**3**) as beige powders as previously described (Scheme 2.1).^[80]

Complex **4**, $\text{CrCl}[\text{O}_2\text{NO}]^{\text{BuBu}}$, was synthesized via a previously reported method where it was characterized by MALDI-TOF, UV-Vis and X-ray crystallography.^[81] Complex **5** ($\text{CrCl}[\text{ONO}]^{\text{BuBuBn}}$) and **6** ($\text{CrCl}[\text{ONO}]^{\text{tAm/AmBn}}$) are novel and were synthesized via similar methods (Scheme 2.1). The synthesis involved stirring a cooled mixture of $\text{H}_2[\mathbf{L2}]$ or $\text{H}_2[\mathbf{L3}]$ and *n*-butyllithium in THF under nitrogen for 2 h followed by transferring the resulting solution into a cooled suspension of $\text{CrCl}_3(\text{THF})_3$ in THF and then stirring for 18 h at room temperature. In the presence of ligands $\text{H}_2[\mathbf{L2}]$ and $\text{H}_2[\mathbf{L3}]$, green powders were obtained, giving **5** and **6**. Purification of crude **5** and **6** by recrystallization from toluene produced green, crystalline material that was characterized by mass spectrometry, UV-visible spectroscopy and elemental analysis. Complex **5** was also characterized by single crystal X-ray diffraction.



Scheme 2.1. Synthetic routes to Cr^{III} complexes.

2.3 Characterization of Chromium^{III} Amine-bis(phenolate) Complexes

2.3.1 MALDI-TOF MS

Using NMR to characterize Cr^{III} complexes is relatively difficult due to their paramagnetic properties. MALDI-TOF MS, on the other hand, is a simple and fast method that can be used to characterize coordination complexes regardless of whether they are paramagnetic or diamagnetic.

The phenolate groups of amine-bis(phenolate) ligands may absorb the laser energy, and this leads to ionization of samples.^[82] For the Cr complexes described here, a simple aromatic matrix such as anthracene was required to get spectra with good signal-to-noise ratios. The mass spectra of the Cr^{III} complexes could be interpreted through the m/z ratio and isotope patterns of the peaks. The mass spectra obtained from the prepared sample mixtures show series of peaks consistent with the expected products.

The spectrum of complex **5** shows peaks at m/z 628.28 corresponding to the $[\text{CrCl}[\text{ONO}]^{\text{BuBuBn}}]^+$ ion, as shown in Figure 2.1. Ligand fragment ion peaks are shown at m/z 538.15 and the fragment ion corresponding to the loss of the chloride, $[\text{Cr}[\text{ONO}]^{\text{BuBuBn}}]^+$ occurred at m/z 593.33 (Figure 2.1). As shown in Figure 2.2, the isotopic distribution pattern of the experimental $[\text{CrCl}[\text{ONO}]^{\text{BuBuBn}}]^+$ is in agreement with the theory for **5**, providing strong evidence for the observed molecular structure. In addition to peaks corresponding to monomeric complexes peaks at higher masses were observed at m/z 1221.6 suggesting the presence of bimetallic fragments corresponding to $\{[\text{Cr}[\text{ONO}]^{\text{BuBuBn}}]\}_2\text{Cl}^+$ (Figure 2.3). Crystallographic evidence supporting the existence of bimetallic species will be discussed in Section 2.3.3.

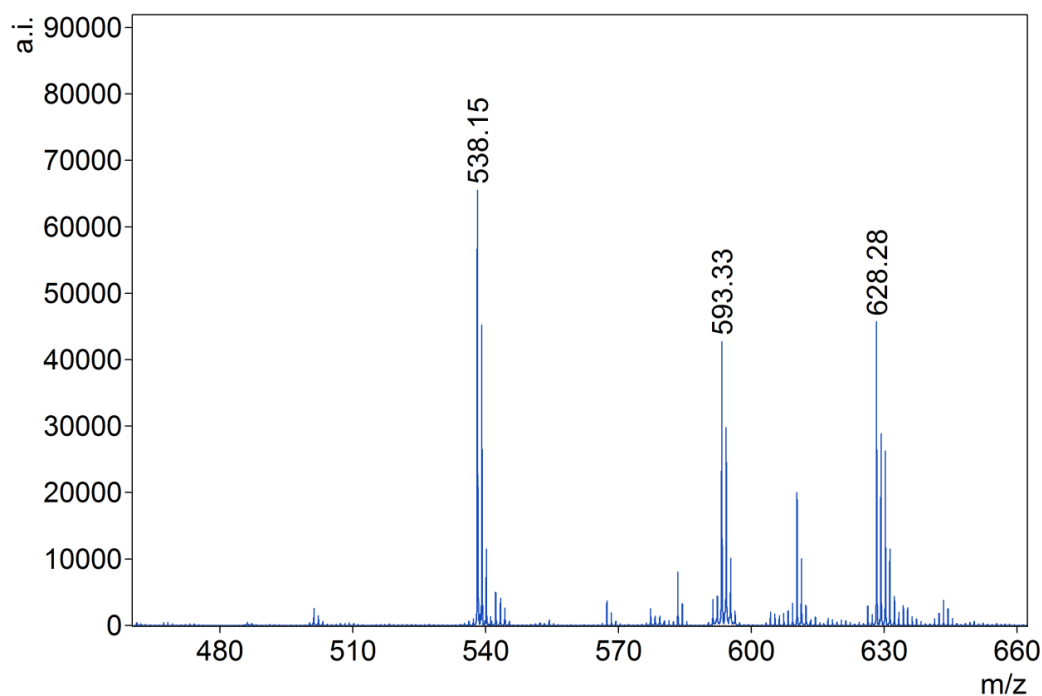


Figure 2.1. MALDI-TOF mass spectrum (lower mass region) of $\text{CrCl}[\text{ONO}]^{\text{BuBuBn}}$ (**5**).

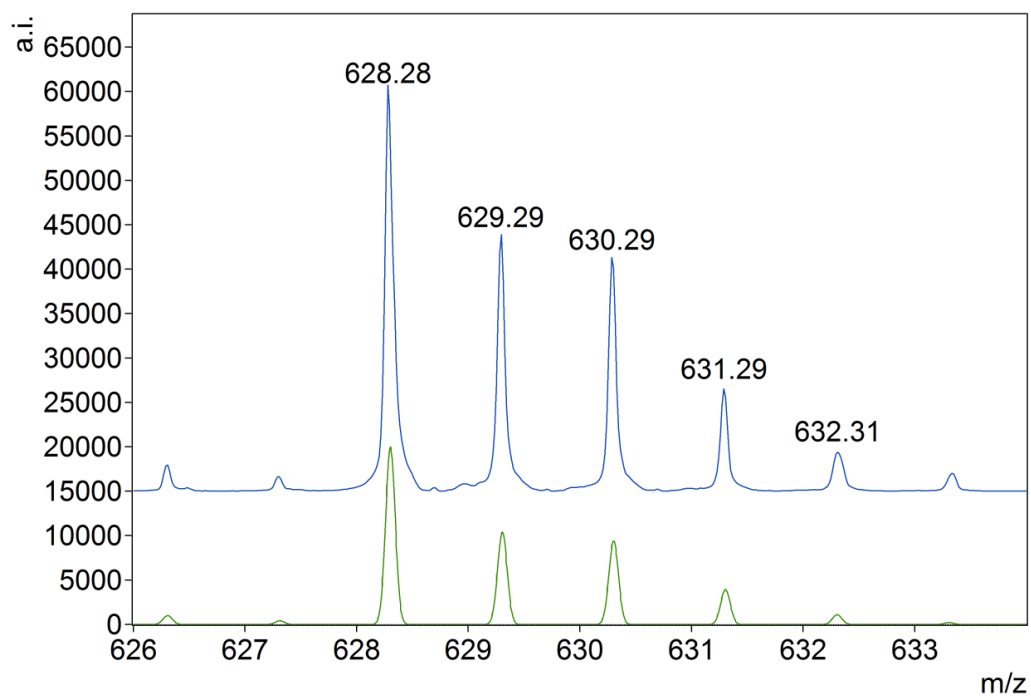


Figure 2.2. Experimental (top blue) and theoretical (bottom, green) MALDI-TOF isotopic distribution pattern for the $[M]^+$ peak of **5**.

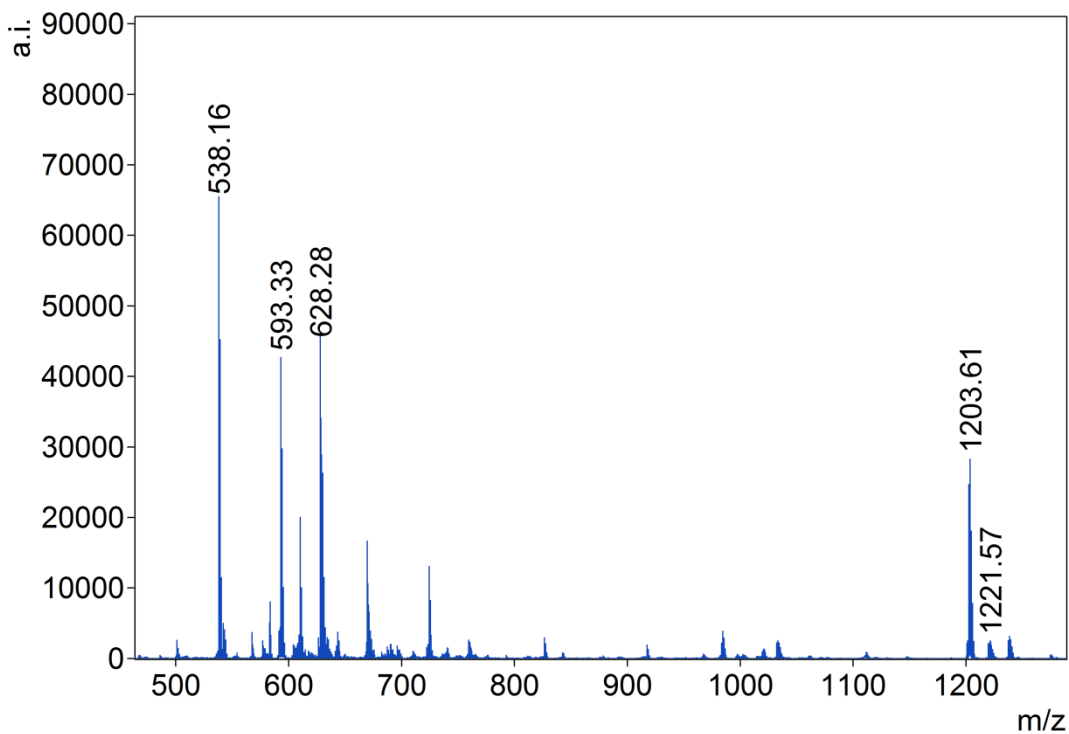


Figure 2.3. MALDI-TOF mass spectrum of (5) showing the higher mass region.

Similarly, compound **6** shows the loss of the chloride ion from the parent ion at m/z 649.31 in the mass spectrum (Figure 2.4). The intense peak for **6** at m/z of 684.27 corresponds to $[\text{CrCl}[\text{ONO}]^{\text{tAmzAmBn}}]^+$. Good matches of the theoretical and experimental isotope patterns of **6** are shown in Figure 2.5. In addition to these peaks, evidence of bimetallic fragments in **6** also exists, e.g. $[\{[\text{Cr}[\text{ONO}]^{\text{tAmzAmBn}}]\}_2\text{Cl}]^+$ at m/z 1333.50 (Figure 2.6).

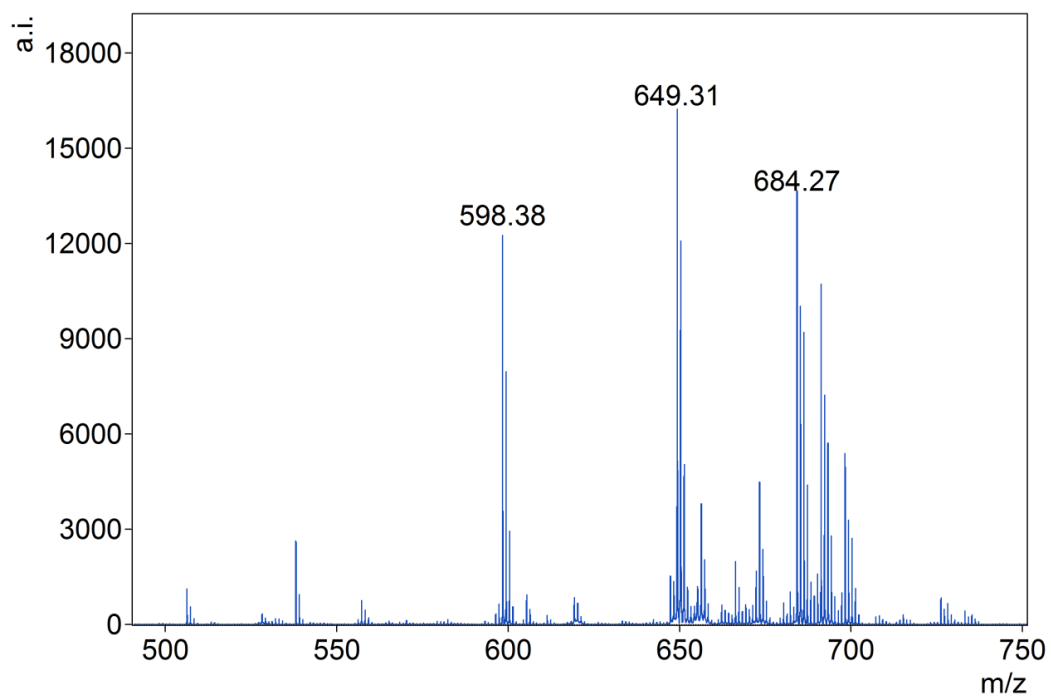


Figure 2.4. MALDI-TOF mass spectrum (lower mass region) of $\text{CrCl}[\text{ONO}]^{\text{tAmAmBenzyl}}$

(6).

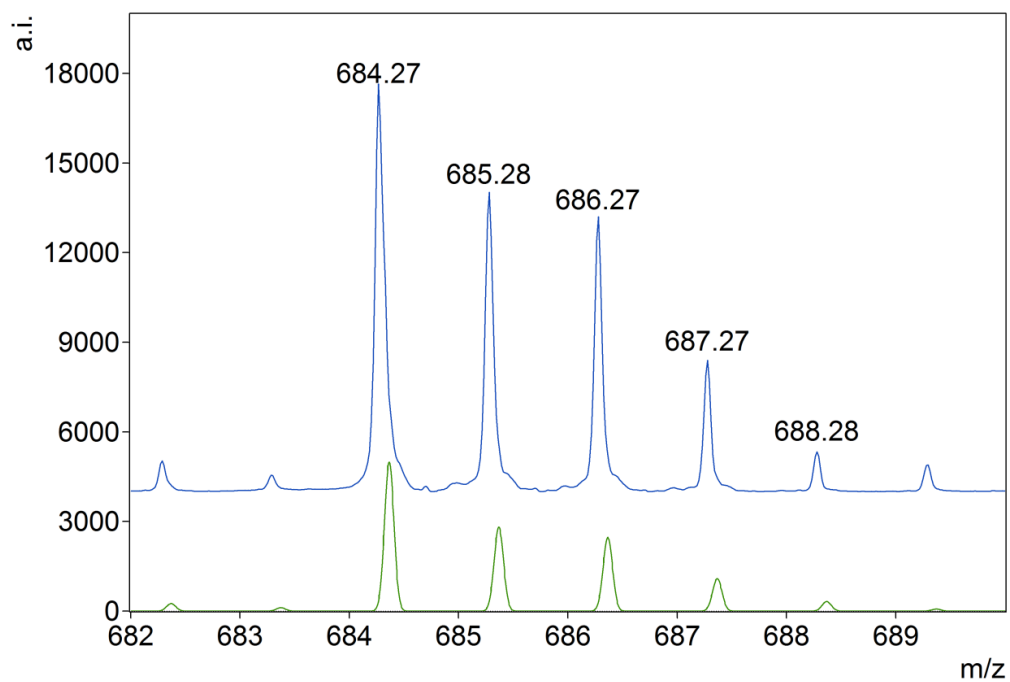


Figure 2.5. Experimental (top, blue) and theoretical (bottom, green) MALDI-TOF isotopic distribution pattern for the molecular ion of the $[M]^+$ peak of **6**.

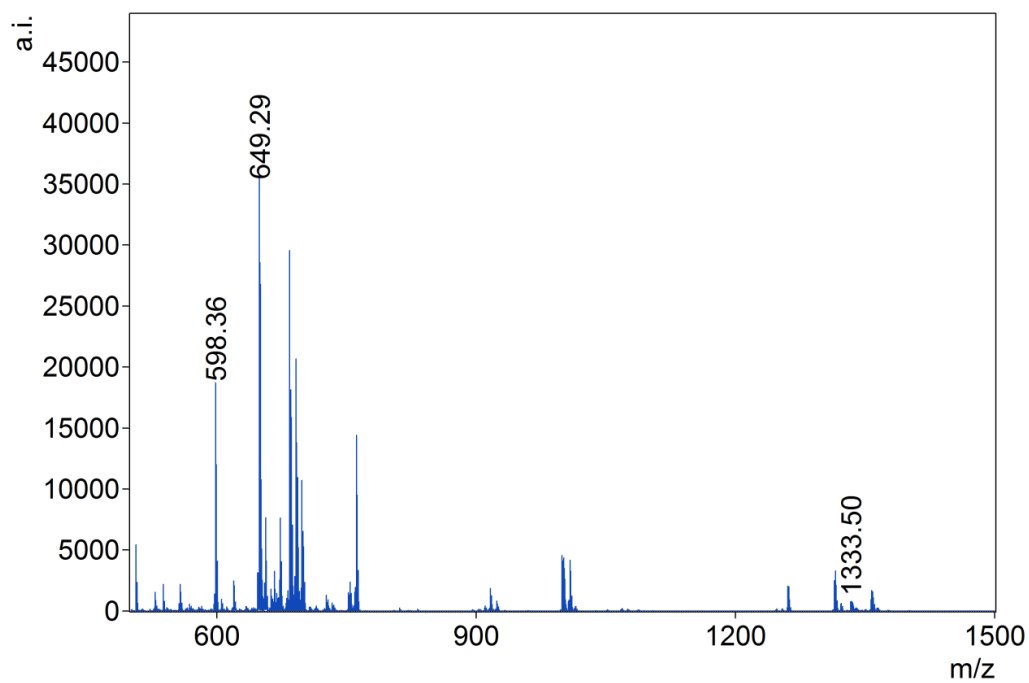


Figure 2.6. MALDI-TOF mass spectrum of (**6**) showing the higher mass region.

2.3.2 UV-Visible Spectroscopy

Electronic absorption spectra of complexes **5** and **6** show multiple bands in the UV and visible regions. In this study, dichloromethane solutions at concentrations of 1×10^{-4} mol L⁻¹ were employed and the spectra are shown in Figures 2.7 and 2.8. The absorption maxima observed in the UV region (below 300 nm) are caused by $\pi \rightarrow \pi^*$ transitions involving the phenolate units. High energy bands are also observed in the region between 300 and 400 nm, which were assigned to charge transfer transitions from the p_{π} orbital (HOMO) of the phenolate oxygen to the empty $d_{x^2-y^2}/d_{z^2}$ and the half-filled d_{π} , orbitals of Cr^{III}. Weaker bands arising from d-d transitions were observed at 560 and 720 nm.

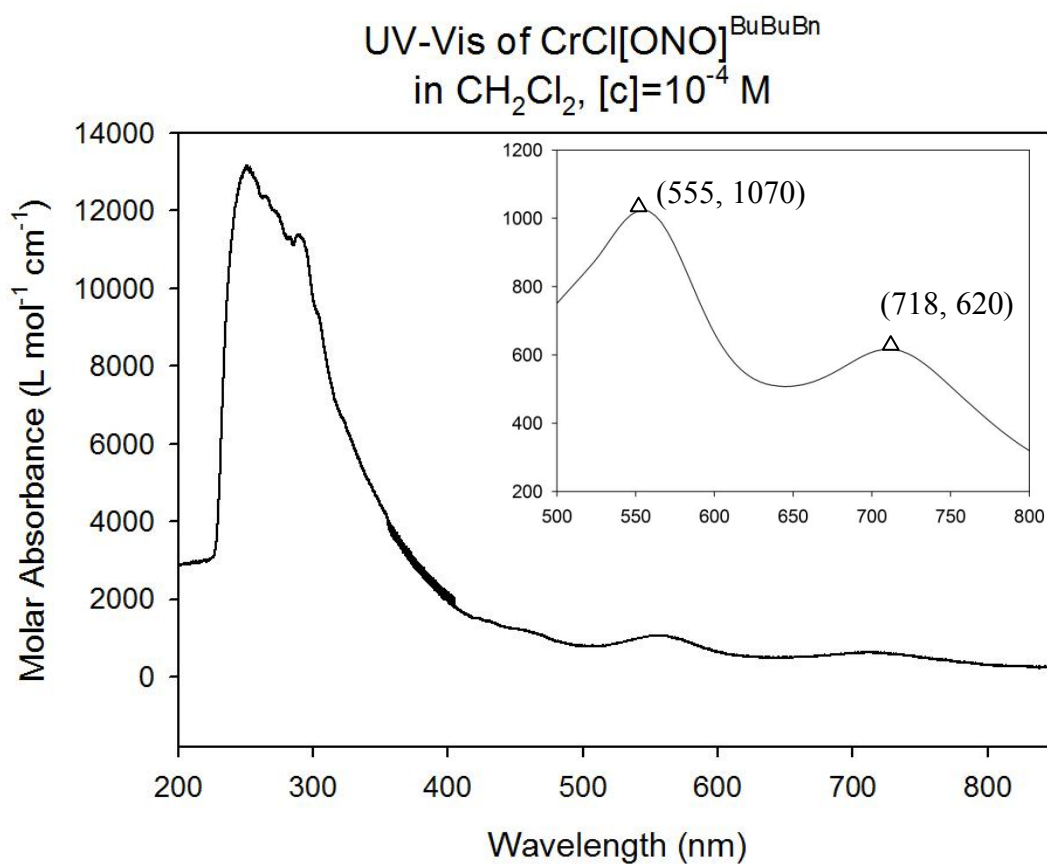


Figure 2.7. UV-Vis absorption spectrum of **5** in CH_2Cl_2 . Inset: Expansion of visible region showing peak wavelength and molar extinction coefficients, and wavelength of two maximum absorptions in region 500-800 nm are assigned.

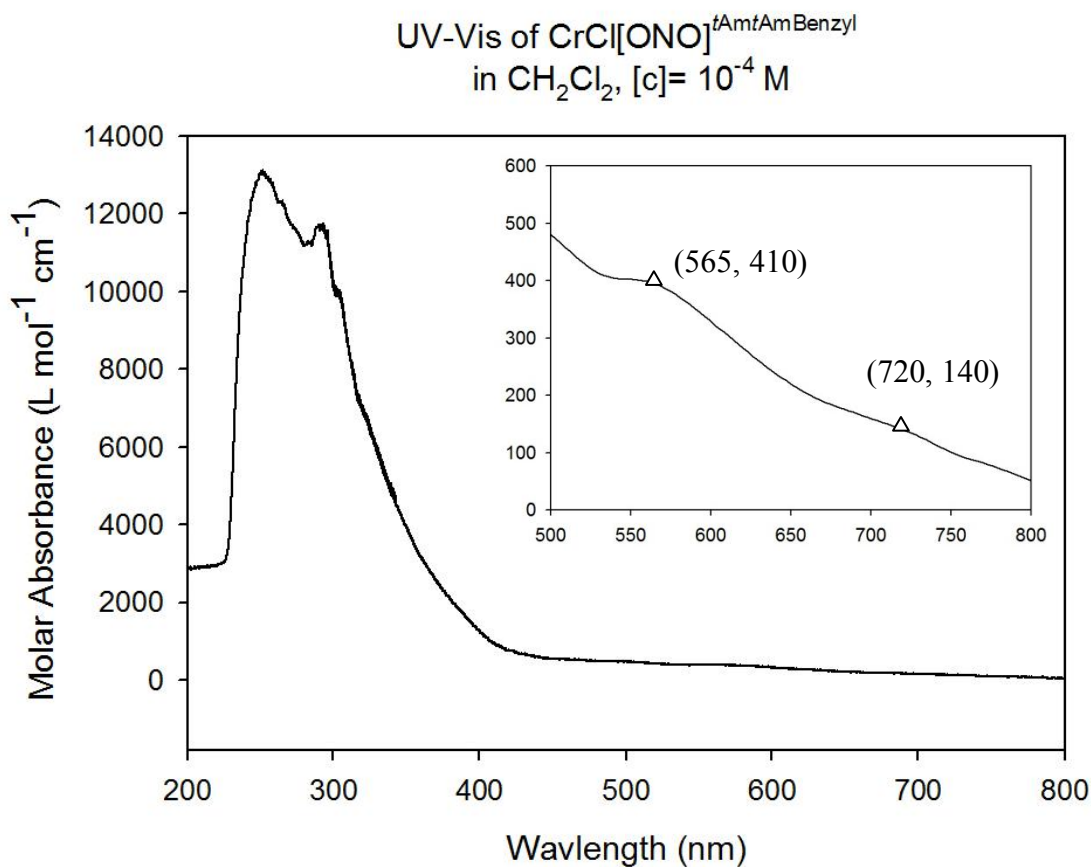


Figure 2.8. UV-Vis absorption spectrum of **6** in CH_2Cl_2 . Inset: Expansion of visible region showing peak wavelength and molar extinction coefficients, and wavelength of two maximum absorptions in region 500-800 nm are assigned.

2.3.3 Single Crystal X-ray Diffraction

Single crystals of an adduct of **5** suitable for X-ray diffraction analysis were isolated by slow evaporation of a toluene solution of **5** under a N_2 atmosphere in a glove box. The resulting structure is shown in Figure 2.9 and selected bond distances and angles are listed in Table 2.1. Crystallographic and structure refinement data are given in the

Appendix. It is immediately obvious that an adduct has formed possessing the formula $(\mathbf{5})_2 \cdot \text{LiCl} \cdot \text{THF}$.

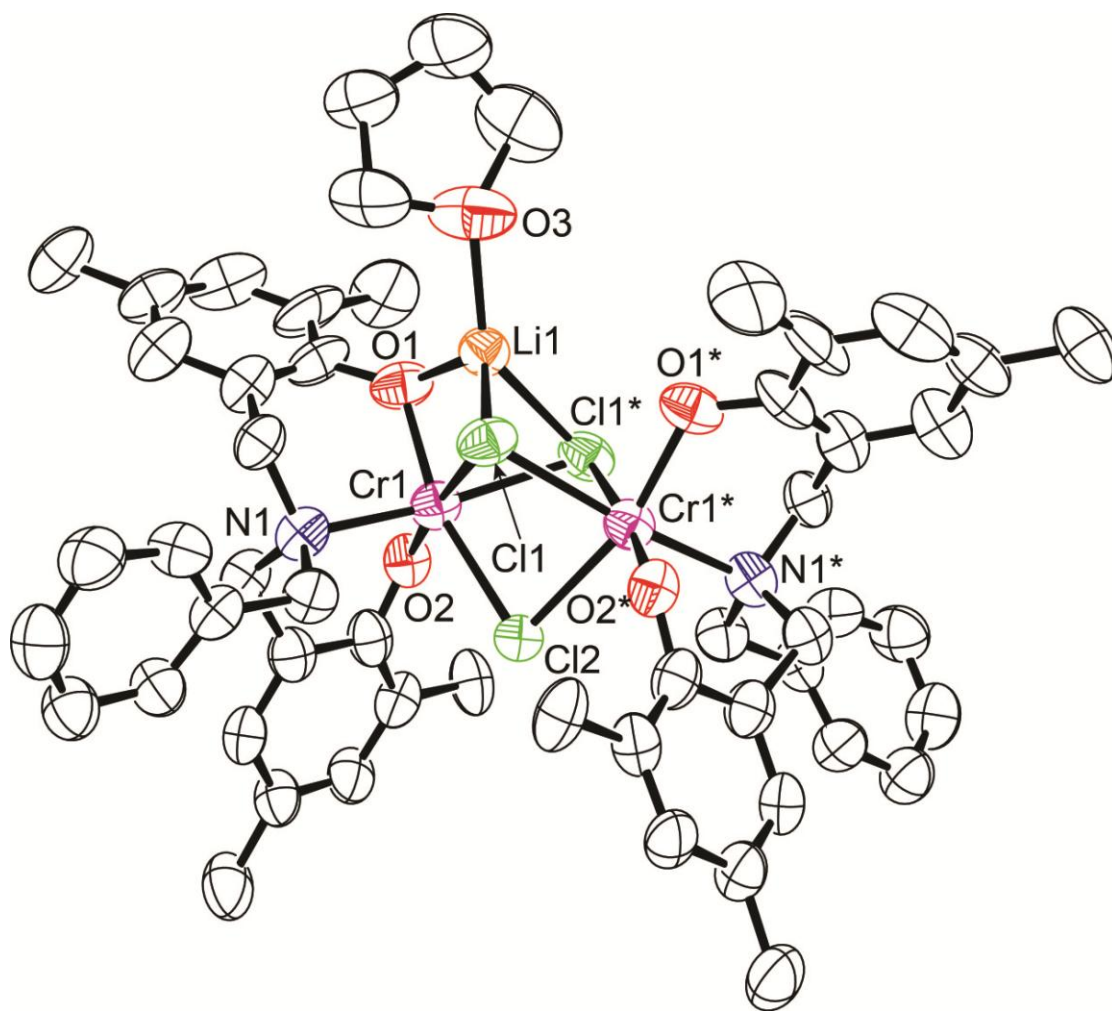


Figure 2.9. Molecular structure (ORTEP) and partially labelled numbering scheme of $(\mathbf{5})_2 \cdot \text{LiCl} \cdot \text{THF}$. Ellipsoids are shown at 50% probability. Hydrogen atoms and methyl groups on phenolate t-butyl groups are omitted for clarity. Symmetry operations used to generate equivalent atoms (*): $-x+2, -x+y+1, -z+1/3$.

The complex was obtained as a dark green crystalline solid. The structure was elucidated by X-ray diffraction, showing the dinuclear complex containing two trivalent chromium atoms with face sharing octahedral geometries. The bridging interaction between the two metal centers is composed of three chlorine atoms. One partially solvated lithium cation forms part of the trimetallic cluster structure and is bridged to the two transition metals by one oxygen and two chlorine atoms.

Many related Cl-bridged Cr complexes have been reported in the literature.^[68, 69, 83-87] One closely related example is shown in Figure 2.10.^[84] This complex possesses N-donor ligands having a narrow bite angle and an anionic charge, formulated as $[(t\text{-Bu})\text{NP}(\text{Ph})_2\text{N}(t\text{-Bu})]$. This bimetallic complex contains face-sharing octahedra, similar to what is observed in $(\mathbf{5})_2 \cdot \text{LiCl} \cdot \text{THF}$ having three bridging Cl^- ions. The bond distances of $\text{Cr}-\text{Cl}_{\text{bridge}}$ (2.425(3) Å and 2.386(2) Å) in $(\mathbf{5})_2 \cdot \text{LiCl} \cdot \text{THF}$ are slightly shorter than those in the previously reported complex, $\{[(t\text{-Bu})\text{NP}(\text{Ph})_2\text{N}(t\text{-Bu})]\text{Cr}\}_2(\mu_2\text{-Cl})_3(\mu_3\text{-Cl})_2\{\text{Li}(\text{THF})_2\}$, where distances of 2.435(3) Å and 2.439(3) Å were reported. The bond angles of $\text{Cr}-\text{Cl}-\text{Cr}$ ($81.08(8)^\circ$ and $82.98(10)^\circ$) in $(\mathbf{5})_2 \cdot \text{LiCl} \cdot \text{THF}$ are slightly smaller than those of the previously reported complex shown in Figure 2.10 ($83.73(10)^\circ$ and $83.00(9)^\circ$). Clearly, the presence of different ancillary ligands (tridentate amine-bis(phenolate) ligand compared to bidentate diamido phosphonium ligands) and their different bite angles will affect the metric parameters of the remaining Cr-to-ligand bonds.

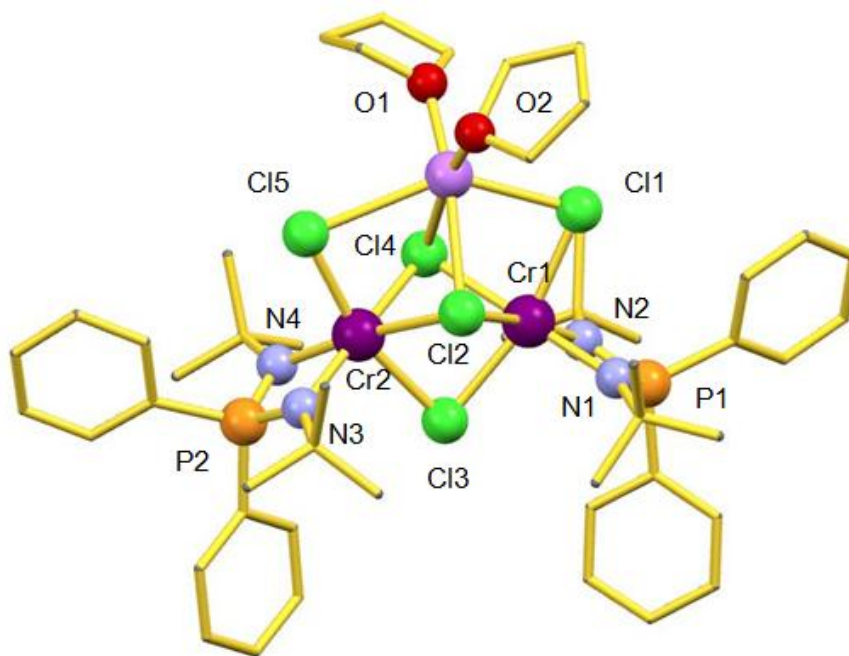


Figure 2.10. Structure of $\{[(t\text{-Bu})\text{NP}(\text{Ph})_2\text{N}(t\text{-Bu})]\text{Cr}\}_2(\mu_2\text{-Cl})_3(\mu_3\text{-Cl})_2\{\text{Li}(\text{THF})_2\}$ containing bridging Cl ions and face-sharing octahedra.^[84]

A related complex possessing a tetradentate amine-bis(phenolate) ligand was reported by the Kozak group.^[68] The complex, abbreviated $\{\text{CrCl}[\text{O}_2\text{NN}']^{\text{BuBu}}\}_2$, contains two bridging Cl⁻ ions resulting in a pair of edge sharing octahedral and showed metric parameters similar to those found in $(\mathbf{5})_2\cdot\text{LiCl}\cdot\text{THF}$. Due to the similar backbones of these two complexes, some of bond angles and lengths are compared. Bond lengths for the Cr-Cl bridge of 2.4050(8) Å and 2.4431(8) Å in $\{\text{CrCl}[\text{O}_2\text{NN}']^{\text{BuBu}}\}_2$ are on average longer than those in $(\mathbf{5})_2\cdot\text{LiCl}\cdot\text{THF}$ (2.425(3) and 2.386(2) Å), and Cr-Cl-Cr bond angles of 84.34(3)° and 95.66(3)° observed in $\{\text{CrCl}[\text{O}_2\text{NN}']^{\text{BuBu}}\}_2$ are larger than those in $(\mathbf{5})_2\cdot\text{LiCl}\cdot\text{THF}$ (81.08(8)° and 82.98(10)°). The Cr-O bond distances (1.870(5) Å and

1.921(6) Å) in $(\mathbf{5})_2 \cdot \text{LiCl} \cdot \text{THF}$ are much more asymmetric than those in $\{\text{CrCl}[\text{O}_2\text{NN}'^{\text{BuBu}}]\}_2$ (1.9050(18) Å and 1.9110(18) Å); whereas the Cr-N bond distance (2.108(7) Å) in $(\mathbf{5})_2 \cdot \text{LiCl} \cdot \text{THF}$ is slightly longer than the corresponding Cr-N distance in $\{\text{CrCl}[\text{O}_2\text{NN}'^{\text{BuBu}}]\}_2$ (2.080(2) Å). One of the O(2)-Cr(1)-N(1) bond angle in $(\mathbf{5})_2 \cdot \text{LiCl} \cdot \text{THF}$ ($91.3(3)^\circ$) is experimentally identical to the angle ($91.15(8)^\circ$) in the $\{\text{CrCl}[\text{O}_2\text{NN}'^{\text{BuBu}}]\}_2$, but the other O(1)-Cr(1)-N(1) bond angle is slightly larger than that of $\{\text{CrCl}[\text{O}_2\text{NN}'^{\text{BuBu}}]\}_2$. The O-Cr-O bond angle ($95.7(3)^\circ$) is slightly larger than that of the $\{\text{CrCl}[\text{O}_2\text{NN}'^{\text{BuBu}}]\}_2$ ($93.33(8)^\circ$). From the comparison between the crystal structures of $(\mathbf{5})_2 \cdot \text{LiCl} \cdot \text{THF}$ and $\{\text{CrCl}[\text{O}_2\text{NN}'^{\text{BuBu}}]\}_2$, the benzyl and pyridyl groups of these two complexes only moderately influence the bond lengths and angles around the chromium atoms.

Table 2.1. Selected bond lengths (Å) and angles (°) for (5)₂·LiCl·THF.

Bond Length (Å)			
Cr(1)-O(2)	1.870(5)	Cr(1)-Cl(1)	2.425(3)
Cr(1)-O(1)	1.921(6)	Cr(1)-Cl(2)	2.386(2)
Cr(1)-N(1)	2.108(7)		
Bond Angles (°)			
O(2)-Cr(1)-N(1)	91.3(3)	Cl(2)-Cr(1)-Cl(1)	82.25(7)
O(1)-Cr(1)-N(1)	92.6(3)	O(2)-Cr(1)-Cl(1)	174.19(19)
O(1)-Cr(1)-Cl(2)	164.4(2)	O(1)-Cr(1)-Cl(1)	89.5(2)
N(1)-Cr(1)-Cl(2)	100.5(2)	N(1)-Cr(1)-Cl(1)	91.2(2)
O(2)-Cr(1)-Cl(1)	96.59(19)	Cl(2)-Cr(1)-Cl(1)	81.98(7)
O(2)-Cr(1)-O(1)	95.7(3)	Cl(1)-Cr(1)-Cl(1)	81.26(11)
O(1)-Cr(1)-Cl(1)	83.6(2)	Cr(1)-Cl(1)-Cr(1)	81.08(8)
N(1)-Cr(1)-Cl(1)	171.5(2)	Cr(1)-Cl(2)-Cr(1*)	82.98(10)
		O(1)-Cr(1)-Cl(1)	89.5(2)

2.4 Experimental

2.4.1 General Experimental Conditions

All manipulations were performed under an atmosphere of dry oxygen-free nitrogen by using standard Schlenk techniques or an MBraun Labmaster glove box, unless otherwise stated. Reagents were purchased either from Aldrich or Alfa Aesar and used

without further purification. $\text{CrCl}_3(\text{THF})_3$ was prepared by the standard method.^[6] Anhydrous THF was distilled from sodium benzophenone ketyl and stored under nitrogen. Toluene was purified by an MBraun Manual Solvent Purification System and stored under nitrogen. *n*-Butyllithium was purchased as a 1.6 M solution in hexanes and stored under nitrogen. Anthracene was recrystallized, dried under vacuum 18 h and stored in the glove box.

MALDI-TOF Mass Spectrometry was performed by using an Applied Biosystems 4800 MALDI TOF/TOF Analyzer equipped with a reflectron, delayed ion extraction and high performance nitrogen laser. Anthracene was used as the matrix. The matrix and chromium complex were dissolved in toluene at a concentration of 20 mg/mL separately. The matrix and chromium complex solutions were mixed together in a ratio of 1:1, and the mixture was spotted on the MALDI plate and left to dry. Samples were prepared in the glove box and sealed under nitrogen in a Ziploc bag for transport to the spectrometer. UV-Vis spectra were obtained on an Ocean Optics USB4000+ fiber optic spectrophotometer. Elemental analyses were performed at Guelph Chemical Laboratories, Guelph, ON, Canada.

2.4.2 Synthesis of Cr^{III} Complexes



$\text{H}_2[\text{ONO}]^{\text{BuBuBn}}$ (4.89 g, 9.00 mmol) was dissolved in THF (50 mL) and cooled to $-78\text{ }^\circ\text{C}$. *n*-Butyllithium (12.37 mL, 19.79 mmol) was slowly added to give a clear red solution, which was warmed to room temperature and further stirred for 2 h. This solution

was transferred via cannula to a suspension of $\text{CrCl}_3(\text{THF})_3$ (3.37 g, 9.00 mmol) in THF (50 mL) cooled to $-78\text{ }^\circ\text{C}$ to give a dark green mixture. Upon warming to room temperature and stirring for 18 h the solids dissolved giving a dark green solution. The solvent was removed *in vacuo* and the solid residue was extracted into toluene. The mixture was filtered through Celite and the solvent was removed under vacuum. The product was washed with pentane and dried to yield 6.01 g of dark green powder. Elemental analysis is unable to unequivocally differentiate between the THF-free or the solvent-containing complex.

$$\text{Yield} = 95.4\% \{ \text{CrCl}[\text{ONO}]^{\text{BuBuBn}} \cdot (\text{THF}) \}$$

Anal. Calcd for $\text{C}_{37}\text{H}_{51}\text{ClCrNO}_2$: C, 70.62; H, 8.17; N, 2.23. Anal. Calcd for $\text{C}_{37}\text{H}_{51}\text{ClCrNO}_2 \cdot (\text{C}_4\text{H}_8\text{O})$: C, 70.21; H, 8.48; N, 2.00. Found: C, 70.57; H, 8.33; N, 1.96. MS (MALDI-TOF) m/z (% ion): 628.4 (100, $[\text{CrCl}[\text{L}]^+]$), 593.4 (95, $[\text{Cr}[\text{L}]^+]$). UV-Vis (CH_2Cl_2) λ_{max} , nm (ϵ): 251 (13160).



$\text{H}_2[\text{ONO}]^{\text{tAmzAmBn}}$ (4.06 g, 6.77 mmol) was dissolved in THF (50 mL) and the solution was cooled to $-78\text{ }^\circ\text{C}$. *n*-Butyllithium (9.31 mL, 14.90 mmol) was slowly added to give a bright red solution of $\text{Li}_2[\text{ONO}]^{\text{tAmzAmBn}}$, which was warmed to room temperature and further stirred for 2 h. This mixture was transferred via cannula to a suspension of $\text{CrCl}_3(\text{THF})_3$ (2.54 g, 6.77 mmol) in THF (50 mL) cooled to $-78\text{ }^\circ\text{C}$ to give a dark green mixture. Upon warming to room temperature and stirring for 18 h the solids dissolved giving a dark green solution. The solvent was removed *in vacuo* and the residue was extracted into toluene. The mixture was filtered through Celite and the solvent was

removed under vacuum. The product was washed with pentane and dried to yield 4.57 g of dark green powder. Elemental analysis is unable to unequivocally differentiate between the THF-free or the solvent-containing complex.

$$\text{Yield} = 98.6\% \{ \text{CrCl}[\text{ONO}]^{t\text{Am}t\text{AmBn}} \cdot (\text{THF}) \}$$

Anal. Calcd for $\text{C}_{41}\text{H}_{59}\text{ClCrNO}_2$: C, 71.85; H, 8.68; N, 2.04. Anal. Calcd for $\text{C}_{41}\text{H}_{59}\text{ClCrNO}_2 \cdot (\text{C}_4\text{H}_8\text{O})$: C, 71.35; H, 8.92; N, 1.85. Found: C, 71.61; H, 8.45; N, 1.90. MS (MALDI-TOF) m/z (% ion): 628.4 (83, $[\text{CrCl}[\text{L}]^+]$), 593.4 (100, $[\text{Cr}[\text{L}]^+]$). UV-Vis (CH_2Cl_2) λ_{max} , nm (ϵ): 250 (13060).

2.5 Conclusions

Three amine-bis(phenolate) chromium complexes were synthesized and characterized. All of these three complexes were made via salt metathesis. Since complex **4** has already been reported in the literature, no other characterization is reported here. The other two complexes were fully characterized by several methods, including solid state single crystal X-ray diffraction for complex **5**. The magnetic behaviour of Cr^{III} compounds previously reported by Kozak's group shows them to be spin-isolated d^3 centres as expected, hence not particularly interesting for further magnetic study.^[68, 81] Interestingly, **5** was obtained in the solid state as a dichromium lithium chloride adduct complex. Attempts were made to obtain crystals of the product of mixing our chromium compounds with co-catalysts, but none were obtained. The following chapter will describe the utilization of these three Cr complexes synthesized for the copolymerization of cyclohexene oxide with carbon dioxide.

Chapter 3

Chromium Amine-bis(phenolate) Complexes for the Copolymerization of Cyclohexene oxide and Carbon Dioxide

3.1 Introduction

The copolymerization of epoxides and carbon dioxide to yield polycarbonates has gained great interest as a process for generating potentially valuable materials from renewable starting materials as described in Chapter 1. Carbon dioxide is appealing as a C1 feedstock,^[49] due to its widespread availability, low cost, and nontoxicity. Also many homogeneous catalysts have been examined for use in the copolymerization of CO₂ and epoxides.^[43, 53, 54, 88-94] However, the high thermodynamic stability of CO₂ requires highly active catalyst and judicious ligand design. Clues for suitable ligands capable of forming active catalysts for CO₂/epoxide copolymerization may be obtained from complexes used for polymerization reactions.

Notably, remarkable achievements in cyclic ester ring-opening polymerization catalysis have been made with metal complexes of various tetradentate ligands, such as [ONOX] (X = OR, NR₂)^[95] and [ONNO].^[96, 97] The [ONNO] ligands may be branched at the central nitrogen (giving a tripodal diamine bis(phenolate) ligand) or linear as in the salen, salan or salalen ligands (see Figure 1.1). However, the tridentate variations, particularly ONO lacking an extra N-tethered donor, are not well explored.^[96, 98-100]

Tetradentate ligand-containing catalyst **4** (see scheme 2.1) was first synthesized and characterized by Rebecca Dean in the Kozak group, but its catalytic activity was not explored.^[81] The activity of catalyst **4** in the copolymerization of CHO and CO₂ will be described in this chapter.

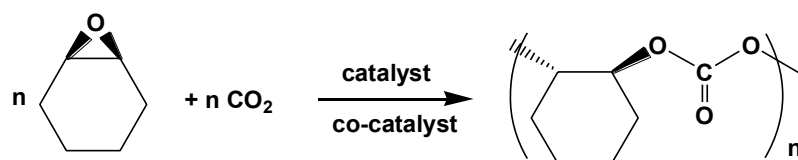
It was deemed worthwhile to extend this study to tridentate amine bis(phenolate) ligands as well, since the studies of these related complexes are still limited. To better understand the effect of these tridentate amine bis(phenolate) ligands on the structure and reactivity of the derived metal complexes, we became interested in employing tridentate Cr^{III} complexes **5** and **6** in the copolymerization of CHO and CO₂. For example, does the presence of the pendent donor stabilize the catalyst or will a more active catalyst be obtained in a more coordinatively unsaturated compound? Will steric effects due to the phenolate group substituents influence activity? Is the nature of the pendant donor (whether O- or N-containing groups are used) significant for activity?

Since chromium^{III} catalysts have shown excellent activity for CO₂/epoxide copolymerization,^[66, 68, 69, 101-103] a study was undertaken to explore the potential of the Cr^{III} amine-bis(phenolate) complexes described in Chapter 2 for this reaction. This chapter will focus on the activity of CrCl[O₂NO]^{BuBu} (**4**), CrCl[ONO]^{BuBuBn} (**5**) and CrCl[ONO]^{tAmtAmBn} (**6**) for copolymerization of cyclohexene oxide (CHO) with CO₂.

3.2 Copolymerization of Cyclohexene Oxide and CO₂

The copolymerization of cyclohexene oxide (CHO) and CO₂ was investigated using catalysts **4**, **5** and **6** (Scheme 3.1). In this chapter, common previously reported co-

catalysts that were effective with Co and Cr-containing complexes for copolymerization, including those previously studied by our group were used.^[43, 65, 68, 69] Specifically, the co-catalysts used were (4-dimethylamino)pyridine (DMAP), bis(triphenylphosphoranylidene)iminium chloride and azide (PPNCl and PPNN₃) (Figure 3.1). When CHO, CO₂, chromium catalysts and co-catalysts were combined, poly(cyclohexene carbonate) (PCHC) was obtained. It has also been previously shown by our group and others that in the absence of catalyst but co-catalyst alone does not give polycarbonate.^[65, 68]



Scheme 3.1. Copolymerization of CHO and CO₂.

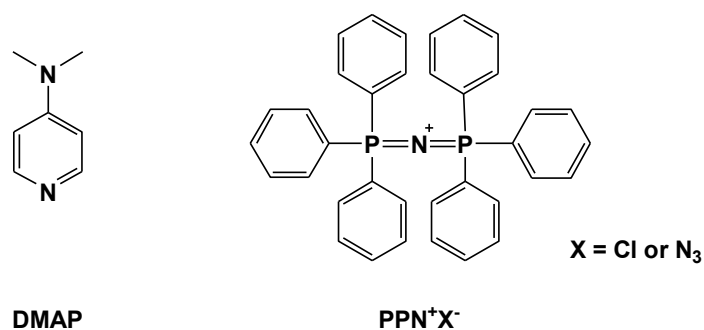


Figure 3.1. Common co-catalysts used in CO₂/epoxide copolymerization reactions.

Table 3.1. Results of the Copolymerization of CHO and CO₂ by Catalyst **5** and **6** with DMAP or PPNX salts.^a

Entry	Catalyst	Co-Catalyst	Time (h)	Temp (°C)	Pressure (bar)	% Conversion ^b	%Yield ^c	TON ^d	TOF ^e (/h)	M_n^f (kg/mol)	PDI ^f (M_w/M_n)
1	5	DMAP	24	60	45	33.8	12.7	169	7.1	2.3	1.58
2 ^g	5	PPNCl	24	60	45	51.5	44.3	258	11	2.8	1.56
3 ^{g, h}	5	PPNCl	24	60	43	38.1	32.5	191	8.0	ND	ND
4 ^g	5	PPNN ₃	24	60	42	44.8	27.0	224	9.3	3.8	1.48
5	6	DMAP	24	60	40	18.7	6.63	93.5	3.9	1.1	2.10
6 ^h	6	DMAP	24	60	42	13.7	5.41	68.5	2.9	ND	ND

^a Copolymerization reactions were carried out in neat CHO (5 mL), using catalyst and co-catalyst of loading of 0.2 mol%. ^b Calculated by ¹H NMR.

^c Isolated yield. ^d Calculated by conversion. ^e Turnover frequency is moles of PCHC produced per mol of Cr per hour. ^f Determined by gel permeation chromatography in CHCl₃, calibrated with polystyrene standards. ^g Dissolved in 4 mL dichloromethane prior to adding CHO.

^h Duplicate run of previous entry. ¹ ND = not determined.

Table 3.2. Results of the Copolymerization of CHO and CO₂ by Catalyst **4** and DMAP or PPNX salts.^a

Entry	Co-Catalyst	Time (h)	Temp (°C)	Pressure (bar)	% Conversion ^b	%Yield ^c	TON ^d	TOF ^e (/h)	M_n^f (kg/mol)	PDI ^f (M_w/M_n)
1	DMAP	24	60	40	68.0	58.9	340	14	5.7	1.48
2 ^g	DMAP	24	60	43	59.9	60.8	300	12	ND	ND
3 ^h	DMAP	24	60	43	28.6	16.4	286	12	2.8	1.67
4 ⁱ	PPNCl	24	60	42	76.3	73.7	382	16	5.7	1.46
5 ⁱ	PPNN ₃	24	60	41	76.3	64.1	382	16	6.4	1.42
6 ⁱ	PPNCl	6	60	41	49.5	37.3	248	41	4.5	1.39
7 ⁱ	PPNCl	3	60	43	33.0	22.8	165	55	3.0	1.63
8 ^h	None	6	60	42	0	0	0	0	NA ^j	NA ^j

^a Copolymerization reactions were carried out in neat CHO (5 mL), using catalyst and co-catalyst of loading of 0.2 mol%. ^b Calculated by ¹H NMR.

^c Isolated yield. ^d Calculated from % conversion. ^e Turnover frequency is moles of PCHC produced per mol of Cr per hour. ^f Determined by gel permeation chromatography in CHCl₃, calibrated with polystyrene standards. ^g Duplicate run of previous entry. ^h Catalyst and co-catalyst of loading of 0.1%. ⁱ Dissolved in 4 mL dichloromethane prior to adding CHO. ^j NA = not applicable (no polymer obtained). ND = not determined.

In the copolymerization study, reactions performed at 60 °C and 40 bar for 24 h using catalyst **4** (possessing a tetradentate ligand) and with PPnCl or PPnN₃ as co-catalyst gave the best results (76.3% conversion of PCHC, entries 4 and 5, Table 3.2). However, the poor solubility of these co-catalysts in CHO required dissolving the catalyst and co-catalyst in dichloromethane, whereupon removal of solvent gives a material now soluble in CHO. This procedure has also been used when these ionic co-catalysts are used with salen- or salan-based Cr^{III} catalysts.^[104] Similar results from recent copolymerization studies by our group were also obtained when an analogue of **4** was employed with PPnCl, and the highest conversion obtained was 72% (at 60 °C, 40 bar and 24 h).^[68] A highly active Cr(salen) catalyst reported by Darensbourg and co-workers exhibited a TOF of 1057 h⁻¹ (at 80 °C, 34.5 bar) for this reaction by using catalyst and co-catalyst of loading of 0.043%.^[105]

On the other hand, the co-catalyst DMAP with catalyst **4** (Entries 1 and 2, Table 3.2) gave lower conversions and yields of polycarbonate compared to using PPnCl and PPnN₃ under the same conditions (Entries 4 and 5, Table 3.2). Similarly, DMAP (Entry 1, Table 3.1) was found to be inferior to PPnCl or PPnN₃ (Entries 2 and 4, Table 3.1) under the same conditions when catalyst **5** was investigated in the copolymerization.

Generally, compared with tetradentate catalyst **4**, tridentate catalysts **5** and **6** showed lower activity for the copolymerization of CO₂/CHO (Table 3.1 and Table 3.2). Tridentate catalyst **6**, which was applied only once for the copolymerization of CO₂ and CHO (Entries 5 and 6, Table 3.1), was found to be much less active than catalyst **5** (Entry 1, Table 3.2) under the same conditions. The fact that isolated yields were lower than the conversions calculated by NMR can be attributed to the loss of products in the isolation

process. This suggests low molecular weight polymers were obtained that were not isolated by precipitation. The crude material was first dissolved in dichloromethane, and then the solution was transferred into an empty round bottom flask. Cold methanol was added to the dichloromethane solution to precipitate solid polymer and the mixture was then refrigerated at 5 °C. After the mixture settled for one to three days, the clear supernatant solution was removed using a pipette and the precipitate was dried under vacuum overnight. Three runs were performed in duplicate (Table 3.1, entries 2 and 3, entries 5 and 6 and Table 3.2, entries 1 and 2) with good reproducibility.

Furthermore, using PPNCl as the co-catalyst gave good conversion (76.3%) for polycarbonate, but required long reaction times (24 h). Shortening the reaction time to 6 h or 3 h, caused the conversions of CHO to decrease to 49.5% and 33.0% respectively (Entries 6 and 7, Table 3.2). This suggests a relatively slow reaction rate under these conditions.

The catalyst loading of Cr and DMAP vs CHO was halved in entry 3, Table 3.2, resulting in a significant decrease in conversion of CHO. A similar trend was previously reported for an analogue of **4**.^[68] Co-catalysts played a crucial role in copolymerization of CO₂/CHO, supported by the fact that no polymer was obtained when no co-catalyst was used. (Entry 8, Table 3.2).

It is worth noting that solid polycarbonates produced with catalyst **4** were almost colorless, while solid polycarbonates were light-green in color when catalyst **5** and **6** were applied.

3.3 Characterization of poly(cyclohexene) carbonate

3.3.1 NMR of polymer

The ^1H NMR spectrum of PCHC obtained according to Table 3.1, entry 1 is shown in Figure 3.2. The methine protons of the non-terminal cyclohexane rings appear as the broad peak at 4.60 ppm.^[93] The presence of ether linkages was typically either not found or was less than 1%, and also no evidence of cyclic carbonate was observed. In Figure 3.2, the appearance of methine protons of the terminal cyclohexane ring, $\text{H}_b + \text{H}_c$, can help to estimate molecular weight of the polymer ($n \approx (\text{H}_{a'} + \text{H}_a) / (\text{H}_b + \text{H}_c)$). Also the presence of unreacted CHO, observed at 3.10 ppm, allows conversion calculations (conversion = $\text{H}_{a'}/(\text{H}_{a'} + \text{H}_{\text{CHO}}) \times 100\%$).

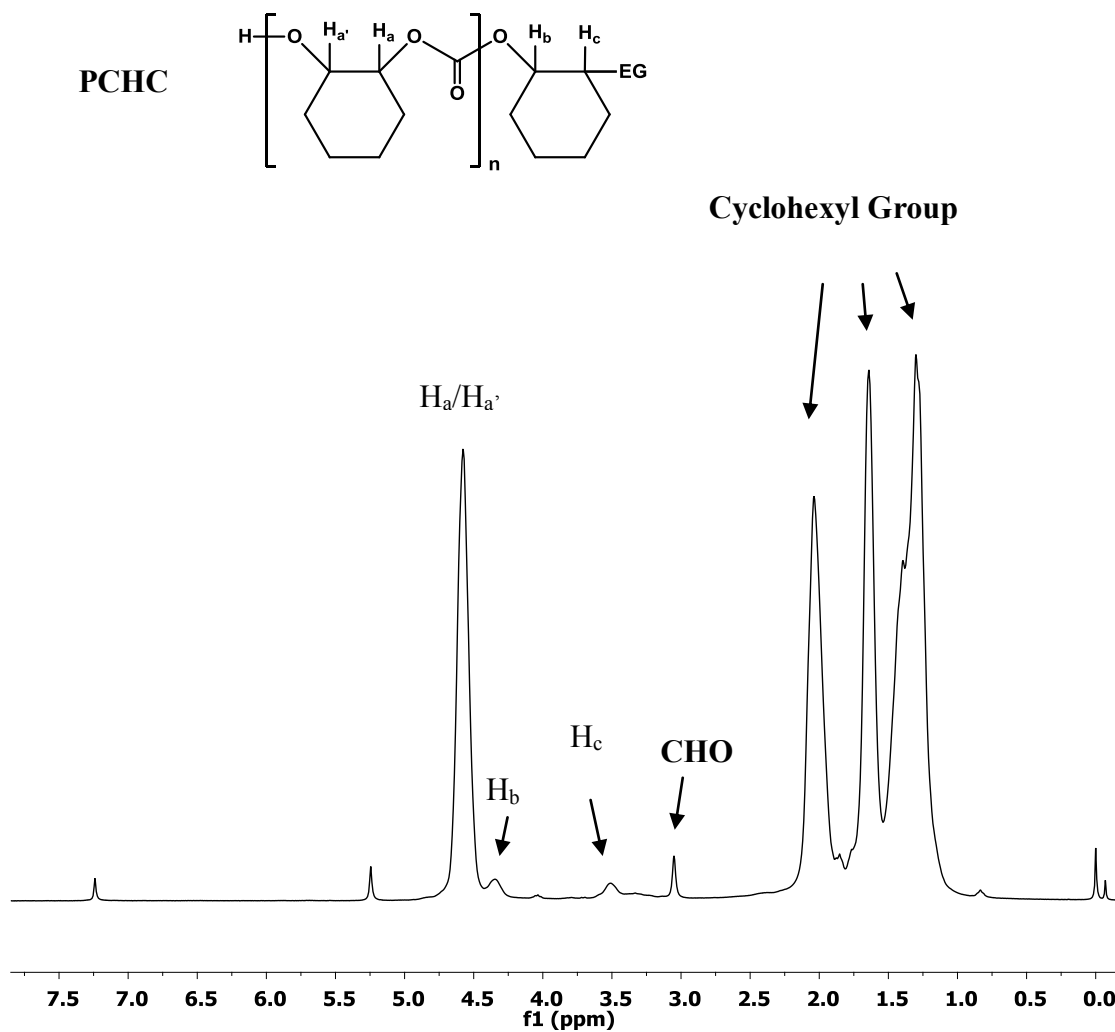


Figure 3.2. Typical ^1H NMR spectrum of PCHC in CDCl_3 (Table 3.1 Entry 1), EG = end group (see section 3.3.2).

The isolated poly(cyclohexene carbonate) stereochemistry was analyzed by ^{13}C NMR spectroscopy, as shown in Figure 3.3. Through quantitative ^{13}C NMR spectroscopy of the carbonyl region, approximately equal amounts of isotactic and syndiotactic units were detected in the polymer spectra when employing chromium catalysts and co-

catalysts, providing evidence that the dominant configuration of the polymer is atactic (Figure 3.4).^[68, 93]

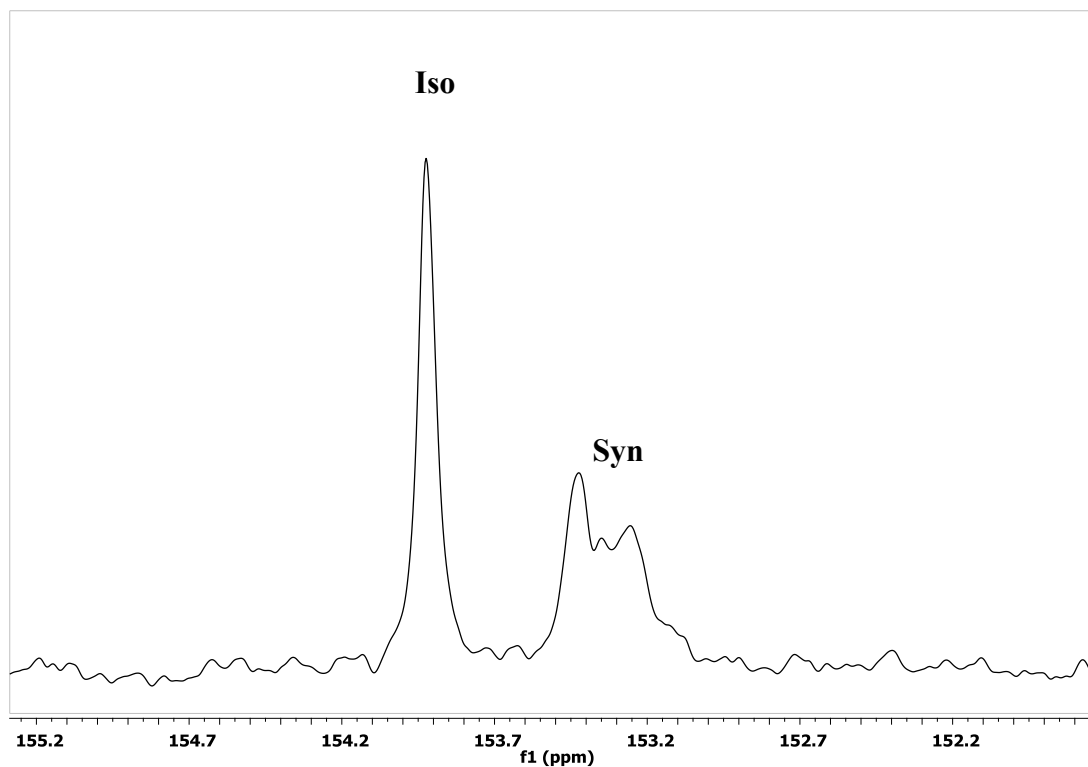


Figure 3.3. Carbonyl region of the ¹³C NMR spectrum (75.5 MHz, CDCl₃) of CHO/CO₂ copolymer prepared as described in Table 3.1, entry 1.

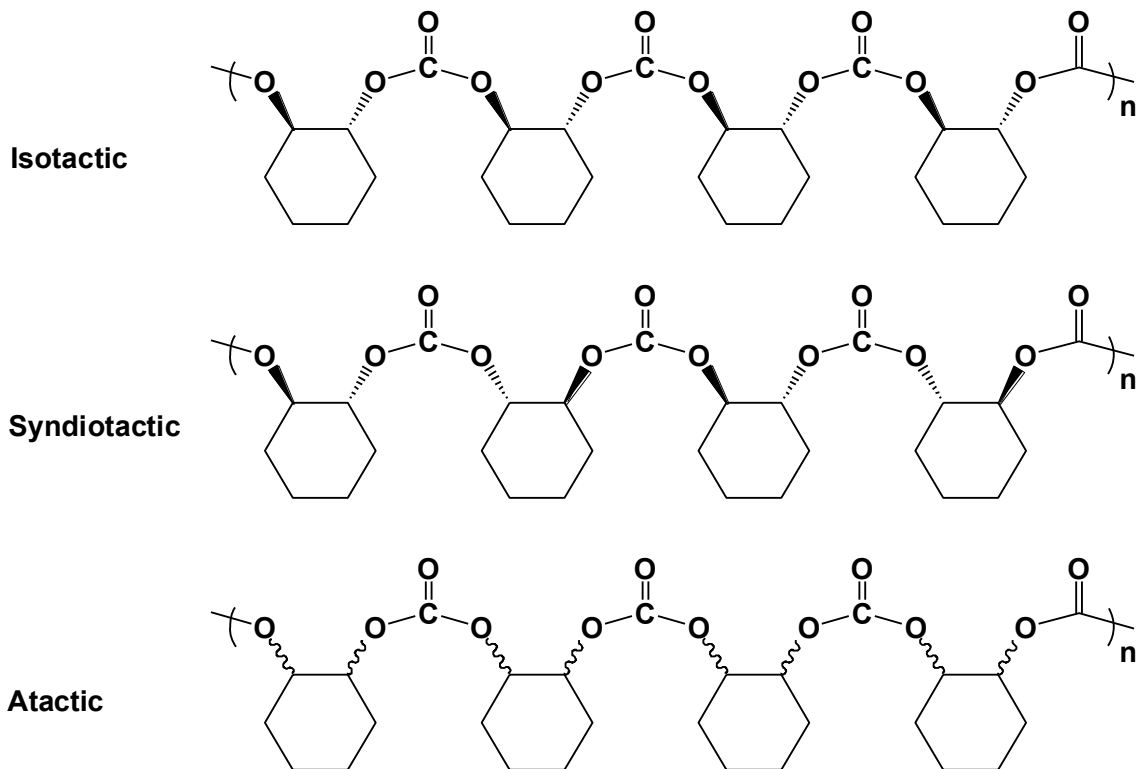
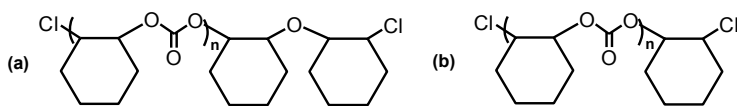
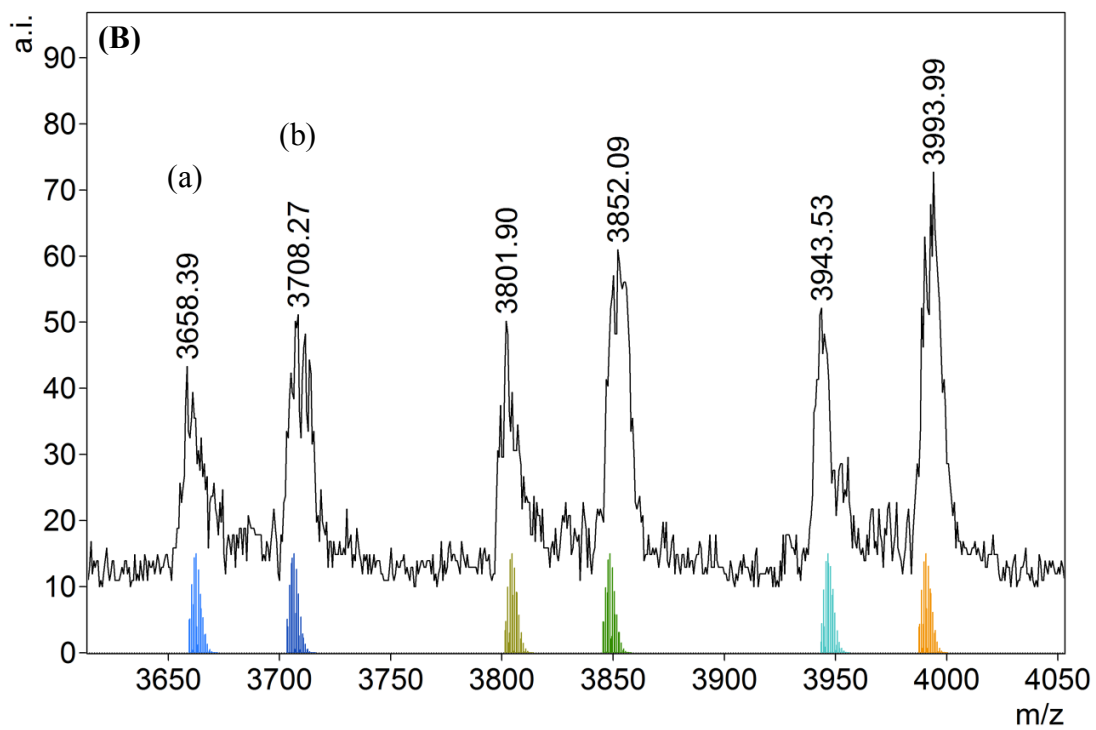
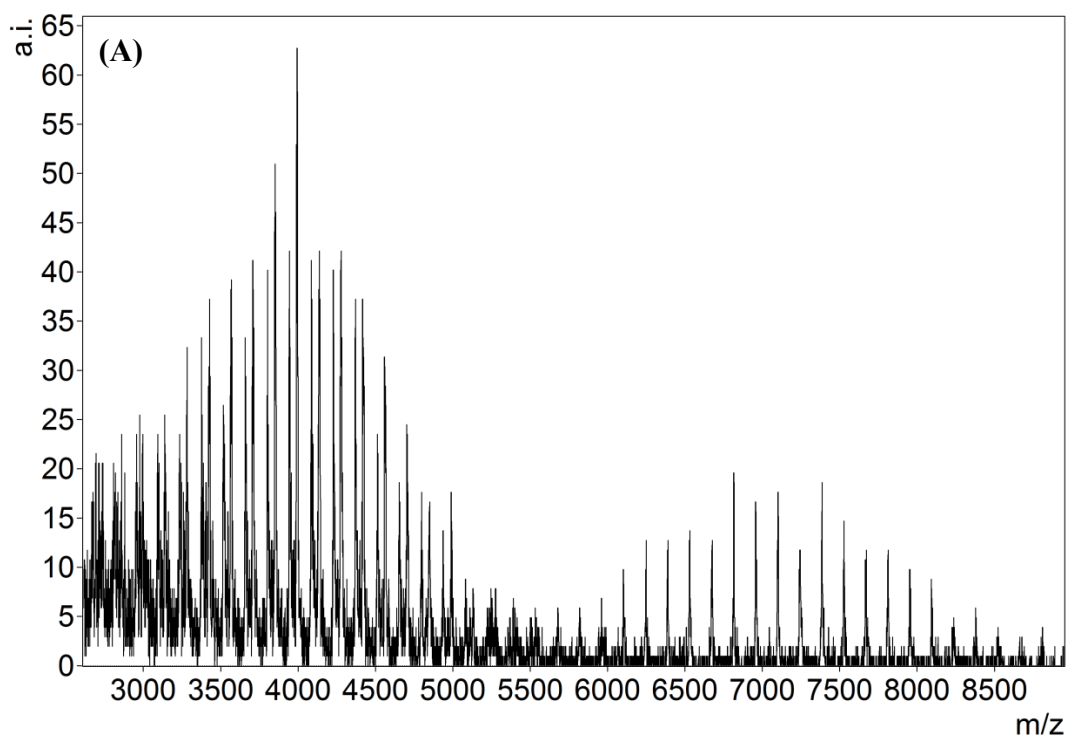


Figure 3.4. Stereochemistry of PCHC.

3.3.2 Mass Spectrometry

MALDI-TOF MS studies were performed in order to gain insight into experimental values of the number average molecular weights of the copolymers and analysis of possible end-groups providing mechanistic details for this system. In the MALDI-TOF mass spectra of these copolymers, multi-modal molecular weight distributions were observed showing multiple end group series, all separated with a repeating unit of 142 g/mol. The different end groups can be attributed to the mechanism, in particular the initiation step involved in the copolymerization process, and the catalyst systems used.

For catalyst **5**, using PPnCl or PPnN₃ as co-catalyst gives approximately 50% conversion of CHO to polymer (Table 3.1, entries 2 and 4). Three polymer chains possessing different end groups were observed when PPnN₃ was used as co-catalyst with catalyst **5** (Figure 3.5). The lower molecular weight series, (a), consists of an ether linkage [35 (Cl) + 142*n* (repeating unit) + 180 (C₁₂H₂₀O) + 35 (Cl)], which may be a result of the double epoxide insertion or chain transfer; (b), consists of both chain ends being chlorides [35 (Cl) + 142*n* (repeating unit) + 82 (C₆H₁₀) + 35 (Cl)], and suggests that the chlorides from complex **5** are involved in initiation of the production of PCHC and also the termination process. Series (b) could result from chain transfer between two growing polymer chains resulting in a single polymer containing two initiation sites as end groups. The higher molecular weight series (c) is the expected series if copolymerization is initiated by ring-opening of an epoxide monomer by a Cl⁻ and terminated by either hydrolysis^[55, 101] or protonation when adding methanol in the polymer purification process, [17 (OH) + 142*n* (repeating unit) + 82 (C₆H₁₀) + 35 (Cl)]. Isotopic masses modeled for all three polymer chains are found to agree with assigned peaks in the experimental spectra.



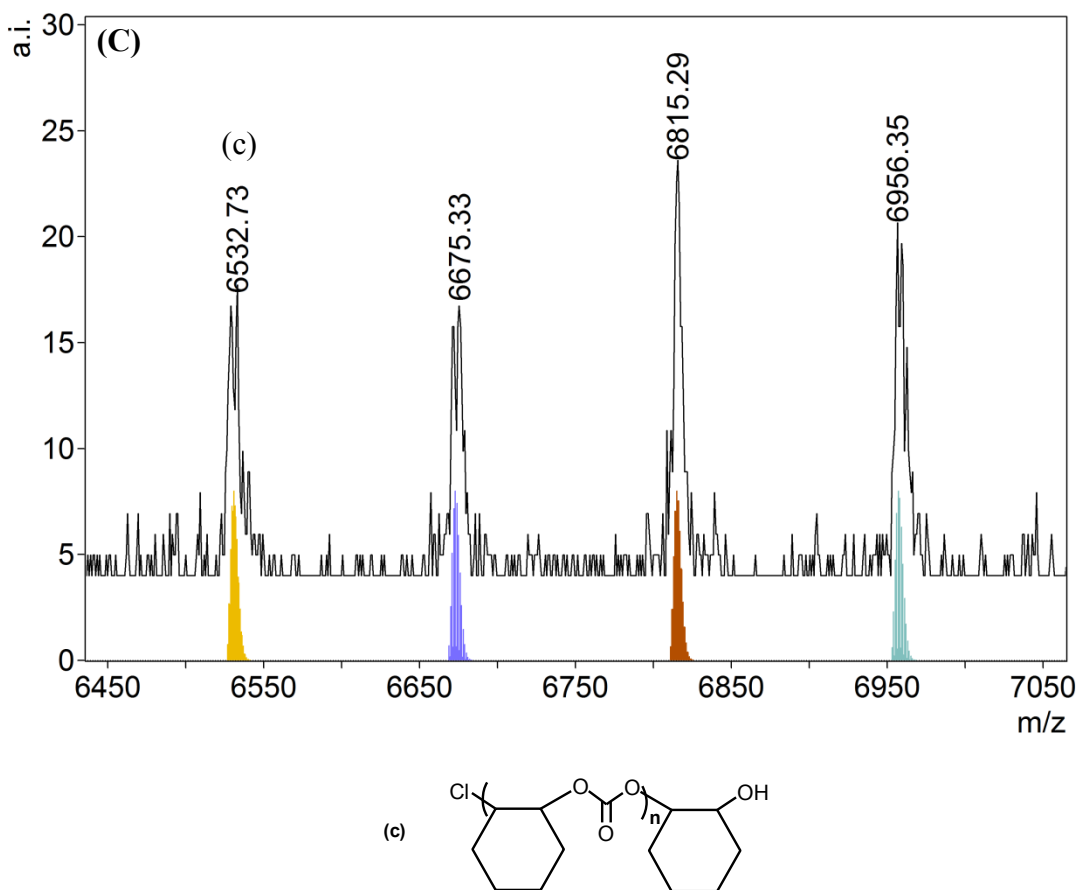
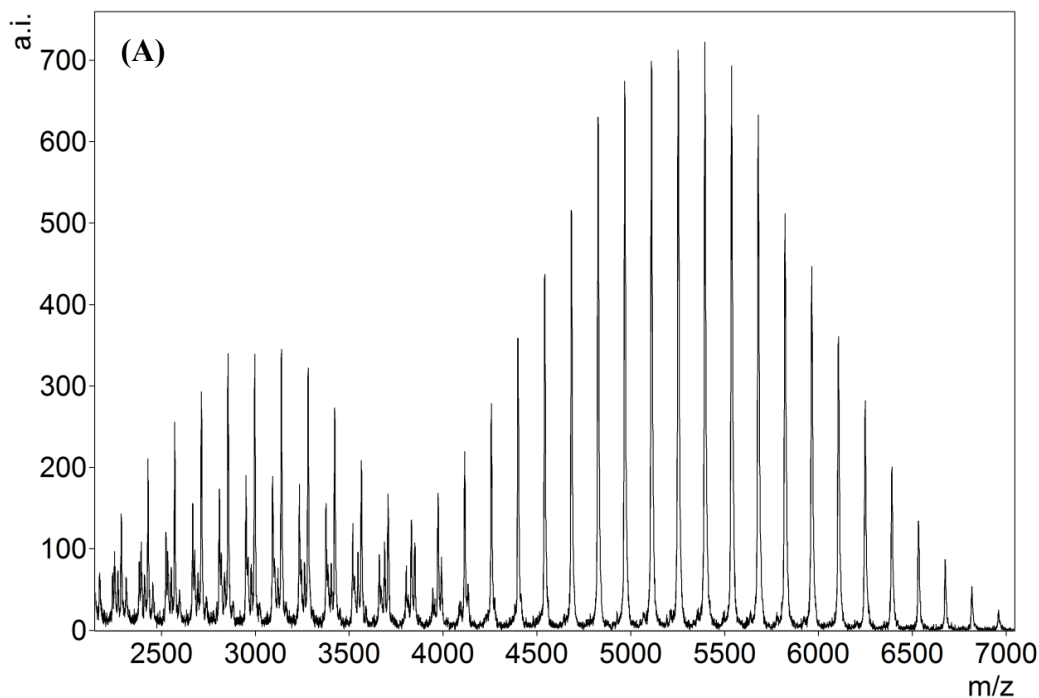
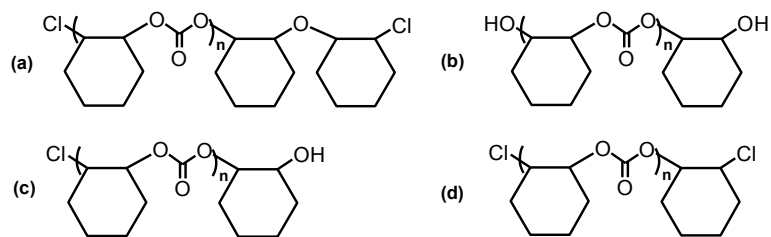
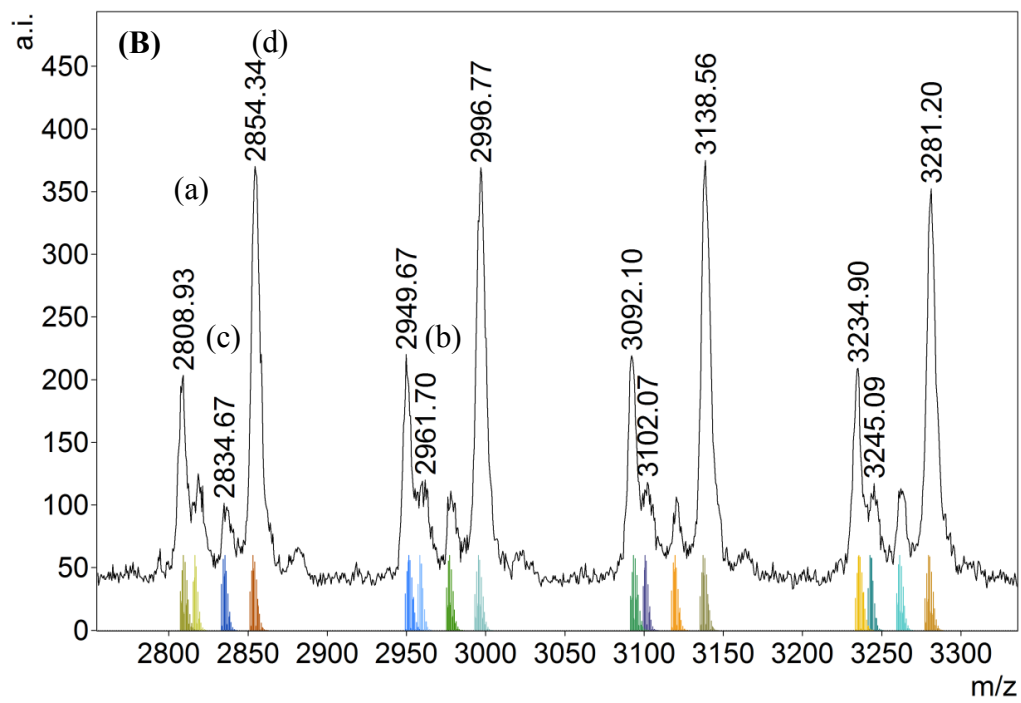


Figure 3.5. (A) MALDI-TOF MS of PCHC produced by **5** (Table 3.1, entry 4). (B) Magnified region of the spectrum ($n = 24-27$). (C) Magnified region of the spectrum ($n = 45-48$). Modeled isotopic masses and images for the polymer chains with end groups (a, b and c).

Furthermore, different end groups of four polymer chains were observed in entry 2, Table 3.1 by using catalyst **5** and PPnCl co-catalyst (Figure 3.6). In the 2000 m/z to 4000 m/z region of MALDI-TOF MS spectrum, four series of polymer chains are detected. Series (a) consists of an ether linkage [35 (Cl) + $142n$ (repeating unit) + 180 ($C_{12}H_{20}O$) + 35 (Cl)], which may be a result of double epoxide insertion or chain transfer^[106]; series (b)

consists of two hydroxyl-end groups [17 (OH) + 142*n* (repeating unit) + 82 (C₆H₁₀) + 17 (OH)] suggesting evidence of chain-transfer as a result of hydrolysis;^[55, 101] series (d), contains Cl groups at both termini of the polymer [35 (Cl) + 142*n* (repeating unit) + 82 (C₆H₁₀) + 35 (Cl)], which indicates that the chlorides from complex **5** (or co-catalyst PPnCl) are involved in initiation of the production of PCHC and also termination process likely via chain transfer. However, series (c), consists of one chloride and hydroxyl-end group the same as series (c) analyzed in entry 4, Table 3.1 (Figure 3.5 (C)), [17 (OH) + 142*n* (repeating unit) + 82 (C₆H₁₀) + 35 (Cl)], which ranges from 2000 *m/z* to 7000 *m/z* in the spectrum (Figure 3.6 (B) and (C)).





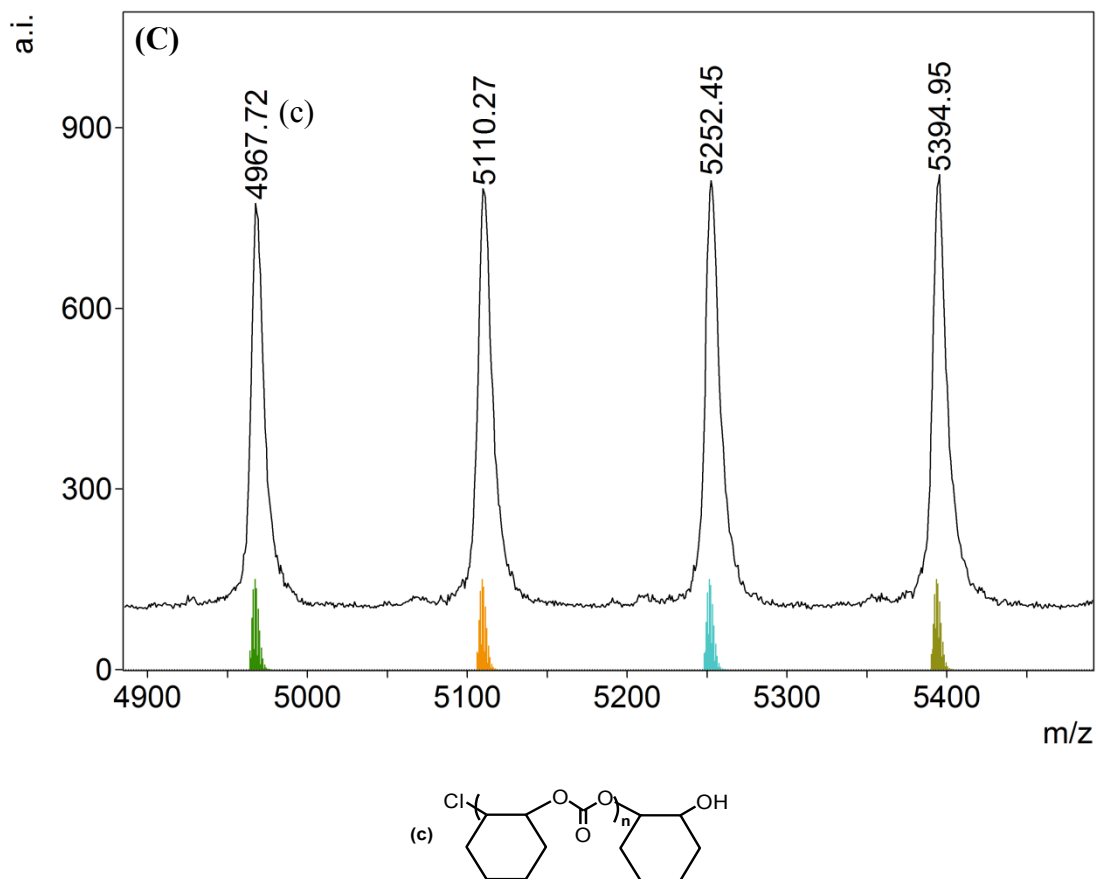
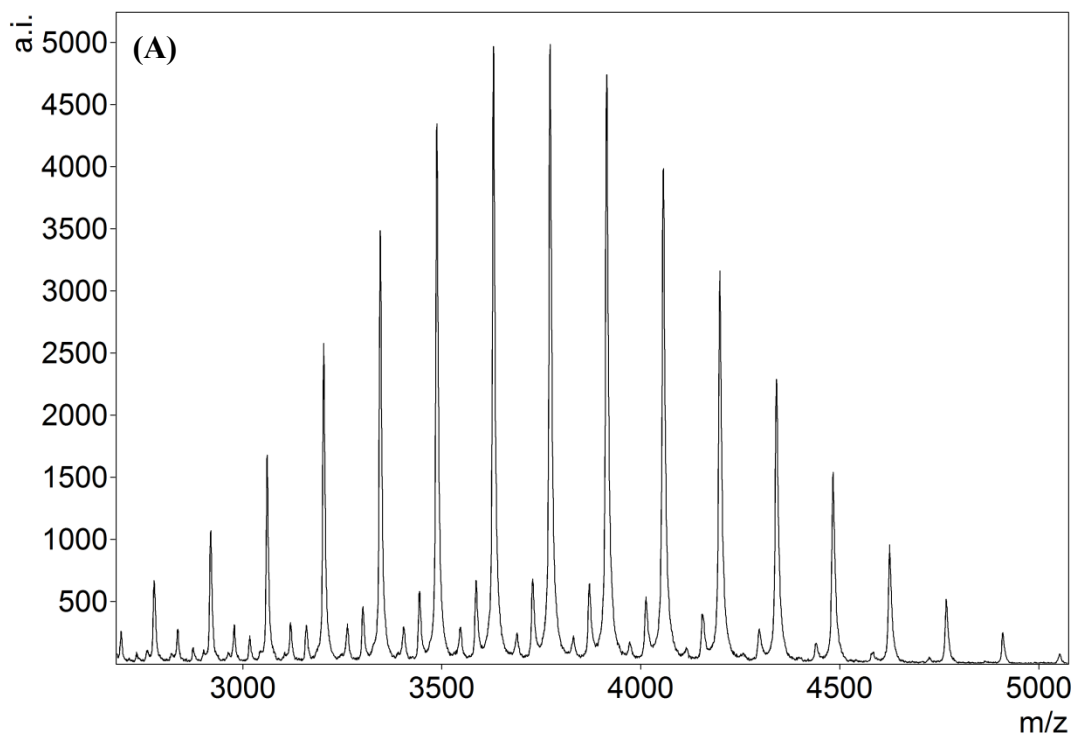


Figure 3.6. (A) MALDI-TOF MS of PCHC produced by **5** (Table 3.1, entry 2). (B) Magnified region of the spectrum ($n = 18-21$). (C) Magnified region of the spectrum ($n = 34-37$) and modeled isotopic masses and images for the polymer chains with end groups (a-d).

DMAP is the only co-catalyst applied with catalyst **6** in copolymerization of CHO and CO₂. Three different end groups resulting from three polymer chains of various molecular weights were found in the mass spectrum of the resulting polymer (Figure 3.7). The lowest molecular weight series, (a), is modeled as $[35 (\text{Cl}) + 142n (\text{repeating unit}) + 82 (\text{C}_6\text{H}_{10}) + 17 (\text{OH})]$. For series (a) the chlorides from complex **6** are involved in

initiation of the production of PCHC and the termination process due to protonolysis.^{[55,}

^{101]} Series (b), consists of a DMAP initiated polymer, $[122 (\text{C}_7\text{H}_{10}\text{N}_2) + 142n$ (repeating unit) $+ 180 (\text{C}_{12}\text{H}_{20}\text{O}) + 17 (\text{OH})]$; series (c), is modeled to have DMAP-containing end groups as observed in the other examples,^[107, 108] $[122 (\text{C}_7\text{H}_{10}\text{N}_2) + 142n$ (repeating unit) $+ 82 (\text{C}_6\text{H}_{10}) + 17 (\text{OH})]$. Specifically, DMAP was found in both series (b) and (c) indicating that the co-catalyst could be acting as the initiator of the copolymerization (Figure 3.7), like other examples where DMAP-containing end groups have been observed.^[107, 108]



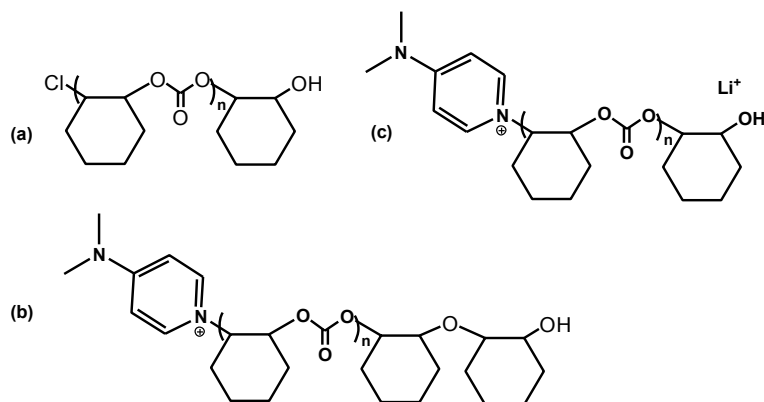
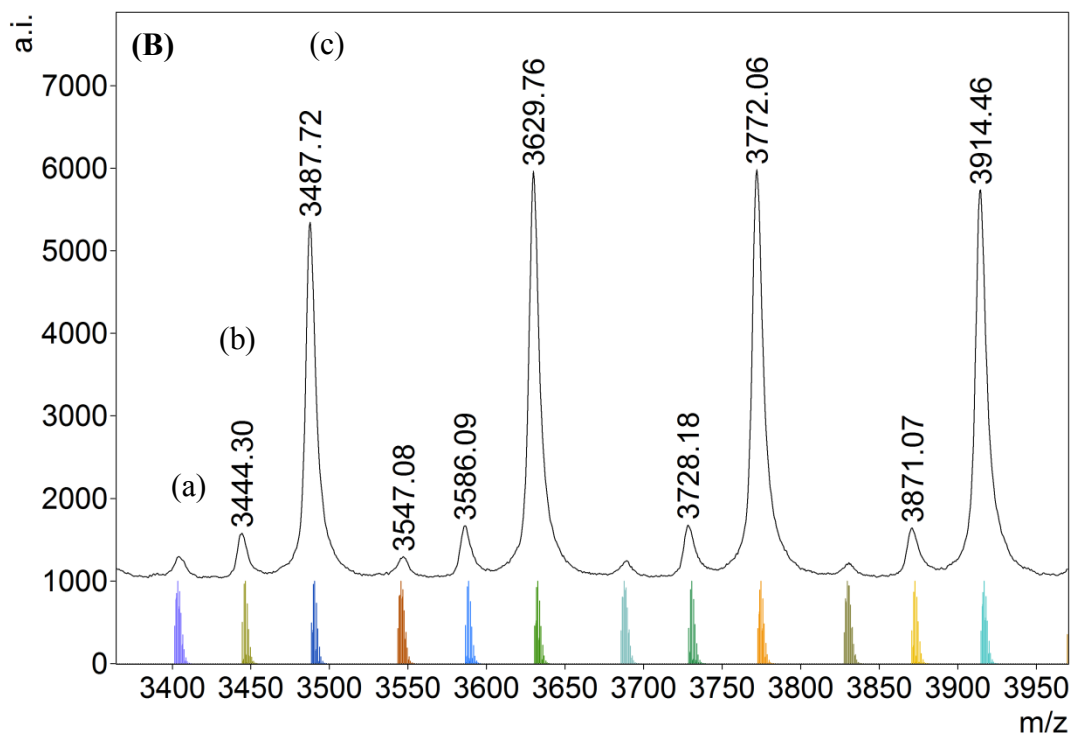
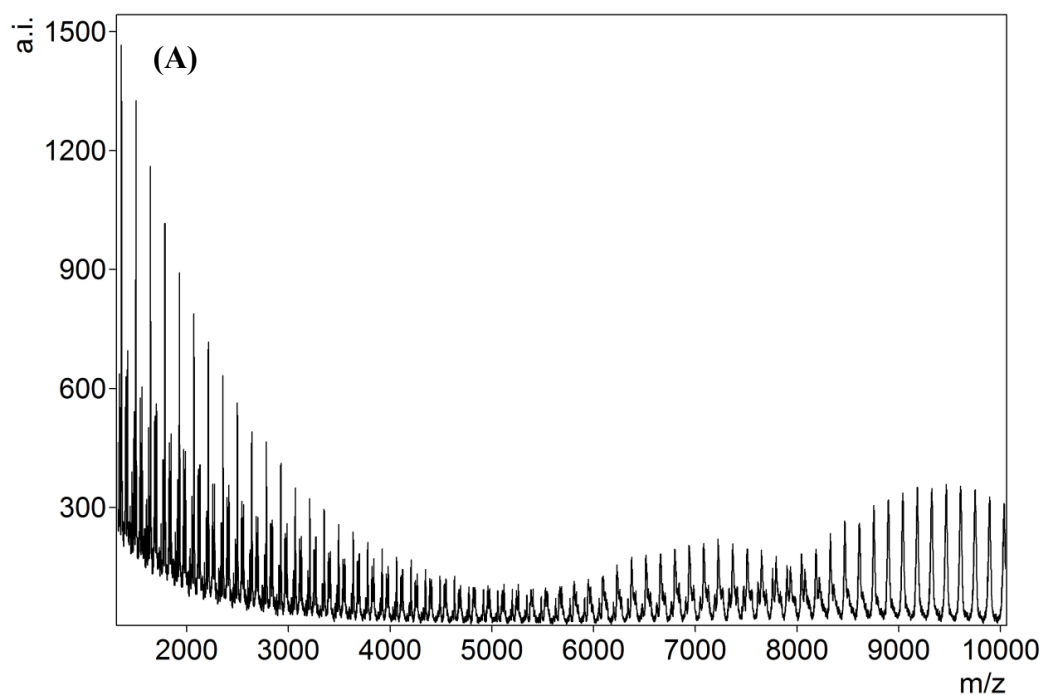


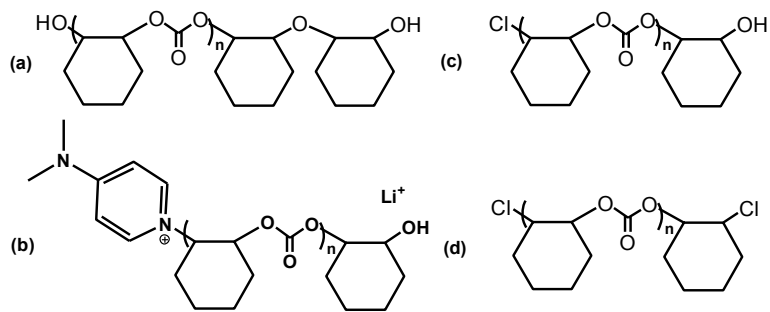
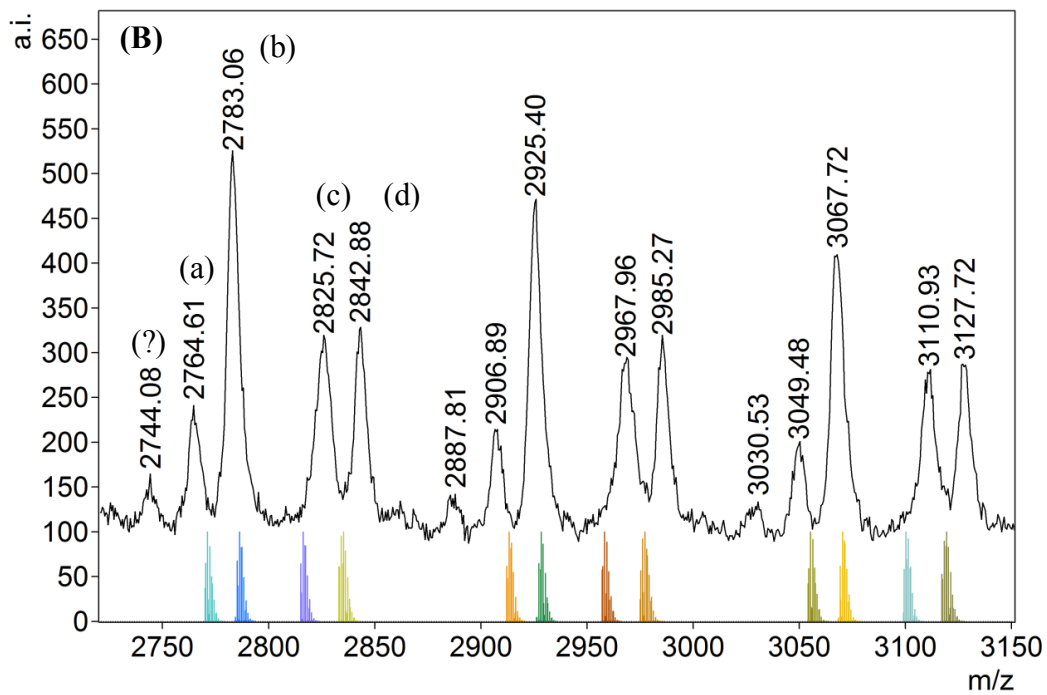
Figure 3.7. (A) MALDI-TOF MS of PCHC produced by **6** (Table 3.1, entry 5). (B) Magnified region of the spectrum ($n = 22-25$) and modeled isotopic masses and images for the polymer chains with end groups (a-c).

MALDI-TOF MS of polymers formed by **4** are more complicated than those obtained using catalyst **5** or **6**. Some peaks in the spectra are still unidentified after end group analysis.

For catalyst **4**, DMAP used as co-catalyst gives 68% conversion to polymer (Table 3.2, entry 1). The differing end groups result from six polymer chains attributed to various molecular weights (Figure 3.8). The lower molecular weight series, (a), contains an ether linkage, $[17 (\text{OH}) + 142n (\text{repeating unit}) + 180 (\text{C}_{12}\text{H}_{20}\text{O}) + 17 (\text{OH})]$, and either water contamination^[55, 101] or protonation in the polymer purification process could be involved in the initiation and termination process of the reaction. Series (b) also contains one DMAP which could be the result of DMAP initiation, $[122 (\text{C}_7\text{H}_{10}\text{N}_2) + 142n (\text{repeating unit}) + 180 (\text{C}_{12}\text{H}_{20}\text{O}) + 17 (\text{OH})]$. The copolymerization could be initiated by ring-opening of an epoxide monomer by a Cl^- and terminated by hydrolysis or protonation^[55, 101] in series (c), $[17 (\text{OH}) + 142n (\text{repeating unit}) + 82 (\text{C}_6\text{H}_{10}) + 35 (\text{Cl})]$. Series (d) contains Cl groups at both termini of the polymer and suggests that the chlorides from complex **4** are involved in the initiation and termination process of the copolymerization, $[35 (\text{Cl}) + 142n (\text{repeating unit}) + 82 (\text{C}_6\text{H}_{10}) + 35 (\text{Cl})]$. The higher molecular weight series, (e), consists of an ether linkage, $[35 (\text{Cl}) + 142n (\text{repeating unit}) + 180 (\text{C}_{12}\text{H}_{20}\text{O}) + 17 (\text{OH})]$. Series (f) ends with two hydroxyl groups, $[17 (\text{OH}) + 142n (\text{repeating unit}) + 82 (\text{C}_6\text{H}_{10}) + 17 (\text{OH})]$, suggesting evidence of chain-transfer as a result of protonolysis. Series (d) is the same as the series (d) in the lower molecular region. Series (c) in the region over 8000 m/z is the same as the series (c) in the lower molecular region. The presence of Li^+ arises from the *n*-butyllithium added in the synthesis of the chromium complexes and the binding of LiCl adducts is possible, as shown by the

structure of $(\mathbf{5})_2\cdot\text{LiCl}\cdot\text{THF}$. Figure 3.9 and Figure 3.10 also show polymer fragments cationized by Li^+ ions. Isotopic masses modeled for all six polymer chains are found to agree with the experimental spectra. However, the series in the lower molecular weight region and the series in the higher molecular weight region remained unknown after end group analysis.





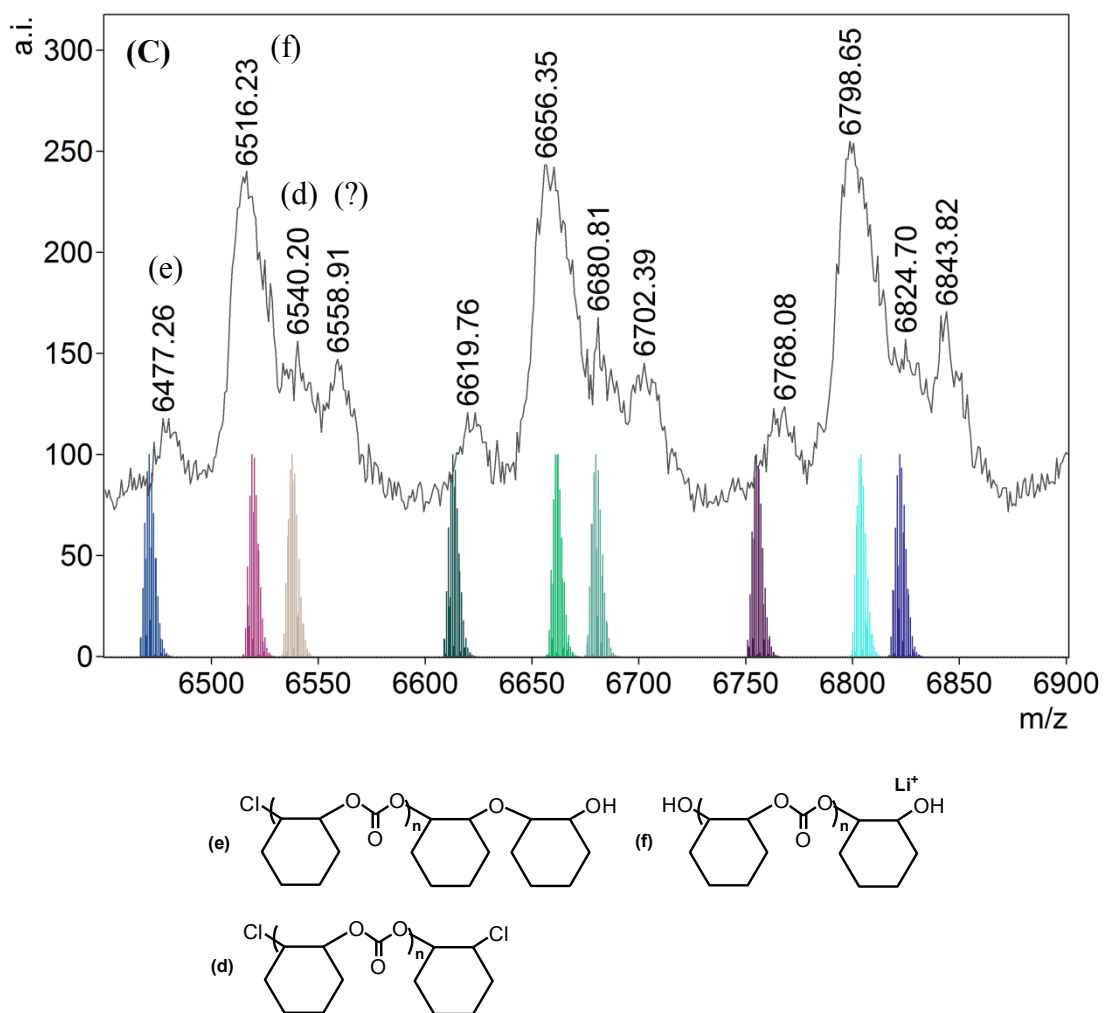
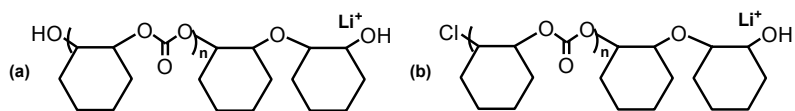
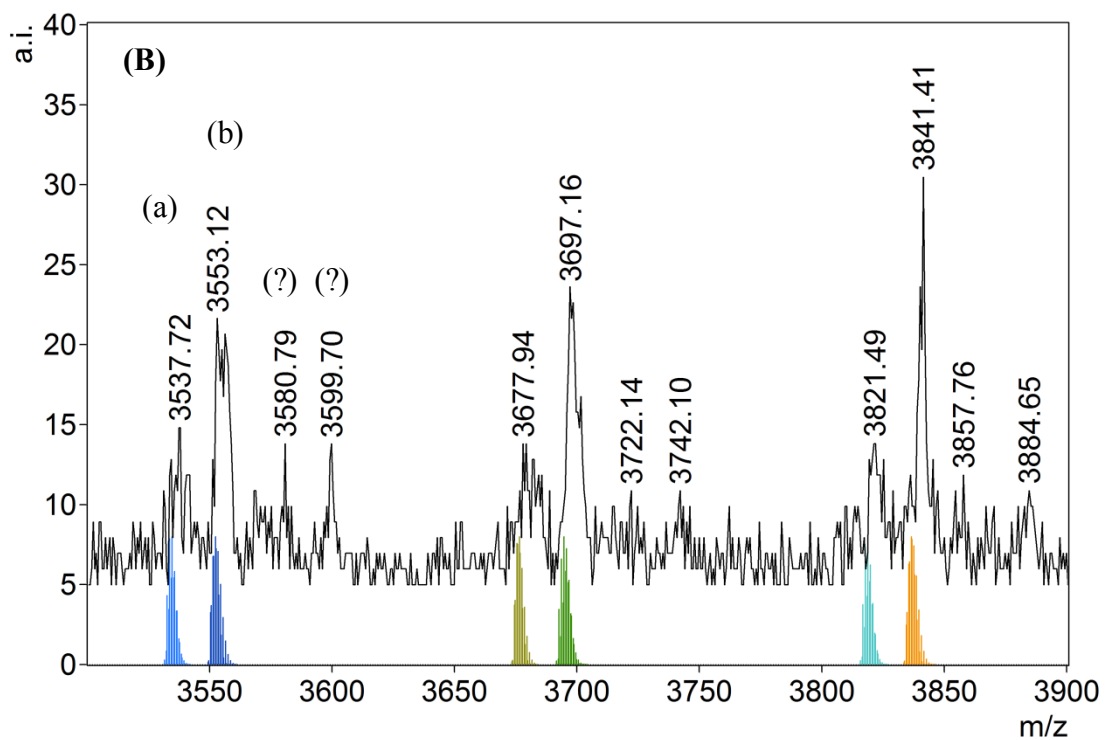
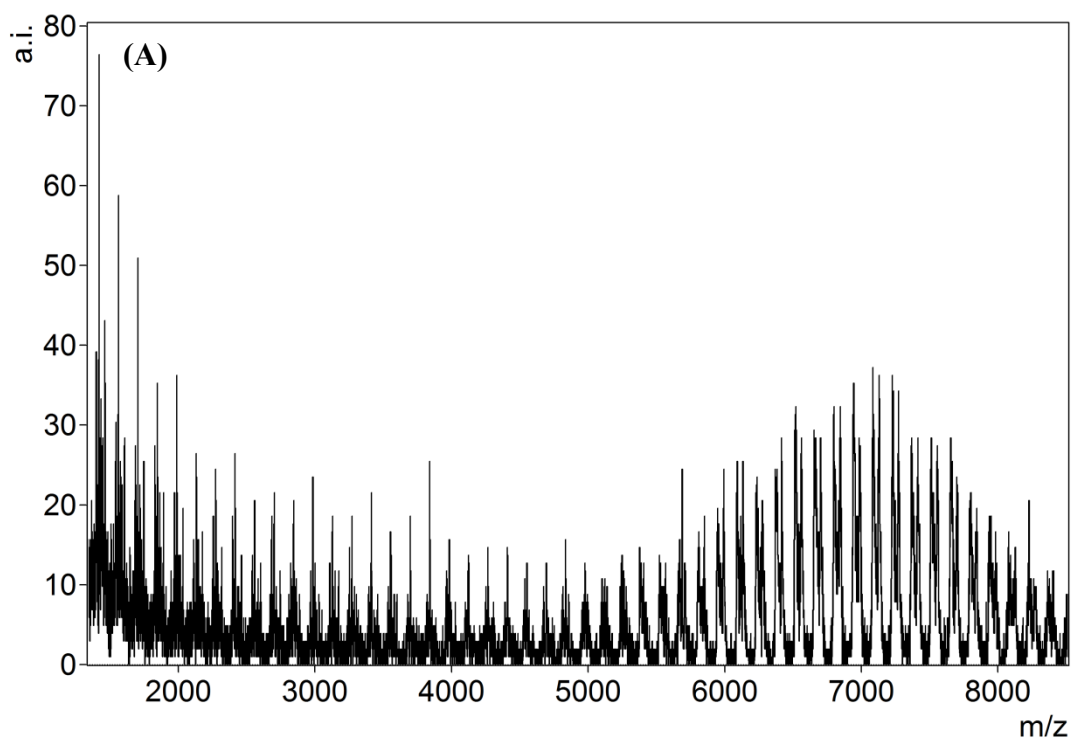


Figure 3.8. (A) MALDI-TOF MS of PCHC produced by **4** (Table 3.2, entry 1). (B) Magnified low molecular weight region of the spectrum ($n = 18-20$). (C) Magnified high molecular weight region of the spectrum ($n = 44-47$). Modeled isotopic masses and images for the polymer chains with end groups (a-f).

Furthermore, PPNCl used as co-catalyst gives 76% conversion to polymer. (Table 3.2, entry 4) The differing end groups result from six polymer chains attributed to various

molecular weights (Figure 3.9). In the lower molecular weight region, series (a) is modeled to have an ether linkage, which may be caused by double epoxide insertion, $[17 \text{ (OH)} + 142n \text{ (repeating unit)} + 180 \text{ (C}_{12}\text{H}_{20}\text{O)} + 17 \text{ (OH)}]$, and two hydroxyl end groups could be the result of protonolysis.^[55, 101] Series (b) contains an ether linkage, suggesting the double epoxide insertion, $[35 \text{ (Cl)} + 142n \text{ (repeating unit)} + 180 \text{ (C}_{12}\text{H}_{20}\text{O)} + 17 \text{ (OH)}]$. In the higher molecular weight region, series (c), consists of two hydroxyl end-groups $[17 \text{ (OH)} + 142n \text{ (repeating unit)} + 82 \text{ (C}_6\text{H}_{10}) + 17 \text{ (OH)}]$, suggesting evidence of chain-transfer as a result of protonolysis; series (d), contains chloride groups at both termini of the polymer, $[35 \text{ (Cl)} + 142n \text{ (repeating unit)} + 82 \text{ (C}_6\text{H}_{10}) + 35 \text{ (Cl)}]$. Isotopic masses modeled for all four polymer chains are found to agree with the experimental spectra. However, two series in the lower molecular weight region remained unknown after end group analysis.



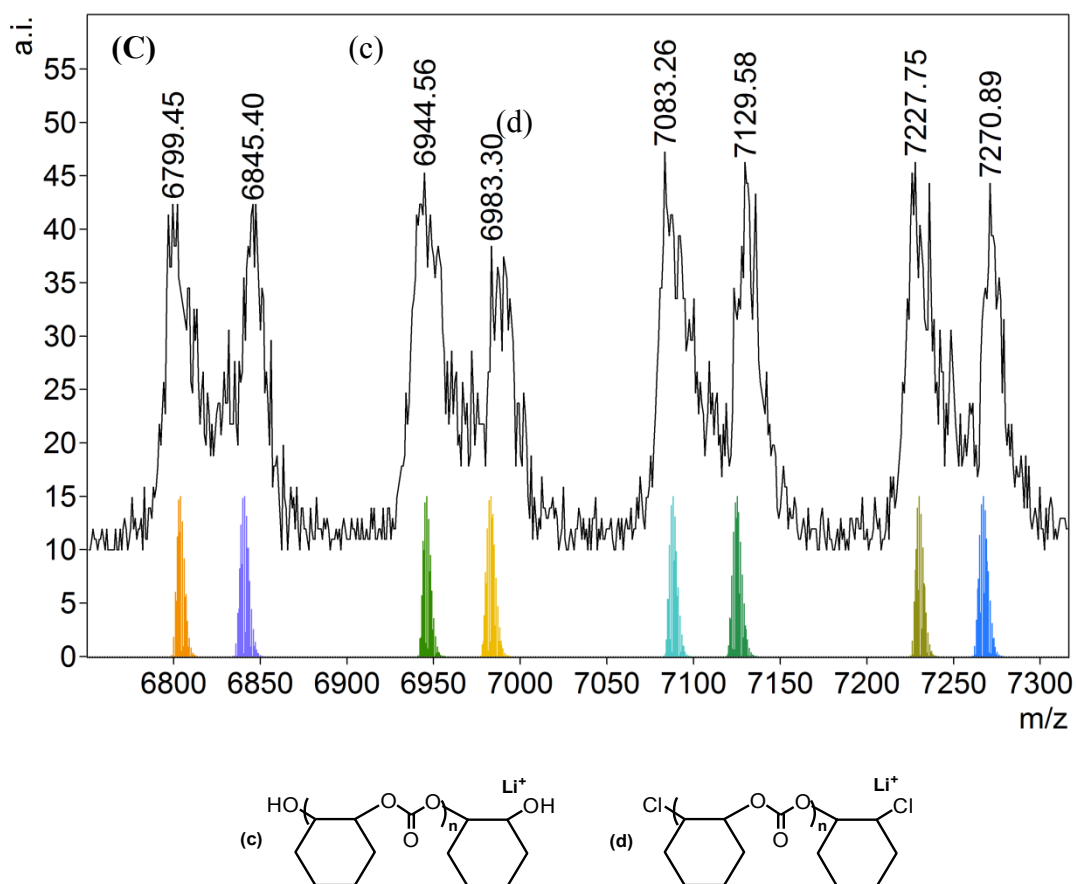
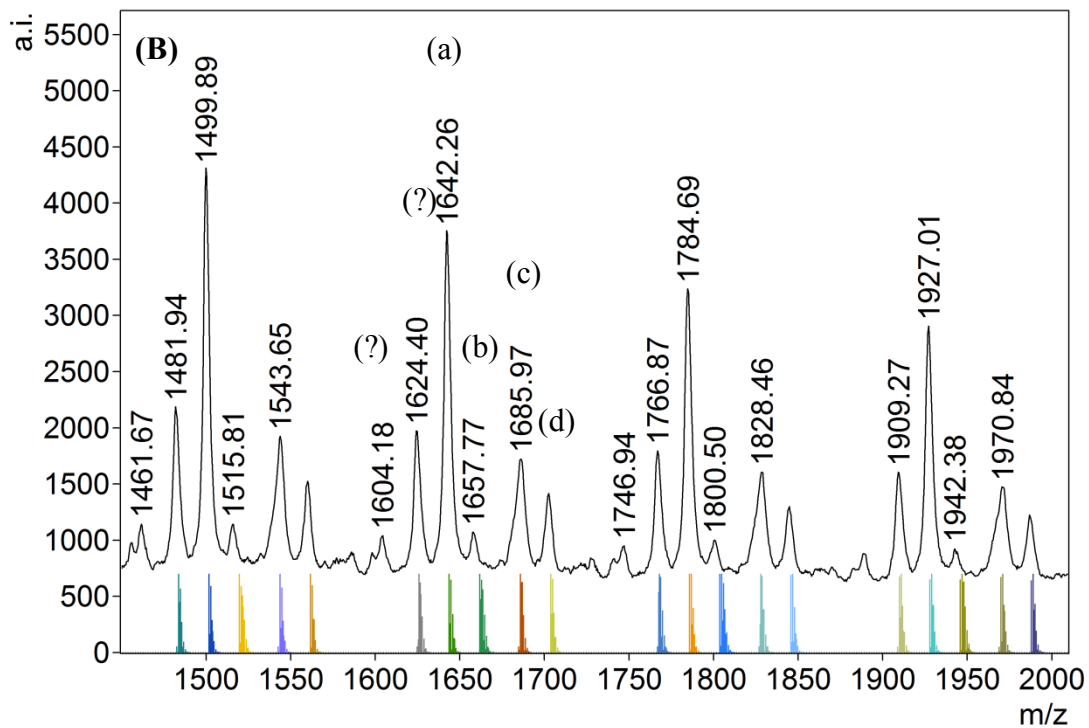
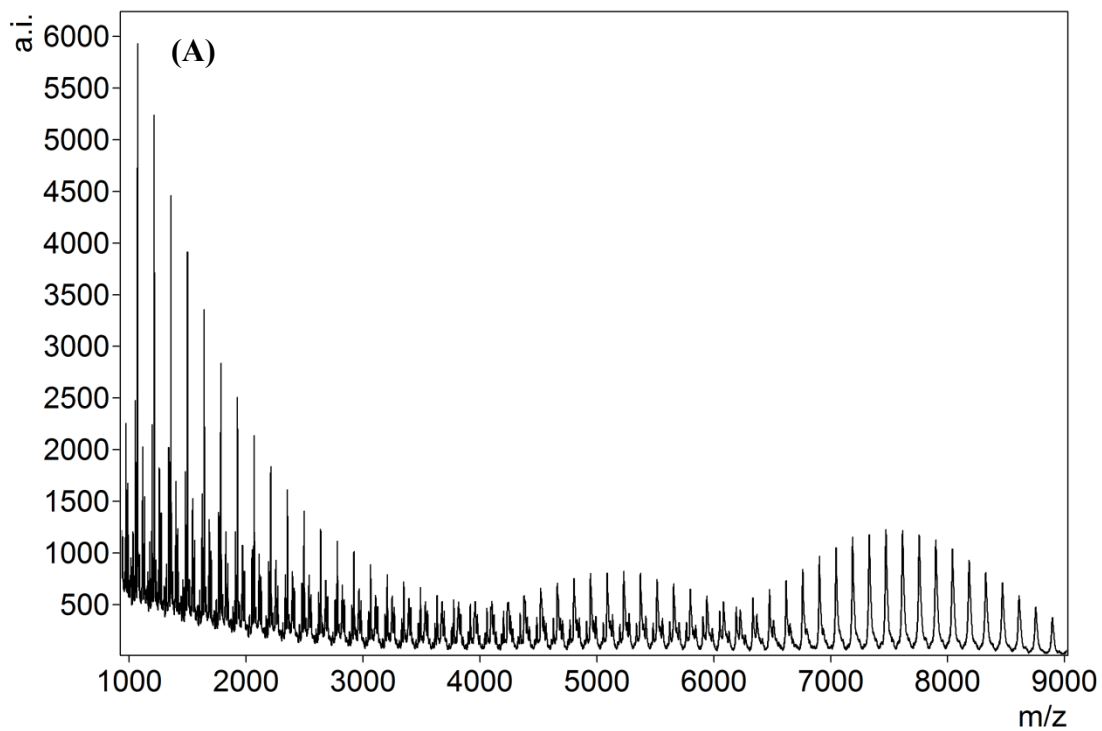


Figure 3.9. (A) MALDI-TOF MS of PCHC produced by **4** (Table 3.2, entry 4). (B) Magnified low molecular weight region of the spectrum ($n = 24-26$). (C) Magnified high molecular weight region of the spectrum ($n = 47-50$). Modeled isotopic masses and images for the polymer chains with end groups (a-d).

Moreover, PPNN₃ used as co-catalyst also gives 76% conversion to polymer (Table 3.2, entry 5). The differing end groups result from seven polymer chains attributed to various molecular weights (Figure 3.10). In the lower molecular weight region, series (a) is modeled to have an ether linkage, $[17 (\text{OH}) + 142n (\text{repeating unit}) + 180 (\text{C}_{12}\text{H}_{20}\text{O}) +$

17 (OH)]. Series (b) $[42 (\text{N}_3) + 142n (\text{repeating unit}) + 180 (\text{C}_{12}\text{H}_{20}\text{O}) + 17 (\text{OH})]$ was initiated by an azide anion and then chain transfers which terminated by protonolysis. Series (c) contains two hydroxyl groups, $[17 (\text{OH}) + 142n (\text{repeating unit}) + 82 (\text{C}_6\text{H}_{10}) + 17 (\text{OH})]$, suggesting evidence of chain-transfer. Series (d), $[42 (\text{N}_3) + 142n (\text{repeating unit}) + 82 (\text{C}_6\text{H}_{10}) + 17 (\text{OH})]$ could also be initiated by an azide anion and terminated by the expected hydroxyl group. In the higher molecular weight region, series (a) and (d) are the same as series of (a) and (d) in the lower molecular weight region. The rest series in the high molecular weight region, series (e), could be initiated by a chloride and terminated by a hydroxyl group, which also suggesting the double epoxide insertion, $[35 (\text{Cl}) + 142n (\text{repeating unit}) + 180 (\text{C}_{12}\text{H}_{20}\text{O}) + 17 (\text{OH})]$; series (f) could be the result of the double epoxide insertion with an ether linkage, $[42 (\text{N}_3) + 142n (\text{repeating unit}) + 180 (\text{C}_{12}\text{H}_{20}\text{O}) + 35 (\text{Cl})]$. Series (g) $[42 (\text{N}_3) + 142n (\text{repeating unit}) + 82 (\text{C}_6\text{H}_{10}) + 35 (\text{Cl})]$ as one might be expected when an azide anion initiated the copolymerization which was terminated by a chloride from catalyst **4**. The series in the region of MALDI-TOF MS spectra over 6500 m/z is the same as the series (e) in the higher molecular region. Isotopic masses modeled for all seven polymer chains are found to agree with the experimental spectra. However, two series in the lower molecular weight region remained unknown after end group analysis.



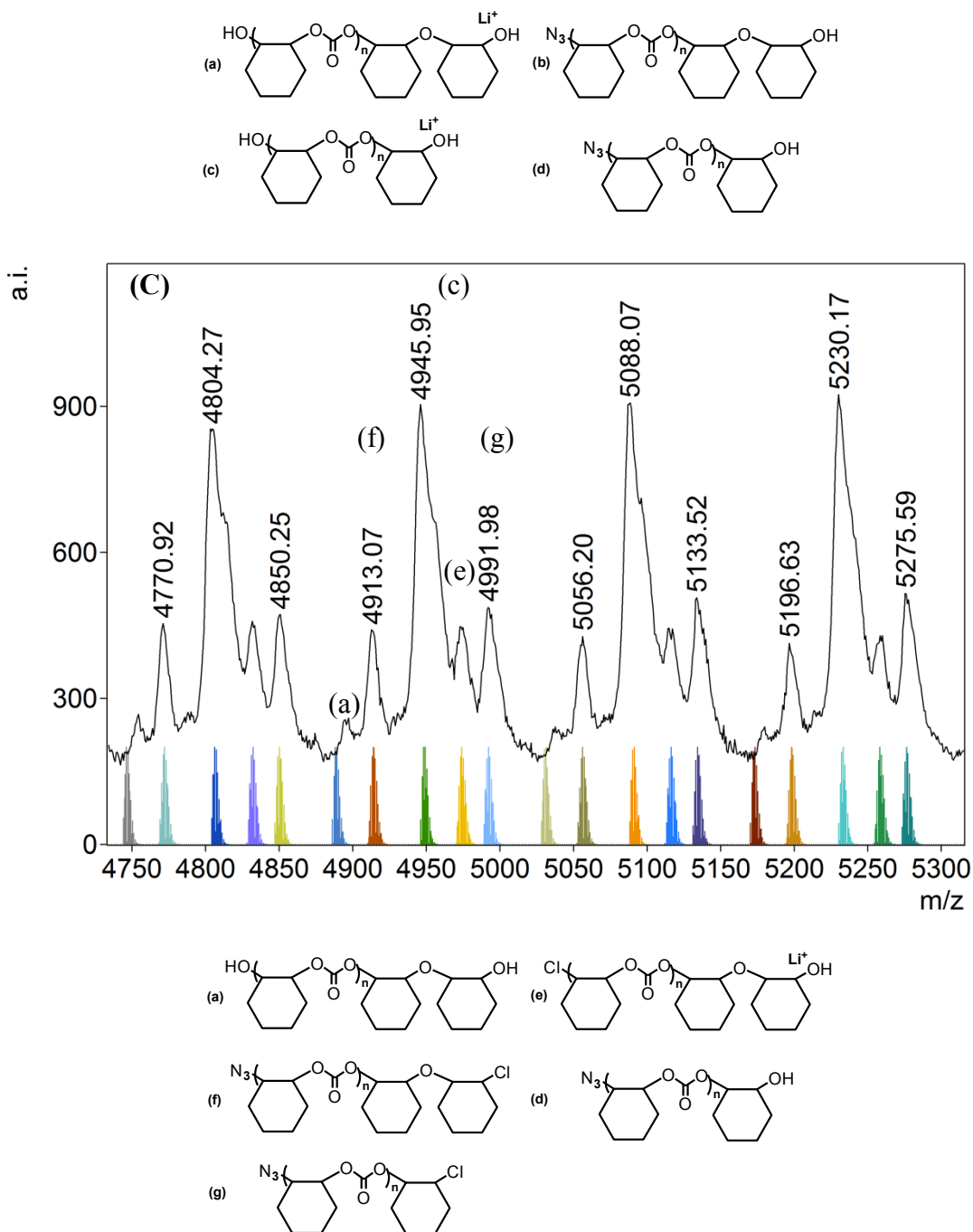


Figure 3.10. (A) MALDI-TOF MS of PCHC produced by **4** (Table 3.2, entry 5). (B) Magnified low molecular weight region of the spectrum ($n = 9-11$). (C) Magnified high molecular weight region of the spectrum ($n = 32-35$). Modeled isotopic masses and images for the polymer chains with end groups (a-g).

3.3.3 Gel Permeation Chromatography

Gel permeation chromatography (GPC) was used to analyze polymer samples in the determination of polymer molecular weights and polydispersity indices (PDIs). From the results of Table 3.1 and 3.2, PDIs were generally observed to be narrow, with most ranging between 1.4 and 1.7. Lower polydispersity (M_w/M_n) values were obtained when PPNCI and PPNN₃ co-catalysts were applied, compared to when DMAP was used. The lowest PDI was obtained by using catalyst **4** and PPNCI (entry 6, Table 3.2), and a reaction time of 6 h. In entries 4, 6 and 7, Table 3.2, molecular weights were found to be dependent on time. As expected, higher molecular weights were obtained with longer reaction time.

In 24-hour reactions, molecular weights between 2.3 and 3.8 kg/mol and polydispersities between 1.48 and 1.58 were found by employing catalyst **5** (possessing a tridentate ligand) with catalyst and co-catalyst loading of 0.2%. Higher molecular weights between 5.7 and 6.4 kg/mol and narrower polydispersities between 1.42 and 1.48 were found, when catalyst **4** (possessing a tetradentate ligand) was used under the same conditions. However, for catalyst **6** bearing a tridentate ligand, molecular weights observed were the lowest and broadest polydispersity (2.10) was obtained in this study. This suggests that the bulky *t*-amyl groups have a deleterious effect on copolymerization activity and possibly lead to increased chain transfer. Some polymer was not characterized by GPC because the yield was very low or the run was a duplicate.

3.4 Experimental

3.4.1 General Experimental Conditions

All manipulations were performed under an atmosphere of dry oxygen-free nitrogen by means of standard Schlenk techniques or using an MBraun Labmaster glove box. CHO was purchased from Aldrich and freshly distilled from CaH₂ and vacuum transferred into a sealed ampule prior to use. All solvents were purified by an MBraun Manual Solvent Purification System, except anhydrous THF, which was distilled from sodium benzophenone ketyl and stored in ampules under nitrogen. PPNN₃ and PPNCI were prepared according to the literature procedure.^[109] 4.8 (99.998%) Supercritical Fluid Chromatography Grade CO₂ was obtained from Praxair in a high-pressure cylinder equipped with a liquid dip tube. All ¹H and ¹³C NMR were performed in CDCl₃ purchased from Cambridge Isotope Laboratories. All ¹H NMR spectra were recorded on a Bruker AVANCE III 300 MHz spectrometer and all ¹³C NMR spectra were recorded on the same spectrometer at 75 MHz. Chemical shifts are given in ppm relative to TMS. All copolymerization reactions were carried out in either a 100 mL or 300 mL stainless steel Parr[®] 5500 autoclave reactor with a Parr[®] 4836 controller.

3.4.2 Copolymerization Procedure

For all reactions carried out in neat cyclohexene oxide (CHO), the appropriate amount of CHO was added to the catalyst and co-catalyst in a glove box. The reactant solution was added via a long-needled syringe to a Parr[®] autoclave, which was pre-dried

under vacuum overnight at 80 °C. The autoclave was then charged with the appropriate pressure of CO₂ and left to stir at the desired temperature and time period. After the desired time the autoclave was cooled in an ice bath until the temperature reached 0 to 4 °C and then vented in the fume hood. An aliquot for NMR was taken immediately after opening the reactor for the determination of conversion. The copolymer was extracted with CH₂Cl₂ and re-precipitated in cold acidic methanol. For reactions done in the presence of PPNC1 or PPNN₃, catalyst and the co-catalyst were first combined in 4 mL of CH₂Cl₂ in the glove box and allowed to stir for 30 minutes and then dried *in vacuo*. This generated a material that was soluble in cyclohexene oxide. The remaining procedure was the same as the neat reactions.

3.4.3 Mass Spectrometry

An Applied Biosystems 4800 MALDI TOF/TOF Analyzer equipped with a reflectron, delayed ion extraction and high performance nitrogen laser (200 Hz operating at 355 nm) was used for polymer analysis. Either 2,5-dihydroxybenzoic acid (DHBA) or 1,8,9-trihydroxyanthracene^[110] with sodium trifluoroacetate was used as the matrix. The matrix was dissolved in THF at a concentration of 2 mg/mL. The polymer was dissolved at approximately 2 mg/mL. The matrix and polymer solutions were mixed together in a ratio of 1:1. One µL of this mixture was spotted on the MALDI plate and left to dry.

3.4.4 Gel Permeation Chromatography

Gel permeation chromatography (GPC) analysis was performed on a Viscotek VE 2001 GPCMax at 35 °C equipped with a Viscotek VE 3580 Refractive Index Detector. Phenogel narrow-bore 5 μm 100 Å, 5 μm Linear(2) columns (300 x 4.60 mm) and a 5 μm guard column were used. The calibration curve was calculated using eight polystyrene standards with molar masses between 1000 and 400,000 daltons. Samples were prepared at a concentration of 2 mg/mL in HPLC grade chloroform and filtered through syringe filters before analysis. The GPC columns were eluted with chloroform (HPLC grade) at a flow rate of 0.35 mL/min with a 200 μL injection volume. No further corrections were performed on the molecular weights obtained.

3.5 Conclusions

In conclusion, the chromium amine-bis(phenolate) complexes, $\text{CrCl}[\text{O}_2\text{NO}]^{\text{BuBu}}$ (**4**), $\text{CrCl}[\text{ONO}]^{\text{BuBuBn}}$ (**5**), $\text{CrCl}[\text{ONO}]^{\text{tAmtAmBn}}$ (**6**) were used for copolymerization of CHO/CO₂. Good activities were observed for the formation of PCHC when complex **4** was applied with PPnCl and PPnN₃ co-catalysts. Under the same condition, the anionic co-catalyst system PPnN₃ or PPnCl was discovered more effective than Lewis Base co-catalyst DMAP by giving polycarbonates with higher yields. These catalytic results agree with the previous reported ones.^[65] The addition of the anionic co-catalyst to the metal center, the chromium nucleophile bond is weakened with the amount of electron density

around the metal center. This destabilization allows for the epoxide to interact or be activated by the metal center, resulting in a rapid epoxide ring opening.^[65]

The steric effect of substituents on the phenolate fragments of the amine-bis(phenolate) ligand appeared to influence the catalyst activity. Catalyst **6**, containing *t*-amyl substituents on the phenolate, shows lower catalyst activity than **5**, which possesses *t*-butyl groups. In this study, catalyst **5** gave approximately 50% conversion of CHO to polymer. It would be worthwhile to change the *t*-amyl or *t*-butyl substituents on the phenolate fragments to substituents with less steric hindrance, such as methyl groups.

Compared to tetradentate chromium^{III} complexes, the tridentate ligands are more coordinatively unsaturated, which was expected to foster co-catalyst or epoxide binding to achieve higher activities in copolymerization. However, from the investigation into the influence of the pendant donor of the amine-bis(phenolate) ligand, tridentate complexes **5** showed inferior activities to tetradentate complex **4** in copolymerization of CHO and CO₂. To explain this, we believe that polymer chain growth is better controlled by occupying two vacant sites in Cr^{III} metal center in tetradentate chromium complex **4** instead of three vacant sites in complex **5**. Also, the PDI values of polycarbonates produced by using tridentate complexes **5** have slightly broader molecular weight distributions than using tetradentate complexes **4**.

Also, H₂[**L**₁] was easier to obtain in high yield after recrystallization than tridentate ligands H₂[**L**₂] and H₂[**L**₃]. Therefore, more attempts can be focused on catalyst **4**. Conditions to examine include varying experimental pressure. Ideally, pressures of 1 bar would be desirable, but this may require the reaction temperature to be increased to 80 °C. Furthermore, the co-catalyst can be changed to N-MeIm^[43, 111], and monomers

other than CHO can be applied with catalyst **4**. The polydispersities observed were generally narrow, when 0.2% loading of catalyst **4** or **5** with co-catalysts was used. Compared to catalyst **5** and **6**, copolymerization reactions were better controlled by using catalyst **4**, which produced polymers with higher molecular weights and narrower polydispersities.

References

- [1] Theopold, K. H., Chromium: Inorganic & Coordination Chemistry, In *Encyclopedia of Inorganic Chemistry*, John Wiley & Sons, Ltd: (2006).
- [2] Constable, E. C.; Housecroft, C. E., *Chem. Soc. Rev.*, (2013) **42**, 1429.
- [3] Kauffman, G. B., Coordination Chemistry: History, In *Encyclopedia of Inorganic Chemistry*, John Wiley & Sons, Ltd: (2006).
- [4] Theopold, K. H.; Kucharczyk, R. R., Chromium: Organometallic Chemistry, In *Encyclopedia of Inorganic and Bioinorganic Chemistry*, John Wiley & Sons, Ltd: (2011).
- [5] Irwin, G.; Kirk, A. D., *Coord. Chem. Rev.*, (2001) **211**, 25.
- [6] So, J. H.; Boudjouk, P., *Inorg. Chem.*, (1990) **29**, 1592.
- [7] Garnovskii, A. D.; Vasilchenko, I. S.; Garnovskii, D. A.; Kharisov, B. I., *J. Coord. Chem.*, (2009) **62**, 151.
- [8] Garnovskii, A. D.; Kharisov, B. I.; Blanco, L. M.; Sadimenko, A. P.; Uraev, A. I.; Vasilchenko, I. S.; Garnovskii, D. A., *J. Coord. Chem.*, (2002) **55**, 1119.
- [9] Gupta, K. C.; Sutar, A. K., *Coord. Chem. Rev.*, (2008) **252**, 1420.
- [10] Cozzi, P. G., *Chem. Soc. Rev.*, (2004) **33**, 410.
- [11] Bellemin-Laponnaz, S.; Dagorne, S., Coordination Chemistry and Applications of Salen, Salan and Salalen Metal Complexes, In *Patai's Chemistry of Functional Groups*, John Wiley & Sons, Ltd: (2009).
- [12] Diehl, H.; Hach, C. C.; Bailar, J. C., Bis(N,N'-Disalicylaethylenediamine)- μ -Aquodnicobalt(II), In *Inorganic Syntheses*, John Wiley & Sons, Inc.: (2007); pp 196.

- [13] Berkessel, A.; Brandenburg, M.; Leitterstorf, E.; Frey, J.; Lex, J.; Schäfer, M., *Adv. Synth. Catal.*, (2007) **349**, 2385.
- [14] Coggon, P.; McPhail, A. T.; Mabbs, F. E.; Richards, A.; Thornley, A. S., *J. Chem. Soc. A: Inorg, Phys, Theor.*, (1970), 3296.
- [15] Bandini, M.; Cozzi, P. G.; Umani-Ronchi, A., *Pure Appl. Chem.*, (2001) **73**, 325.
- [16] Gibson, V. C.; Mastroianni, S.; Newton, C.; Redshaw, C.; Solan, G. A.; White, A. J. P.; Williams, D. J., *J. Chem. Soc., Dalton Trans.*, (2000), 1969.
- [17] Trentin, F.; Scarso, A.; Strukul, G., *Tetrahedron Lett.*, (2011) **52**, 6978.
- [18] Takenaka, N.; Huang, Y.; Rawal, V. H., *Tetrahedron*, (2002) **58**, 8299.
- [19] Huang, Y.; Iwama, T.; Rawal, V. H., *Org. Lett.*, (2002) **4**, 1163.
- [20] Gigante, B.; Corma, A.; García, H.; Sabater, M., *Catal. Lett.*, (2000) **68**, 113.
- [21] Protesescu, L.; Tudorache, M.; Neatu, S.; Grecu, M. N.; Kemnitz, E.; Filip, P.; Parvulescu, V. I.; Coman, S. M., *J. Phys. Chem. C*, (2011) **115**, 1112.
- [22] Paddock, R. L.; Nguyen, S. T., *J. Am. Chem. Soc.*, (2001) **123**, 11498.
- [23] Shen, Y.-M.; Duan, W.-L.; Shi, M., *J. Org. Chem.*, (2003) **68**, 1559.
- [24] Darensbourg, D. J.; Moncada, A. I.; Choi, W.; Reibenspies, J. H., *J. Am. Chem. Soc.*, (2008) **130**, 6523.
- [25] Darensbourg, D. J.; Mackiewicz, R. M.; Rodgers, J. L.; Fang, C. C.; Billodeaux, D. R.; Reibenspies, J. H., *Inorg. Chem.*, (2004) **43**, 6024.
- [26] Jeon, J. Y.; Lee, J. J.; Varghese, J. K.; Na, S. J.; Sujith, S.; Go, M. J.; Lee, J.; Ok, M.-A.; Lee, B. Y., *Dalton Trans.*, (2013) **42**, 9245.
- [27] Bryliakov, K. P.; Talsi, E. P., *Inorg. Chem.*, (2003) **42**, 7258.
- [28] Srinivasan, K.; Kochi, J. K., *Inorg. Chem.*, (1985) **24**, 4671.

- [29] Bousquet, C.; Gilheany, D. G., *Tetrahedron Lett.*, (1995) **36**, 7739.
- [30] Ryan, K. M.; Bousquet, C.; Gilheany, D. G., *Tetrahedron Lett.*, (1999) **40**, 3613.
- [31] Groysman, S.; Goldberg, I.; Kol, M.; Genizi, E.; Goldschmidt, Z., *Inorg. Chim. Acta*, (2003) **345**, 137.
- [32] Danner, H.; Braun, R., *Chem. Soc. Rev.*, (1999) **28**, 395.
- [33] Gerngross. T.U.; Slater, S. C., *Sci. Am.*, (2000) **283**, 37.
- [34] Gross, R. A.; Kalra, B., *Science*, (2002) **297**, 803.
- [35] Okada, M., *Prog. Polym. Sci.*, (2002) **27**, 87.
- [36] Department of Energy (US); International Energy Agency Report-0484, (2013).
- [37] Sakakura, T.; Kohno, K., *Chem. Commun.*, (2009), 1312.
- [38] Haszeldine, R. S., *Science*, (2009) **325**, 1647.
- [39] Azar, C.; Lindgren, K.; Larson, E.; Möllersten, K., *Climatic Change*, (2006) **74**, 47.
- [40] Cooper, A. I., *J. Mater. Chem.*, (2000) **10**, 207.
- [41] Schäffner, B.; Schäffner, F.; Verevkin, S. P.; Börner, A., *Chem. Rev.*, (2010) **110**, 4554.
- [42] Darensbourg, D. J.; Holtcamp, M. W., *Coord. Chem. Rev.*, (1996) **153**, 155.
- [43] Kember, M. R.; Buchard, A.; Williams, C. K., *Chem. Commun.*, (2011) **47**, 141.
- [44] Mecking, S., *Angew. Chem. Int. Ed.*, (2004) **43**, 1078.
- [45] vom Saal, F. S.; Hughes, C., *Environ. Health Perspect.*, (2005) **113**, 926.
- [46] Eldik, R. V.; Hubbard, C. D., *Adv. Inorg. Chem.*, (2009) **61**.
- [47] Fukuoka, S.; Kawamura, M.; Komiya, K.; Tojo, M.; Hachiya, H.; Hasegawa, K.; Aminaka, M.; Okamoto, H.; Fukawa, I.; Konno, S., *Green Chem.*, (2003) **5**, 497.

- [48] Ragauskas, A. J.; Williams, C. K.; Davison, B. H.; Britovsek, G.; Cairney, J.; Eckert, C. A.; Frederick, W. J.; Hallett, J. P.; Leak, D. J.; Liotta, C. L.; Mielenz, J. R.; Murphy, R.; Templer, R.; Tschaplinski, T., *Science*, (2006) **311**, 484.
- [49] Klaus, S.; Lehenmeier, M. W.; Anderson, C. E.; Rieger, B., *Coord. Chem. Rev.*, (2011) **255**, 1460.
- [50] Brunelle, D. J., *J. Am. Chem. Soc.*, (2005) **898**, 1.
- [51] Webster, D. C., *Prog. Org. Coat.*, (2003) **47**, 77.
- [52] Inoue, S.; Koinuma, H.; Tsuruta, T., *Macromol. Chem. Phys.*, (1969) **130**, 210.
- [53] Sugimoto, H.; Inoue, S., *J. Polym. Sci., Part A: Polym. Chem.*, (2004) **42**, 5561.
- [54] Cheng, M.; Lobkovsky, E. B.; Coates, G. W., *J. Am. Chem. Soc.*, (1998) **120**, 11018.
- [55] Sugimoto, H.; Ohtsuka, H.; Inoue, S., *J. Polym. Sci., Part A: Polym. Chem.*, (2005) **43**, 4172.
- [56] Qin, Z.; Thomas, C. M.; Lee, S.; Coates, G. W., *Angew. Chem. Int. Ed.*, (2003) **42**, 5484.
- [57] Cheng, M.; Moore, D. R.; Reczek, J. J.; Chamberlain, B. M.; Lobkovsky, E. B.; Coates, G. W., *J. Am. Chem. Soc.*, (2001) **123**, 8738.
- [58] Moore, D. R.; Cheng, M.; Lobkovsky, E. B.; Coates, G. W., *J. Am. Chem. Soc.*, (2003) **125**, 11911.
- [59] Ikpo, N.; Flogeras, J. C.; Kerton, F. M., *Dalton Trans.*, (2013) **42**, 8998.
- [60] Darensbourg, D. J., *Chem. Rev.*, (2007) **107**, 2388.
- [61] Kember, M. R.; White, A. J. P.; Williams, C. K., *Macromolecules*, (2010) **43**, 2291.
- [62] Yoo, J.; Na, S. J.; Park, H. C.; Cyriac, A.; Lee, B. Y., *Dalton Trans.*, (2010) **39**, 2622.

- [63] Sujith, S.; Min, J. K.; Seong, J. E.; Na, S. J.; Lee, B. Y., *Angew. Chem. Int. Ed.*, (2008) **47**, 7306.
- [64] Mang, S.; Cooper, A. I.; Colclough, M. E.; Chauhan, N.; Holmes, A. B., *Macromolecules*, (1999) **33**, 303.
- [65] Darensbourg, D. J.; Mackiewicz, R. M., *J. Am. Chem. Soc.*, (2005) **127**, 14026.
- [66] Darensbourg, D. J.; Mackiewicz, R. M.; Rodgers, J. L.; Phelps, A. L., *Inorg. Chem.*, (2004) **43**, 1831.
- [67] Darensbourg, D. J.; Phelps, A. L., *Inorg. Chem.*, (2005) **44**, 4622.
- [68] Dean, R. K.; Dawe, L. N.; Kozak, C. M., *Inorg. Chem.*, (2012) **51**, 9095.
- [69] Dean, R. K.; Devaine-Pressing, K.; Dawe, L. N.; Kozak, C. M., *Dalton Trans.*, (2013) **42**, 9233.
- [70] Sandler, S. R.; Karo, W.; Bonesteel, J.-A.; Pearce, E. M., Gel permeation chromatography, In *Polymer Synthesis and Characterization*, Academic Press: San Diego, (1998), 140.
- [71] Wichmann, O.; Sillanpää, R.; Lehtonen, A., *Coord. Chem. Rev.*, (2012) **256**, 371.
- [72] Kerton, F. M.; Holloway, S.; Power, A.; Soper, R. G.; Sheridan, K.; Lynam, J. M.; Whitwood, A. C.; Willans, C. E., *Can. J. Chem.*, (2008) **86**, 435.
- [73] Hinshaw, C. J.; Peng, G.; Singh, R.; Spence, J. T.; Enemark, J. H.; Bruck, M.; Kristofzski, J.; Merbs, S. L.; Ortega, R. B.; Wexler, P. A., *Inorg. Chem.*, (1989) **28**, 4483.
- [74] Tshuva, E. Y.; Goldberg, I.; Kol, M.; Goldschmidt, Z., *Organometallics*, (2001) **20**, 3017.

- [75] Groysman, S.; Tshuva, E.; Goldberg, I.; Kol, M.; Goldschmidt, Z.; Shuster, M., *Organometallics*, (2004) **23**, 5291.
- [76] Conte, V.; Coletti, A.; Floris, B.; Licini, G.; Zonta, C., *Coord. Chem. Rev.*, (2011) **255**, 2165.
- [77] Qian, X.; Dawe, L. N.; Kozak, C. M., *Dalton Trans.*, (2011) **40**, 933.
- [78] Chowdhury, R. R.; Crane, A. K.; Fowler, C.; Kwong, P.; Kozak, C. M., *Chem. Commun.*, (2008), 94.
- [79] Chard, E. F.; Dawe, L. N.; Kozak, C. M., *J. Organomet. Chem.*, (2013) **737**, 32.
- [80] Dean, R. K.; Reckling, A. M.; Chen, H.; Dawe, L. N.; Schneider, C. M.; Kozak, C. M., *Dalton Trans.*, (2013) **42**, 3504.
- [81] Dean, R. K.; Granville, S. L.; Dawe, L. N.; Decken, A.; Hattenhauer, K. M.; Kozak, C. M., *Dalton Trans.*, (2010) **39**, 548.
- [82] Ikpo, N.; Butt, S. M.; Collins, K. L.; Kerton, F. M., *Organometallics*, (2009) **28**, 837.
- [83] Kreisel, K. A.; Yap, G. P. A.; Theopold, K. H., *Organometallics*, (2006) **25**, 4670.
- [84] Albahily, K.; Licciulli, S.; Gambarotta, S.; Korobkov, I.; Chevalier, R.; Schuhen, K.; Duchateau, R., *Organometallics*, (2011) **30**, 3346.
- [85] Kreisel, K. A.; Yap, G. P. A.; Theopold, K. H., *Inorg. Chem.*, (2008) **47**, 5293.
- [86] Kim, S.-K.; Kim, T.-J.; Chung, J.-H.; Hahn, T.-K.; Chae, S.-S.; Lee, H.-S.; Cheong, M.; Kang, S. O., *Organometallics*, (2010) **29**, 5805.
- [87] Gao, B.; Luo, X.; Gao, W.; Huang, L.; Gao, S.-m.; Liu, X.; Wu, Q.; Mu, Y., *Dalton Trans.*, (2012) **41**, 2755.
- [88] Darensbourg, D. J.; Billodeaux, D. R., *Inorg. Chem.*, (2005) **44**, 1433.
- [89] Kojima, F.; Aida, T.; Inoue, S., *J. Am. Chem. Soc.*, (1986) **108**, 391.

- [90] Xiao, Y. L.; Wang, Z.; Ding, K. L., *Chem.-Eur. J.*, (2005) **11**, 3668.
- [91] Stamp, L. M.; Mang, S. A.; Holmes, A. B.; Knights, K. A.; de Miguel, Y. R.; McConvey, I. F., *Chem. Commun.*, (2001), 2502.
- [92] Cohen, C. T.; Chu, T.; Coates, G. W., *J. Am. Chem. Soc.*, (2005) **127**, 10869.
- [93] Buchard, A.; Kember, M. R.; Sandeman, K. G.; Williams, C. K., *Chem. Commun.*, (2011) **47**, 212.
- [94] Lu, X. B.; Darensbourg, D. J., *Chem. Soc. Rev.*, (2012) **41**, 1462.
- [95] Zelikoff, A. L.; Kopilov, J.; Goldberg, I.; Coates, G. W.; Kol, M., *Chem. Commun.*, (2009), 6804.
- [96] Tshuva, E. Y.; Goldberg, I.; Kol, M.; Goldschmidt, Z., *Inorg. Chem.*, (2001) **40**, 4263.
- [97] Gendler, S.; Segal, S.; Goldberg, I.; Goldschmidt, Z.; Kol, M., *Inorg. Chem.*, (2006) **45**, 4783.
- [98] Chen, Q. H.; Huang, J. L.; Yu, J., *Inorg. Chem. Commun.*, (2005) **8**, 444.
- [99] Seena, E. B.; Mathew, N.; Kuriakose, M.; Kurup, M. R. P., *Polyhedron*, (2008) **27**, 1455.
- [100] Shujah, S.; Zia ur, R.; Muhammad, N.; Ali, S.; Khalid, N.; Tahir, M. N., *J. Organomet. Chem.*, (2011) **696**, 2772.
- [101] Nakano, K.; Nakamura, M.; Nozaki, K., *Macromolecules*, (2009) **42**, 6972.
- [102] Guo, L.; Wang, C.; Zhao, W.; Li, H.; Sun, W.; Shen, Z., *Dalton Trans.*, (2009), 5406.
- [103] Darensbourg, D. J. Ulusoy, M. Karroonnirum, . . . oland, . . . eibenspies, J. H. etinkaya, B., *Macromolecules*, (2009) **42**, 6992.

- [104] Sutar, A. K.; Maharana, T.; Dutta, S.; Chen, C.-T.; Lin, C.-C., *Chem. Soc. Rev.*, (2010) **39**, 1724.
- [105] Darensbourg, D. J.; Mackiewicz, R. M.; Billodeaux, D. R., *Organometallics*, (2004) **24**, 144.
- [106] Jutz, F.; Buchard, A.; Kember, M. R.; Fredriksen, S. B.; Williams, C. K., *J. Am. Chem. Soc.*, (2011) **133**, 17395.
- [107] Niu, Y. S.; Zhang, W. X.; Pang, X.; Chen, X. S.; Zhuang, X. L.; Jing, X. B., *J. Polym. Sci., Part A: Polym. Chem.*, (2007) **45**, 5050.
- [108] Rao, D. Y.; Li, B.; Zhang, R.; Wang, H.; Lu, X. B.; . *Inorg. Chem.*, (2009) **48**, 2830.
- [109] Demadis, K. D.; Meyer, T. J.; White, P. S., *Inorg. Chem.*, (1998) **37**, 3610.
- [110] Trimpin, S. K., S.; Raeder, H. J.; Muellen, K., *J. Am. Soc. Mass. Spectrom.*, (2006) **17**, 661.
- [111] Darensbourg, D. J.; Rodgers, J. L.; Fang, C. C., *Inorg. Chem.*, (2003) **42**, 4498.

Appendices

Table A1.1. Crystallographic and Structure Refinement Data for (5)₂·LiCl·THF.

Chemical formula	C ₇₈ H ₁₁₀ Cl ₃ Cr ₂ LiN ₂ O ₅ ·2(C ₇ H ₈)
Colour	Green
Habit	Prism
Formula mass	1557.24
Crystal system	Trigonal
<i>a</i> [Å]	18.945(9)
<i>b</i> [Å]	18.945(9)
<i>c</i> [Å]	25.390(13)
α [°]	90.00
β [°]	90.00
γ [°]	120.00
Unit cell <i>V</i> [Å ³]	7892(7)
Temperature [K]	123(2)
Space group	P3 ₁ 2 1 (#152)
<i>Z</i>	3
<i>D_c</i> /g cm ⁻³	0.983
Radiation type	MoK α
Absorption, μ [cm ⁻¹]	3.24
<i>F</i> (000)	2502
Reflections measured	73179
Independent refl's	7780
<i>R_{int}</i>	0.1281
<i>R_I</i> , ^[a] <i>wR</i> (<i>F</i> ²) ^[b] (<i>all</i>)	0.1351, 0.3327
<i>R_I</i> , ^[a] <i>wR</i> (<i>F</i> ²) ^[b] (<i>I</i> > 2 σ (<i>I</i>))	0.1211, 0.3154
Goodness of fit on <i>F</i> ²	1.187
CCDC Ref no.	974612

[a] $R_I = \Sigma(|F_o| - |F_c|) / \Sigma|F_o|$. [b] $wR_2 = [\Sigma(w(F_o^2 - F_c^2)^2) / \Sigma w(F_o^2)^2]^{1/2}$.

checkCIF/PLATON report

You have not supplied any structure factors. As a result the full set of tests cannot be run.

No syntax errors found. CIF dictionary Interpreting this report

Datablock: HC013

Bond precision: C-C = 0.0178 A Wavelength=0.71075

Cell: a=18.945 (9) b=18.945 (9) c=25.390 (13)
 alpha=90 beta=90 gamma=120

Temperature: 123 K

	Calculated	Reported
Volume	7892 (10)	7892 (7)
Space group	P 31 2 1	P 31 2 1
Hall group	P 31 2"	P 31 2"
Moiety formula	C76 H104 Cl3 Cr2 Li N2 O4, C2 H4 O	C78 H110 Cl3 Cr2 Li N2 O5, 2(C7 H8)
Sum formula	C78 H108 Cl3 Cr2 Li N2 O5	C92 H126 Cl3 Cr2 Li N2 O5
Mr	1370.95	1557.24
Dx, g cm-3	0.865	0.983
Z	3	3
Mu (mm-1)	0.318	0.324
F000	2196.0	2502.0
F000'	2199.96	
h, k, lmax	21, 21, 28	21, 21, 28
Nref	4295 [7787]	7780
Tmin, Tmax	0.878, 0.902	0.888, 0.963
Tmin'	0.878	

Correction method= NUMERICAL

Data completeness= 1.81/1.00 Theta(max)= 23.490

R(reflections)= 0.1211(6060) wR2(reflections)= 0.3327(7780)

S = 1.187 Npar= 561

The following ALERTS were generated. Each ALERT has the format
test-name_ALERT_alert-type_alert-level.

Click on the hyperlinks for more details of the test.

Alert level A

CHEMW03_ALERT_2_A ALERT: The ratio of given/expected molecular weight as
calculated from the _atom_site* data lies outside
the range 0.90 <> 1.10

```

From the CIF: _cell_formula_units_Z          3
From the CIF: _chemical_formula_weight      1557.24
TEST: Calculate formula weight from _atom_site_*
atom      mass      num      sum
C         12.01     78.00    936.86
H          1.01    108.00    108.86
Cl        35.45      3.00    106.36
Cr        52.00      2.00    103.99
N         14.01      2.00     28.01
O         16.00      5.00     79.99
Li         6.94      1.00      6.94
Calculated formula weight                    1371.02

```

Author Response: This structure was treated via Platon's Squeeze procedure. Please see `platon_squeeze_details` for full details. 2 toluene molecules that were omitted from the model were included in the formula for calculation of the intensive properties.

Alert level B

THETM01_ALERT_3_B The value of $\sin(\theta_{\max})/\lambda$ is less than 0.575
 Calculated $\sin(\theta_{\max})/\lambda = 0.5608$

Author Response: 2theta was cut-off at 47 degrees. These crystals diffracted very weakly and no significant diffraction was observed above this level.

PLAT220_ALERT_2_B Large Non-Solvent C Ueq(max)/Ueq(min) ... 4.4 Ratio
 PLAT234_ALERT_4_B Large Hirshfeld Difference C2 -- C3 .. 0.28 Ang.

Author Response: Due to weak diffraction and large structure size some of the light atoms show some discontinuities in anisotropic displacement. Attempts to model the largest differences using SIMU were made (please see `iucr_refine_instructions_details` for a full list of the applied restraints.) The atoms identified by the Hirshfeld Rigid Bond Test were carefully examined to ensure that they are not the result of an incorrect atom-type assignment.

PLAT341_ALERT_3_B Low Bond Precision on C-C Bonds 0.0178 Ang

Author Response: The large associated su's on the C-C bonds, and many of the light atom angles, is the expected result of the weakly diffracting data-set.

PLAT413_ALERT_2_B Short Inter XH3 .. XHn H24C .. H24C .. 1.97 Ang.

Author Response: H-atoms were introduced in calculated positions and refined on a riding model. H-atoms on disordered methyl groups were refined using HFIX 33 instead of HFIX137 due to the weak quality of the collected data.

Alert level C

RFACG01_ALERT_3_C The value of the R factor is > 0.10
R factor given 0.121

Author Response: The crystal under consideration diffracted weakly and therefore the high weighted R factor does not indicate an incorrect model.

RFACR01_ALERT_3_C The value of the weighted R factor is > 0.25
Weighted R factor given 0.333

Author Response: The crystal under consideration diffracted weakly and therefore the high weighted R factor does not indicate an incorrect model.

RINTA01_ALERT_3_C The value of Rint is greater than 0.12
Rint given 0.128

Author Response: The crystal under consideration diffracted weakly.

PLAT020_ALERT_3_C The value of Rint is greater than 0.12 0.128

Author Response: The crystal under consideration diffracted weakly.

PLAT041_ALERT_1_C Calc. and Reported SumFormula Strings Differ ?

Author Response: This structure was treated via Platon's Squeeze procedure. Please see platon_squeeze_details for full details. 2 toluene molecules that were omitted from the model were included in the formula for calculation of the intensive properties.

PLAT068_ALERT_1_C Reported F000 Differs from Calcd (or Missing)... ?

Author Response: This structure was treated via Platon's Squeeze procedure. Please see platon_squeeze_details for full details. 2 toluene molecules that were omitted from the model were included in the formula for calculation of the intensive properties.

PLAT082_ALERT_2_C High R1 Value 0.12

Author Response: The crystal under consideration diffracted weakly and therefore the high weighted R factor does not indicate an incorrect model.

PLAT084_ALERT_2_C High wR2 Value 0.33

Author Response: The crystal under consideration diffracted weakly and therefore the high weighted R factor does not indicate an incorrect model.

PLAT094_ALERT_2_C Ratio of Maximum / Minimum Residual Density 3.21

Author Response: From shelx.lst Electron density synthesis with coefficients Fo-Fc Highest peak 1.09 at 0.9092 0.5223 0.1449 [0.05 A from CR1] Deepest hole -0.34 at 0.1118 0.7292 0.1358 [1.26 A from LI1]

PLAT222_ALERT_3_C Large Non-Solvent H Uiso(max)/Uiso(min) .. 5.5 Ratio

Author Response: H-atoms were introduced in calculated positions and refined on a riding model. Large H-atoms are associated with disordered groups. Attempts to model the disorder are described in `_refine_special_details`.

PLAT230_ALERT_2_C Hirshfeld Test Diff for C1 -- C6 .. 5.3 su

Author Response: Due to weak diffraction and large structure size some of the light atoms show some discontinuities in anisotropic displacement. Attempts to model the largest differences using SIMU were made (please see `iucr_refine_instructions_details` for a full list of the applied restraints.) The atoms identified by the Hirshfeld Rigid Bond Test were carefully examined to ensure that they are not the result of an incorrect atom-type assignment.

PLAT230_ALERT_2_C Hirshfeld Test Diff for C2 -- C22 .. 6.5 su

Author Response: Due to weak diffraction and large structure size some of the light atoms show some discontinuities in anisotropic displacement. Attempts to model the largest differences using SIMU were made (please see `iucr_refine_instructions_details` for a full list of the applied restraints.) The atoms identified by the Hirshfeld Rigid Bond Test were carefully examined to ensure that they are not the result of an incorrect atom-type assignment.

PLAT230_ALERT_2_C Hirshfeld Test Diff for C13 -- C14 .. 6.1 su

Author Response: Due to weak diffraction and large structure size some of the light atoms show some discontinuities in anisotropic displacement. Attempts to model the largest differences using SIMU were made (please see `iucr_refine_instructions_details` for a full list of the applied restraints.) The atoms identified by the Hirshfeld Rigid Bond Test were carefully examined to ensure that they are not the result of an incorrect atom-type assignment.

PLAT234_ALERT_4_C Large Hirshfeld Difference O1 -- C1 .. 0.16 Ang.

Author Response: Due to weak diffraction and large structure size some of the light atoms show some discontinuities in anisotropic displacement. Attempts to model the largest differences using SIMU were made (please see `iucr_refine_instructions_details` for a full list of the applied restraints.) The atoms identified by the Hirshfeld Rigid Bond Test were carefully examined to ensure that they are not the result of an incorrect atom-type assignment.

PLAT234_ALERT_4_C Large Hirshfeld Difference O1 -- Li1 .. 0.19 Ang.

Author Response: Due to weak diffraction and large structure size some of the light atoms show some discontinuities in anisotropic displacement. Attempts to model the largest differences using SIMU were made (please see [iucr_refine_instructions_details](#) for a full list of the applied restraints.) The atoms identified by the Hirshfeld Rigid Bond Test were carefully examined to ensure that they are not the result of an incorrect atom-type assignment.

PLAT234_ALERT_4_C Large Hirshfeld Difference C1 -- C2 .. 0.20 Ang.

Author Response: Due to weak diffraction and large structure size some of the light atoms show some discontinuities in anisotropic displacement. Attempts to model the largest differences using SIMU were made (please see [iucr_refine_instructions_details](#) for a full list of the applied restraints.) The atoms identified by the Hirshfeld Rigid Bond Test were carefully examined to ensure that they are not the result of an incorrect atom-type assignment.

PLAT234_ALERT_4_C Large Hirshfeld Difference C3 -- C4 .. 0.19 Ang.

Author Response: Due to weak diffraction and large structure size some of the light atoms show some discontinuities in anisotropic displacement. Attempts to model the largest differences using SIMU were made (please see [iucr_refine_instructions_details](#) for a full list of the applied restraints.) The atoms identified by the Hirshfeld Rigid Bond Test were carefully examined to ensure that they are not the result of an incorrect atom-type assignment.

PLAT234_ALERT_4_C Large Hirshfeld Difference C4 -- C5 .. 0.17 Ang.

Author Response: Due to weak diffraction and large structure size some of the light atoms show some discontinuities in anisotropic displacement. Attempts to model the largest differences using SIMU were made (please see [iucr_refine_instructions_details](#) for a full list of the applied restraints.) The atoms identified by the Hirshfeld Rigid Bond Test were carefully examined to ensure that they are not the result of an incorrect atom-type assignment.

PLAT234_ALERT_4_C Large Hirshfeld Difference C8 -- C9 .. 0.17 Ang.

Author Response: Due to weak diffraction and large structure size some of the light atoms show some discontinuities in anisotropic displacement. Attempts to model the largest differences using SIMU were made (please see [iucr_refine_instructions_details](#) for a full list of the applied restraints.) The atoms identified by the Hirshfeld Rigid Bond Test were carefully examined to ensure that they are not the result of an incorrect atom-type assignment.

PLAT234_ALERT_4_C Large Hirshfeld Difference C10 -- C11 .. 0.19 Ang.

Author Response: Due to weak diffraction and large structure size some of the light atoms show some discontinuities in anisotropic displacement. Attempts to model the largest differences using SIMU were made (please see `iucr_refine_instructions_details` for a full list of the applied restraints.) The atoms identified by the Hirshfeld Rigid Bond Test were carefully examined to ensure that they are not the result of an incorrect atom-type assignment.

PLAT234_ALERT_4_C Large Hirshfeld Difference C11 -- C12 .. 0.21 Ang.

Author Response: Due to weak diffraction and large structure size some of the light atoms show some discontinuities in anisotropic displacement. Attempts to model the largest differences using SIMU were made (please see `iucr_refine_instructions_details` for a full list of the applied restraints.) The atoms identified by the Hirshfeld Rigid Bond Test were carefully examined to ensure that they are not the result of an incorrect atom-type assignment.

PLAT234_ALERT_4_C Large Hirshfeld Difference C12 -- C13 .. 0.17 Ang.

Author Response: Due to weak diffraction and large structure size some of the light atoms show some discontinuities in anisotropic displacement. Attempts to model the largest differences using SIMU were made (please see `iucr_refine_instructions_details` for a full list of the applied restraints.) The atoms identified by the Hirshfeld Rigid Bond Test were carefully examined to ensure that they are not the result of an incorrect atom-type assignment.

PLAT234_ALERT_4_C Large Hirshfeld Difference C18A -- C19A .. 0.18 Ang.

Author Response: Due to weak diffraction and large structure size some of the light atoms show some discontinuities in anisotropic displacement. Attempts to model the largest differences using SIMU were made (please see `iucr_refine_instructions_details` for a full list of the applied restraints.) The atoms identified by the Hirshfeld Rigid Bond Test were carefully examined to ensure that they are not the result of an incorrect atom-type assignment.

PLAT234_ALERT_4_C Large Hirshfeld Difference C19A -- C20A .. 0.16 Ang.

Author Response: Due to weak diffraction and large structure size some of the light atoms show some discontinuities in anisotropic displacement. Attempts to model the largest differences using SIMU were made (please see `iucr_refine_instructions_details` for a full list of the applied restraints.) The atoms identified by the Hirshfeld Rigid Bond Test were carefully examined to ensure that they are not the result of an incorrect atom-type assignment.

PLAT234_ALERT_4_C Large Hirshfeld Difference C20A -- C21 .. 0.17 Ang.

Author Response: Due to weak diffraction and large structure size some of the light atoms show some discontinuities in anisotropic displacement. Attempts to model the largest differences using SIMU were made (please see [iucr_refine_instructions_details](#) for a full list of the applied restraints.) The atoms identified by the Hirshfeld Rigid Bond Test were carefully examined to ensure that they are not the result of an incorrect atom-type assignment.

PLAT234_ALERT_4_C Large Hirshfeld Difference C22 -- C25 .. 0.25 Ang.

Author Response: Due to weak diffraction and large structure size some of the light atoms show some discontinuities in anisotropic displacement. Attempts to model the largest differences using SIMU were made (please see [iucr_refine_instructions_details](#) for a full list of the applied restraints.) The atoms identified by the Hirshfeld Rigid Bond Test were carefully examined to ensure that they are not the result of an incorrect atom-type assignment.

PLAT234_ALERT_4_C Large Hirshfeld Difference C30 -- C32 .. 0.25 Ang.

Author Response: Due to weak diffraction and large structure size some of the light atoms show some discontinuities in anisotropic displacement. Attempts to model the largest differences using SIMU were made (please see [iucr_refine_instructions_details](#) for a full list of the applied restraints.) The atoms identified by the Hirshfeld Rigid Bond Test were carefully examined to ensure that they are not the result of an incorrect atom-type assignment.

PLAT234_ALERT_4_C Large Hirshfeld Difference C30 -- C33A .. 0.23 Ang.

Author Response: Due to weak diffraction and large structure size some of the light atoms show some discontinuities in anisotropic displacement. Attempts to model the largest differences using SIMU were made (please see [iucr_refine_instructions_details](#) for a full list of the applied restraints.) The atoms identified by the Hirshfeld Rigid Bond Test were carefully examined to ensure that they are not the result of an incorrect atom-type assignment.

PLAT234_ALERT_4_C Large Hirshfeld Difference C34 -- C35 .. 0.18 Ang.

Author Response: Due to weak diffraction and large structure size some of the light atoms show some discontinuities in anisotropic displacement. Attempts to model the largest differences using SIMU were made (please see [iucr_refine_instructions_details](#) for a full list of the applied restraints.) The atoms identified by the Hirshfeld Rigid Bond Test were carefully examined to ensure that they are not the result of an incorrect atom-type assignment.

PLAT234_ALERT_4_C Large Hirshfeld Difference C34 -- C37 .. 0.17 Ang.

Author Response: Due to weak diffraction and large structure size some of the light atoms show some discontinuities in anisotropic displacement. Attempts to model the largest differences using SIMU were made (please see [iucr_refine_instructions_details](#) for a full list of the applied restraints.) The atoms identified by the Hirshfeld Rigid Bond Test were carefully examined to ensure that they are not the result of an incorrect atom-type assignment.

PLAT241_ALERT_2_C Check High Ueq as Compared to Neighbors for C11

Author Response: Due to weak diffraction and large structure size some of the light atoms show some discontinuities in anisotropic displacement. Attempts to model the largest differences using SIMU were made (please see [iucr_refine_instructions_details](#) for a full list of the applied restraints.) The atoms identified by the Hirshfeld Rigid Bond Test were carefully examined to ensure that they are not the result of an incorrect atom-type assignment.

PLAT241_ALERT_2_C Check High Ueq as Compared to Neighbors for O1

Author Response: Due to weak diffraction and large structure size some of the light atoms show some discontinuities in anisotropic displacement. Attempts to model the largest differences using SIMU were made (please see [iucr_refine_instructions_details](#) for a full list of the applied restraints.) The atoms identified by the Hirshfeld Rigid Bond Test were carefully examined to ensure that they are not the result of an incorrect atom-type assignment.

PLAT241_ALERT_2_C Check High Ueq as Compared to Neighbors for C12

Author Response: Due to weak diffraction and large structure size some of the light atoms show some discontinuities in anisotropic displacement. Attempts to model the largest differences using SIMU were made (please see [iucr_refine_instructions_details](#) for a full list of the applied restraints.) The atoms identified by the Hirshfeld Rigid Bond Test were carefully examined to ensure that they are not the result of an incorrect atom-type assignment.

PLAT242_ALERT_2_C Check Low Ueq as Compared to Neighbors for C11

Author Response: Due to weak diffraction and large structure size some of the light atoms show some discontinuities in anisotropic displacement. Attempts to model the largest differences using SIMU were made (please see [iucr_refine_instructions_details](#) for a full list of the applied restraints.) The atoms identified by the Hirshfeld Rigid Bond Test were carefully examined to ensure that they are not the result of an incorrect atom-type assignment.

PLAT242_ALERT_2_C Check Low Ueq as Compared to Neighbors for C22

Author Response: Due to weak diffraction and large structure size some of the light atoms show some discontinuities in anisotropic displacement. Attempts to model the largest differences using SIMU were made (please see `iucr_refine_instructions_details` for a full list of the applied restraints.) The atoms identified by the Hirshfeld Rigid Bond Test were carefully examined to ensure that they are not the result of an incorrect atom-type assignment.

PLAT242_ALERT_2_C Check Low Ueq as Compared to Neighbors for C26

Author Response: Due to weak diffraction and large structure size some of the light atoms show some discontinuities in anisotropic displacement. Attempts to model the largest differences using SIMU were made (please see `iucr_refine_instructions_details` for a full list of the applied restraints.) The atoms identified by the Hirshfeld Rigid Bond Test were carefully examined to ensure that they are not the result of an incorrect atom-type assignment.

PLAT242_ALERT_2_C Check Low Ueq as Compared to Neighbors for C30

Author Response: Due to weak diffraction and large structure size some of the light atoms show some discontinuities in anisotropic displacement. Attempts to model the largest differences using SIMU were made (please see `iucr_refine_instructions_details` for a full list of the applied restraints.) The atoms identified by the Hirshfeld Rigid Bond Test were carefully examined to ensure that they are not the result of an incorrect atom-type assignment.

PLAT309_ALERT_2_C Single Bonded Oxygen (C-O .GT. 1.3 Ang) 03

Author Response: The atoms in question is part of a disordered THF group. The disorder crosses a symmetry element (a two-fold screw axis) and therefore this group was treated with a PART -1 instruction. The O-atom is in fact bonded within THF, and coordinated to a Li atom.

PLAT334_ALERT_2_C Small Average Benzene C-C Dist. C1 -C6 1.37 Ang.

Author Response: Many of the light atoms were involved in various disorders. DFIX restraints were applied to these groups (please see `iucr_refine_instructions_details` for a full list of the applied restraints.)

PLAT366_ALERT_2_C Short? C(sp?)-C(sp?) Bond C16 - C21 ... 1.37 Ang.

Author Response: Many of the light atoms were involved in various disorders. DFIX restraints were applied to these groups (please see `iucr_refine_instructions_details` for a full list of the applied restraints.)

PLAT410_ALERT_2_C Short Intra H...H Contact H15A .. H17 .. 1.98 Ang.

Author Response: H-atoms were introduced in calculated positions and refined on a riding model. H-atoms on disordered methyl groups were refined using HFIX 33 instead of HFIX137 due to the weak quality of the collected data.

PLAT722_ALERT_1_C	Angle	Calc	116.00,	Rep	117.30	Dev...	1.30	Deg.
	C17 -C18 -H18		1.555	1.555	1.555	#	116	

Author Response: Deviations here may be due to applied restraints and that the calculated values by checkCIF are done without access to the variance/covariance matrix.

PLAT722_ALERT_1_C	Angle	Calc	129.00,	Rep	127.80	Dev...	1.20	Deg.
	C18 -C19 -H19		1.555	1.555	1.555	#	118	

Author Response: Deviations here may be due to applied restraints and that the calculated values by checkCIF are done without access to the variance/covariance matrix.

PLAT722_ALERT_1_C	Angle	Calc	126.00,	Rep	127.80	Dev...	1.80	Deg.
	C20 -C19 -H19		1.555	1.555	1.555	#	119	

Author Response: Deviations here may be due to applied restraints and that the calculated values by checkCIF are done without access to the variance/covariance matrix.

PLAT722_ALERT_1_C	Angle	Calc	111.00,	Rep	109.50	Dev...	1.50	Deg.
	H32D -C32A -H32E		1.555	1.555	1.555	#	265	

Author Response: Deviations here may be due to applied restraints and that the calculated values by checkCIF are done without access to the variance/covariance matrix.



Alert level G

FORMU01_ALERT_2_G There is a discrepancy between the atom counts in the `_chemical_formula_sum` and the formula from the `_atom_site*` data.
Atom count from `_chemical_formula_sum`: C92 H126 C13 Cr2 Li1 N2 O5
Atom count from the `_atom_site` data: C78 H108 C13 Cr2 Li1 N2 O5

Author Response: This structure was treated via Platon's Squeeze procedure. Please see `platon_squeeze_details` for full details. 2 toluene molecules that were omitted from the model were included in the formula for calculation of the intensive properties.

CELLZ01_ALERT_1_G Difference between formula and `atom_site` contents detected.

Author Response: This structure was treated via Platon's Squeeze procedure. Please see `platon_squeeze_details` for full details. 2 toluene molecules that were omitted from the model were included in the formula for calculation of the intensive properties.

CELLZ01_ALERT_1_G ALERT: Large difference may be due to a
symmetry error - see SYMMG tests
From the CIF: `_cell_formula_units_Z` 3
From the CIF: `_chemical_formula_sum` C92 H126 Cl3 Cr2 Li N2 O5
TEST: Compare cell contents of formula and `atom_site` data

atom	Z*formula	cif sites	diff
C	276.00	234.00	42.00
H	378.00	324.00	54.00
Cl	9.00	9.00	0.00
Cr	6.00	6.00	0.00
Li	3.00	3.00	0.00
N	6.00	6.00	0.00
O	15.00	15.00	0.00

Author Response: This structure was treated via Platon's Squeeze procedure. Please see `platon_squeeze_details` for full details. 2 toluene molecules that were omitted from the model were included in the formula for calculation of the intensive properties.

PLAT002_ALERT_2_G Number of Distance or Angle Restraints on AtSite 43

Author Response: Due to weak diffraction and large structure size some of the light atoms exhibited non-ideal behaviour. Attempts to model the largest differences using DFIX, SIMU and ISOR were made (please see `iucr_refine_instructions_details` for a full list of the applied restraints.)

PLAT003_ALERT_2_G Number of Uiso or Uij Restrained Atom Sites 33

Author Response: Due to weak diffraction and large structure size some of the light atoms exhibited non-ideal behaviour. Attempts to model the largest differences using DFIX, SIMU and ISOR were made (please see `iucr_refine_instructions_details` for a full list of the applied restraints.)

PLAT033_ALERT_4_G Flack x Value Deviates .gt. 2*sigma from Zero .. 0.120
PLAT042_ALERT_1_G Calc. and Reported MoietyFormula Strings Differ ?

Author Response: This structure was treated via Platon's Squeeze procedure. Please see `platon_squeeze_details` for full details. 2 toluene molecules that were omitted from the model were included in the formula for calculation of the intensive properties.

PLAT072_ALERT_2_G SHELXL First Parameter in WGHT Unusually Large. 0.20
PLAT152_ALERT_1_G The Supplied and Calc. Volume s.1. Differ by ... 3 Units
PLAT242_ALERT_2_G Check Low Ueq as Compared to Neighbors for Li1A

Author Response: Due to weak diffraction and large structure size some of the light atoms show some discontinuities in anisotropic displacement. Attempts to model the largest differences using SIMU were made (please see [iucr_refine_instructions_details](#) for a full list of the applied restraints.) The atoms identified by the Hirshfeld Rigid Bond Test were carefully examined to ensure that they are not the result of an incorrect atom-type assignment.

```

PLAT301_ALERT_3_G Note: Main Residue Disorder ..... 26 Perc.
PLAT302_ALERT_4_G Note: Anion/Solvent Disorder ..... 100 Perc.
PLAT606_ALERT_4_G VERY LARGE Solvent Accessible VOID(S) in Structure !
PLAT764_ALERT_4_G Overcomplete CIF Bond List Detected (Rep/Expd) . 1.11 Ratio
PLAT791_ALERT_4_G Note: The Model has Chirality at N1 (Verify) R
PLAT811_ALERT_5_G No ADDSYM Analysis: Too Many Excluded Atoms .... !
PLAT860_ALERT_3_G Note: Number of Least-Squares Restraints ..... 280
PLAT869_ALERT_4_G ALERTS Related to the use of SQUEEZE Suppressed !

```

```

1 ALERT level A = Most likely a serious problem - resolve or explain
5 ALERT level B = A potentially serious problem, consider carefully
45 ALERT level C = Check. Ensure it is not caused by an omission or oversight
18 ALERT level G = General information/check it is not something unexpected

10 ALERT type 1 CIF construction/syntax error, inconsistent or missing data
25 ALERT type 2 Indicator that the structure model may be wrong or deficient
9 ALERT type 3 Indicator that the structure quality may be low
24 ALERT type 4 Improvement, methodology, query or suggestion
1 ALERT type 5 Informative message, check

```

It is advisable to attempt to resolve as many as possible of the alerts in all categories. Often the minor alerts point to easily fixed oversights, errors and omissions in your CIF or refinement strategy, so attention to these fine details can be worthwhile. In order to resolve some of the more serious problems it may be necessary to carry out additional measurements or structure refinements. However, the purpose of your study may justify the reported deviations and the more serious of these should normally be commented upon in the discussion or experimental section of a paper or in the "special_details" fields of the CIF. checkCIF was carefully designed to identify outliers and unusual parameters, but every test has its limitations and alerts that are not important in a particular case may appear. Conversely, the absence of alerts does not guarantee there are no aspects of the results needing attention. It is up to the individual to critically assess their own results and, if necessary, seek expert advice.

Publication of your CIF in IUCr journals

A basic structural check has been run on your CIF. These basic checks will be run on all CIFs submitted for publication in IUCr journals (*Acta Crystallographica*, *Journal of Applied Crystallography*, *Journal of Synchrotron Radiation*); however, if you intend to submit to *Acta Crystallographica Section C* or *E*, you should make sure that full publication checks are run on the final version of your CIF prior to submission.

Publication of your CIF in other journals

Please refer to the *Notes for Authors* of the relevant journal for any special instructions relating to CIF submission.

PLATON version of 05/11/2012; check.def file version of 05/11/2012

Datablock HC013 - ellipsoid plot

